SRI International

18 March 1980

SWANN'S REMOTE VIEWING PROBE OF MERCURY

Prepared by: B. Humphrey
Radio Physics Laboratory

SRI International
333 Ravenswood Ave. • Menlo Park, California 94025
(415) 326-6200 • Cable: SRI INTL MPK • TWX: 910-373-1246

TABLE OF CONTENTS

INTRODUCTION

This report presents Ingo Swann's probe of the planet Mercury prior to the "Mariner 10" flyby, in addition to the scientific data and analyses which ultimately resulted from the "Mariner" exploration.

Data charts have been included to illuminate both the Swann impressions and representative technical reference quotes, which are relevant to the various planetary topics such as electromagnetism, surface morphology, atmospheric composition, etc. Only a few of the technical excerpts are actually quoted in the data charts: the others are merely listed as references and may be found in their contextual entirety in the appropriate appendices.

All of the impressions and data references are color-coded in the appendices. Surface information is underlined in green; atmospheric is blue; magnetic and electromagnetic, red; gravity, purple; and biological, yellow. For example, if you wished to see the Science News reference for "lobate scarps" on the "surface phenomena" data sheet, you would turn to Appendix III, locate the "Vol. 106" section and note the green color-coded underlining on page 196. There is also a "1a." next to the underscored excerpt, which indicates that this is the first Science News quote ("a") pertaining to the first listed "surface phenomena" Swann impression ("1").

This collection of excerpts is reasonably, although not absolutely inclusive for this particular selection of scientific periodicals. Most importantly, the quotes are meant to depict an accurate picture of what we now know about the various characteristics of Mercury.

EXCERPTS FROM SWANN TRANSCRIPT

TECHNICAL REFERENCES

IMPRESSION CLASSIFICATION	IMPRESSION	DATA
Magnetic and Electromagnetic 1. An unanticipated magnetic field, characteristics, bow shock	1. Do you suppose Mercury has - what shall we call it? a magnetosphere. Like a circular sphere of magnetism, of magnetic belts around it, except with Mercury, they are not a sphere but on the sun-side of Mercury it is set closer to the planet's surface and on the far side of the planet it is sort of pushed out into space. That must be the strength of the solar winds that do that. In other words, on the night-side of the planet, the magnetosphere is pushed farther out into space, and on the sun-side of the planet it is pushed more close to the surface. It sort of trails behind the planet in the opposite direction it is moving. It might not be a magneticsphere, but a plasma of some sort. It feels hot. I'd say that the planet is characterized by sort of a low-keyed electric magnetic splendor.	1. Scientific American, Sept. 1975. a. p. 68: the unanticipated magnetic field That Mercury has a dipole magnetic field aligned with its spin axis, very similar to the earth's field although weaker, is to me particularly unexpected. Granted that Mercury probably has a large iron core, the rotation of the planet is nevertheless so slow at present that before Mariner 10's encounter with the planet no one thought that a Mercurian field might be generated by a fluid-dynamo mechanism of the type postulated for the earth (in which the field arises from electric currents associated with fluid motions in the core of the spinning earth). b. p. 64: magnetic field characteristics Science News, Vol. 105 a. p. 221: the unanticipated magnetic field b. p. 221: a bow shock wave c. p. 221: magnetic field characteristics Science News, Vol. 106 a. p. 196: the unanticipated magnetic field Science News, Vol. 107 a. p. 118: the unanticipated magnetic field b. p. 118: a bow shock wave c. p. 188: the unanticipated magnetic field d. p. 188: a magnetosphere In this third pass Mariner skimmed by only 323 kilometers from the newly intriguing world. The earth's much more powerful magnetic field, points out Ness, of the Goddard Space Flight Center, blocks the solar wind at a distance equal to about 15 times earth's radius. Mercury's little field, however, forms its solar wind shock wave less than half a Mercury radius out from the planet's surface; in other words, the planet itself occupies most of its magnetosphere, making a close flyby a necessity. e. p. 188: drawing of the magnetosphere. 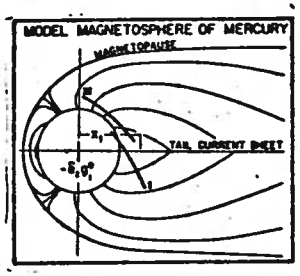

EXCERPTS FROM SWANN TRANSCRIPT

TECHNICAL REFERENCES

IMPRESSION CLASSIFICATION	IMPRESSION	DATA
Magnetic and Electromagnetic (cont)		
1. (continued)	1. (continued) same as previous page	1. Science, Vol. 185, July 12, 1974. a. p. 142: the unanticipated magnetic field b. p. 145: magnetosphere; plasma events Observations at Mercury Encounter by the Plasma Science Experiment on Mariner 10 Abstract. A fully developed bow shock and magnetosheath were observed near Mercury, providing unambiguous evidence for a strong interaction between Mercury and the solar wind. Inside the sheath there is a distinct region analogous to the magnetosphere or magnetotail of Earth, populated by electrons with lower density and higher temperature than the electrons observed in the solar wind or magnetosheath. At the time of encounter, conditions were such that a perpendicular shock was observed on the inbound leg and a parallel shock was observed on the outbound leg of the trajectory, and energetic plasma electron events were detected upstream from the outbound shock crossing. The interaction is most likely not atmospheric, but the data clearly indicate that the obstacle to solar wind flow is magnetic, either intrinsic or induced. The particle fluxes and energy spectra showed large variations while the spacecraft was inside the magnetosphere, and these variations could be either spatial or temporal. (See entire article.) c. p. 151: magnetic field; magnetosphere: "Magnetic Field Observations near Mercury: Preliminary Results from Mariner 10" (see entire article). d. p. 160: particles; magnetosphere: "Electrons and Protons in Mercury's Magnetic Field" (see entire article)
2. Auroras	2. I see rainbows that seem to leap up. They arch - they are more like auroras, I guess. I guess it would have to be an atmospheric type of situation with liquid molecules in it in combination with the fluctuating magnetosphere - it looks like oil on water in a way, that kind of color effects.	2. Science, Vol. 185, July 12, 1974. a. p. 159 If Mercury also has a weak atmosphere, then acceleration of particles in the neutral sheet might lead to precipitation of particles into the polar regions and to "auroral" events. Direct access of particles from the interplanetary medium to the polar region is always possible.

EXCERPTS FROM SWANN TRANSCRIPT

TECHNICAL REFERENCES

IMPRESSION CLASSIFICATION	IMPRESSION	DATA
Atmospheric		
1. Does Mercury possess one?	1. Everything seems very clear. Oh, I know why! There seems to be a thin atmosphere, but it is not enough to - it doesn't make a blue sky like on earth, so you can see blackness except where the sun is, maybe it is purple, I guess. There is not much haze.	1. Scientific American, Sept. 1975. a. p. 60 We now know that Mercury has no atmosphere whatever, and has not had one for billions of years. b. p. 64 c. p. 66 Science, Vol. 185, July 12, 1974 a. p. 166 Mercury's Atmosphere from Mariner 10: Preliminary Results. Abstract. Analysis of data obtained by the ultraviolet experiment on Mariner 10 indicates that Mercury is surrounded by a thin atmosphere consisting in part of helium. The partial pressure of helium at the terminator is about 5×10^{-12} millibar. The total surface pressure of the atmosphere is less than about 2×10^{-9} millibar. Upper limits are set for the abundance of various gases, including hydrogen, oxygen, carbon, argon, neon, and xenon. Science News, Vol. 105 a. p. 221 A major surprise was the discovery that the supposedly airless world has an atmosphere. b. p. 221
2. Clouds	2. I see some clouds - electrical storms now. These clouds come and go very fast, and they form sort of on the day side of the planet, on the two peripheries of the day side.	2. No reference.

EXCERPTS FROM SWANN TRANSCRIPT

TECHNICAL REFERENCES

IMPRESSION CLASSIFICATION	IMPRESSION	DATA
Surface Phenomena		
1. Lobate scarps	1. There are differences in land masses, in a way mountainous, but not too mountainous. Everything looks chewed down, I guess because of the land tides.	1. Scientific American, Sept. 1975. a. p. 63 Another important difference between the heavily cratered regions of Mercury and those of the moon is the ubiquitous presence on Mercury of shallowly scalloped cliffs running for hundreds of kilometers. The structure of these features, termed lobate scarps, suggests they resulted from an early period of crustal shortening on a global scale. Science News, Vol. 106 a. p. 196 Science, Vol. 185, Jul. 12, 1974. a. p. 176
2. Cracks and fissures	2. As the planet turns, the sun creates waves of earth tides, so that the surface has lots of cracks and fissures.	2. Science News, Vol. 105 a. p. 254 There are definite signs of lava flows suggesting volcanic activity, and long, not-too-twisted cliffs and fissures pointing to a planet with at least a somewhat active history. Science, Vol. 185, July 12, 1974. a. p. 174
3. Effect of water and atmosphere on surface topography	3. I see land masses, but they look waterwashed, as if the water just twirls around the planet all the time.	3. Scientific American, Sept. 1975 a. pp. 62-63 Another interesting property of Mercury is that in its equatorial region the subsurface temperatures are always above the freezing point of water and in the polar regions the subsurface temperatures are well below freezing. In contrast, liquid water of internal origin cannot reach the surface of the moon or Mars (except through volcanic activity because the subsurface temperatures are everywhere below freezing for a depth of many kilometers. In view of the large longitudinal variation in the influx of solar radiation and the potential for a latitudinal variation in chemical weathering conceivably associated with the occasional release of subsurface water, one might expect to perceive some characteristic effects on the surface at appropriate geographic locations on the planet. Actually we have been surprised to find no such effects either in radar maps made from the earth or in the photographs sent back by Mariner 10. Science News, Vol. 105 a. p. 254 There are no signs of substantial atmospheric erosion or of worldwide crustal shifts like the plate tectonics of earth.

EXCERPTS FROM SWANN TRANSCRIPT

TECHNICAL REFERENCES

IMPRESSION CLASSIFICATION	IMPRESSION	DATA
Surface (contd.)		
4. Tides	4. I get the impression of humidity - water. And tides huge tides; liquid tides, and also earth tides. As the planet turns, the sun creates waves of earth tides, so that the surface has lots of cracks and fissures. On the surface there is both a liquid - it seems heavier than water, but liquid, its water of some sort - and land tides, both water tides and land tides, and a fast condensation cycle.	4. Scientific American, Sept. 1975 a. p. 61 It is extremely improbable that Mercury exhibits spin-orbit coupling simply by coincidence. It is more likely that tidal interaction with the sun has removed angular momentum and slowed the planet sufficiently from a higher original rate of spin to trap into the present resonant period.
5. Copper	5. I get the impression that there is a lot of copper there.	5. No reference.

EXCERPTS FROM SWANN TRANSCRIPT

TECHNICAL REFERENCES

IMPRESSION CLASSIFICATION	IMPRESSION	DATA
Gravity		
1. Gravity anomalies	1. (a) The gravity must be uneven, pulling more towards the sun at all times. (b) It must have different gravities, depending upon which side you are on.	1. Emphasis on impression (b). Science, Vol. 185, July 12, 1974. a. p. 176 Plains-filled basins conceivably may be the sites of gravity anomalies similar to the lunar mascons. O'Leary (17) has speculated that a nonuniform distribution of regional gravity anomalies might provide the gravitational inhomogeneity required to keep Mercury in its 3/2 spin resonant period. The location of the large Caloris Basin near the mercurian equatorial region, which is preferentially pointed toward the sun at perihelion, is suggestive in this regard. However, detailed measurements of the nonspherical portion of Mercury's gravity field (probably with an orbiting spacecraft will be required to verify if Caloris or other circular basins on Mercury actually exhibit mascon-like gravity anomalies.

EXCERPTS FROM SWANN TRANSCRIPT

TECHNICAL REFERENCES

IMPRESSION CLASSIFICATION	IMPRESSION	DATA
Biological		
1. Lichens	1. Those must be lichens, sort of a water life which attaches itself to the rocks, and goes through its life cycle that way.	1. No reference.

MERCURY PROBE 11 MARCH 1974
SWANN RESPONSE

With Jupiter, I sort of just arrived at Jupiter - but this time I sort of went somewhat outside Earth's pull. I guess I have to go in the direction of the Sun, so I can see the Moon in back of me. There we go.

Do you suppose Mercury has - what shall we call it? - a magnetosphere. Like a circular sphere of of magnetism, of magnetic belts around it, except with Mercury, they are not a sphere but on the sun-side of Mercury it is set closer to the planet's surface and on the far side of the planet it is 1. sort of pushed out into space. That must be the strength of the solar winds that do that. In other words, on the night-side of the planet, the magnetosphere is pushed farther out into space, and on the sun-side of the planet it is pushed more close to the surface. It sort of trails behind the planet in the opposite direction it is moving.

1. It might not be a magneticsphere, but a plasma of some sort. It feels hot.

The sun seems larger, maybe about four times the size if viewed from earth.

1. Everything seems very clear. Oh, I know why! There seems to be a thin atmosphere, but it is not enough to - it doesn't make a blue sky like on earth, so you can see blackness except where the sun is, maybe it is purple, I guess. There is not much haze.

4. [I get the impression of humidity - water. And tides, huge tides; liquid tides, and also earth tides. As the planet turns, the sun creates waves of earth tides, so that the surface has lots of cracks and fissures.] 2

1a. The gravity must be uneven, pulling more towards the Sun at all times.

2. I see some clouds - electrical storms now. These clouds come and go very fast, and they form sort of on the day side of the planet, on the two peripheries of the day side. I see rainbows that seem to leap up. They arch - they are more like auroras, I guess. 2.

4 On the surface there is both a liquid - it seems heavier than water, but liquid, its water of some sort - and land tides, both water tides and land tides, and a fast condensation cycle, I guess that's what you would call it. This creates the leaping rainbows in all directions sometimes.

16. It must have different gravities, depending upon which side you are on. Its beautiful - god its beautiful. The refraction of the sun on those - I guess it would have to be an atmospheric type of situation with liquid molecules in it in combination with the fluctuating magnetosphere - 2 it looks like oil on water in a way, that kind of color effects.

5. I get the impression that there is a lot of copper there.

3. I see land masses, but they look waterwashed, as if the water just twirls around the planet all the time. Those must be lichens, sort of a water life which attaches itself to the rocks, and goes through its life 1. cycle that way.

It seems a lovely little planet. There are differences in land masses, 1. in a way mountainous, but not too mountainous. Everything looks chewed down, I guess because of the land tides.

1. I'd say that the planet is characterized by sort of a low-keyed electric magnetic splendor.

That's all. This time I had the impression of popping out, away from earth and pausing for a minute, looking back, seeing the moon. And then heading for the sun. There are actually two planets there, but I chose the one which seemed to the Sun, small, clear clouds that are not clouds, lovely magnetic fluxes, shifting, things like that.

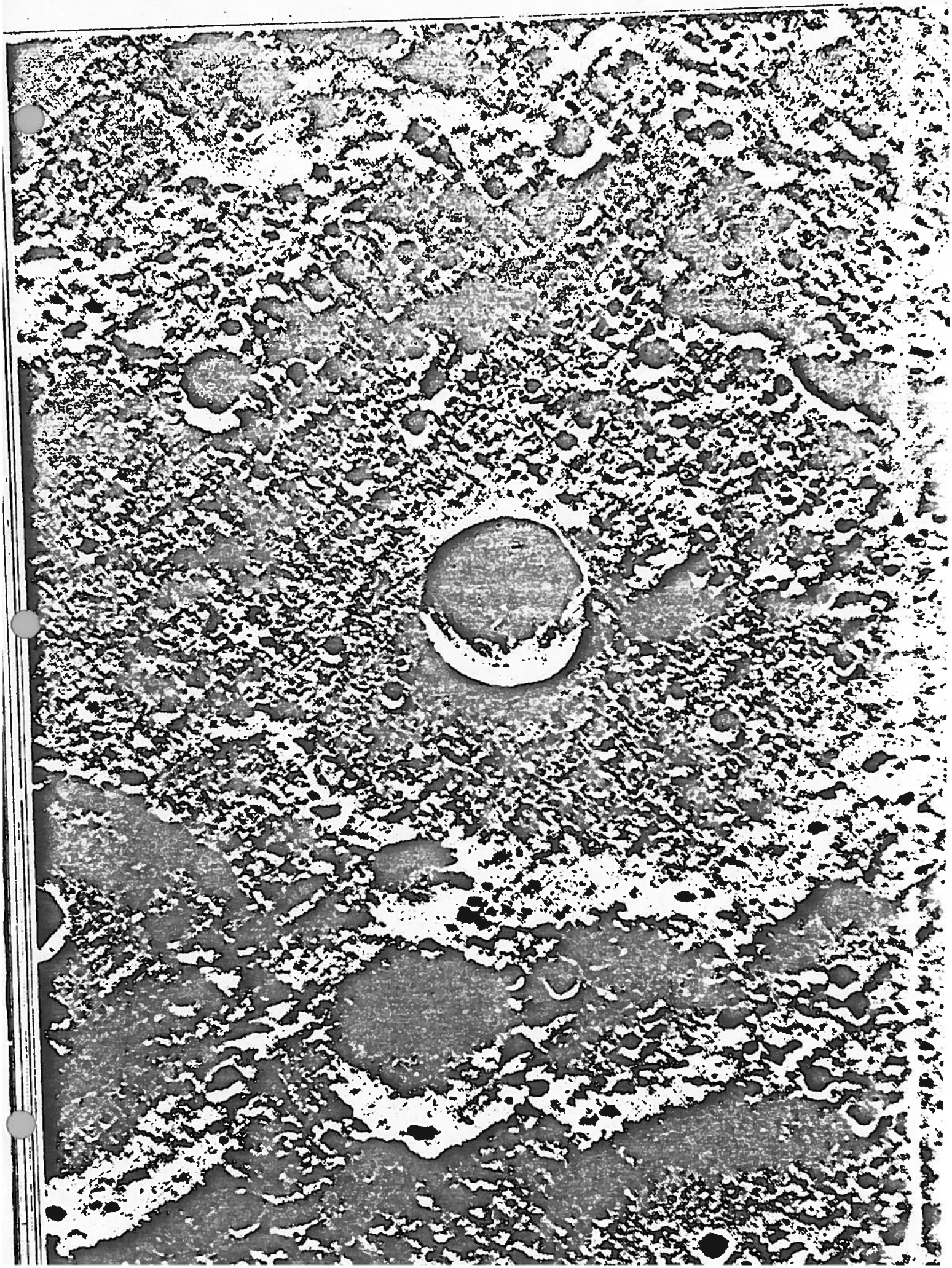

MERCURY

The remarkable pictures made by the spacecraft Mariner 10 have revealed a planetary paradox: Although Mercury is like the earth on the inside, it is like the moon on the outside

by Bruce C. Murray

There is a story that as Copernicus lay on his deathbed he lamented never having seen the planet Mercury. The story seems implausible because in northern Europe the planet is occasionally visible at twilight. Even if Copernicus could have viewed Mercury through a modern telescope, however, he would have been presented with a singularly unrewarding image. Only a few vague markings can be discerned through a telescope. They are so faint that optical astronomers were long misled into assigning the planet an incorrect rate of rotation.

Last year, 501 years after the founder of modern astronomy was born, the spacecraft *Mariner 10* passed within a few hundred kilometers of Mercury, providing both a 5,000-fold increase in photographic resolution of the planet's surface features and entirely new measurements of phenomena in the planet's immediate environment. Suddenly Mercury was plucked from obscurity and placed in an observational status comparable to that of the moon before the modern age of space exploration. Furthermore, *Mariner 10* is in an orbit that carries it back to the vicinity of Mercury every 176 days. As a result the spacecraft transmitted a second set of close-up photographs on September 21, 1974, 176 days after its first encounter with the planet, and an extremely valuable third set of observations, including a limited set of high-resolution pictures, on March 16 of this year, shortly before it exhausted its supply of gas for stabilizing its attitude in space.

Before *Mariner 10's* highly successful voyage it was recognized that Mercury is covered with at least a thin layer of finely divided dark silicate material very similar to that on the moon. Allowing for the difference in distance from the sun, Mercury closely mimics the moon in the way it reflects sunlight and radar pulses and in its emission of infrared radiation and radio waves. Yet it has been known on the basis of Mercury's size and mass that the planet is much denser than the moon or Mars and only slightly less dense than the earth. The earth's bulk density is greater than the laboratory density of its constituent materials, since much of the earth's substance is under high pressure in its interior. Hence the high bulk density of the much less massive Mercury implies that Mercury contains an even greater abundance than the earth of heavy elements, particularly iron.

Even the two most elementary facts about Mercury inferred from ground-based observations—the nature of its surface materials and its density—raised difficult questions. Could Mercury be composed of a homogeneous mixture of iron and silicate materials, as is the case with certain kinds of meteorites? Alternatively, could Mercury have a large earthlike iron core enclosed by a relatively thin silicate mantle and crust? If Mercury is chemically differentiated as the earth is, and the evidence now points in that direction, the diameter of its iron core is fully three-fourths the diameter of the planet, or the size of the moon!

Since Mercury is the innermost planet in the solar system, never more than 28 angular degrees from the sun in the sky, it is notoriously difficult to study by conventional astronomical techniques. We now appreciate how seriously these techniques can be compromised by contamination with sunlight. (Mars, in comparison, presents its largest image in the middle of the night, when the earth lies directly between it and the sun.) As recently as 1962 a leading expert in the visual and photographic observation of the planets wrote in what was then the most authoritative book on planetary astronomy that Mercury rotates at a rate such that one hemisphere constantly faces the sun, as one hemisphere of the moon constantly faces the earth. This synchronous rotation meant that Mercury supposedly turned on its axis once every 88 days, in step with the period of its revolution around the sun. Indeed, the planet was said to be synchronous with the sun to within one part in 10,000. In the same period spectroscopists working at two different wavelengths concluded that Mercury has a thin atmosphere. That conclusion received independent support from purported variations across the disk of the planet in the degree to which reflected [illegible]

CRATERED SURFACE OF MERCURY was photographed for the first time late in March of last year by cameras aboard *Mariner 10*. This high-resolution picture shows a typical heavily cratered region, strongly resembling the surface of the moon, on the equator of the planet. The pictures returned by *Mariner 10* made it possible to relate a previously agreed-on longitude system for Mercury to a specific topographical feature for the purposes of detailed mapping. In 1970 the International Astronomical Union had defined the origin of planetographic longitudes as the meridian crossing the subsolar point of the first perihelion passage of 1950. It has now been agreed that the 20-degree meridian of Mercury passes through the center of a particular small crater immediately adjacent to the large crater near the center of this picture. The small crater, which is 1.5 kilometers in diameter and lies .58 degree south of the equator, is at the foot of the outer rim of the large crater at a position equivalent to eight o'clock on a clock dial. It has been named Hun Kal, which stands for 20 in the language of the Maya, who used a base-20 number system. The photograph is reproduced with north at right in order to include as much of *Mariner 10* frame as possible.

was plane-polarized. We now know that Mercury has no atmosphere whatever, and has not had one for billions of years. And the planet does not revolve synchronously around the sun.

On the other hand, imaginative artists had commonly depicted the surface of Mercury as resembling the surface of the moon, and their intuition has proved to be correct. The *Mariner 10* photographs reveal that Mercury's surface is remarkably similar to the moon's, not only in its features but also in the sequence of events that was required to produce them. Mercury thus presents something of a planetary paradox: it is like the moon on the outside, yet like the earth on the inside, even to exhibiting an earthlike magnetic field.

In 1962, after centuries of unsatisfactory observations at visible wavelengths, radio waves from Mercury were detected. Radio astronomers from the University of Michigan observed the planet near elongation, when half of its disk, as it is seen from the earth, is in sunlight and half is in shadow. If Mercury were in synchronous rotation around the sun, the dark side would never receive any direct radiation from the sun and would be perpetually cold. Hence the thermal emission (including radio waves) from the dark side should be extremely low, well below the limit of detection. The Michigan workers were surprised to discover a substantial total radio flux evidently arising from both the dark and the sunlit halves of the planet, corresponding to an overall average near-surface temperature of 350 to 400 degrees Kelvin (170 to 260 degrees Fahrenheit). Such an average apparent temperature is exactly what any moonlike object would exhibit at the orbit of Mercury if it were rotating on its axis more rapidly than the once-a-revolution synchronous rate. Astronomers were so committed to the idea of synchronous rotation, however, that it was generally presumed that the anom-

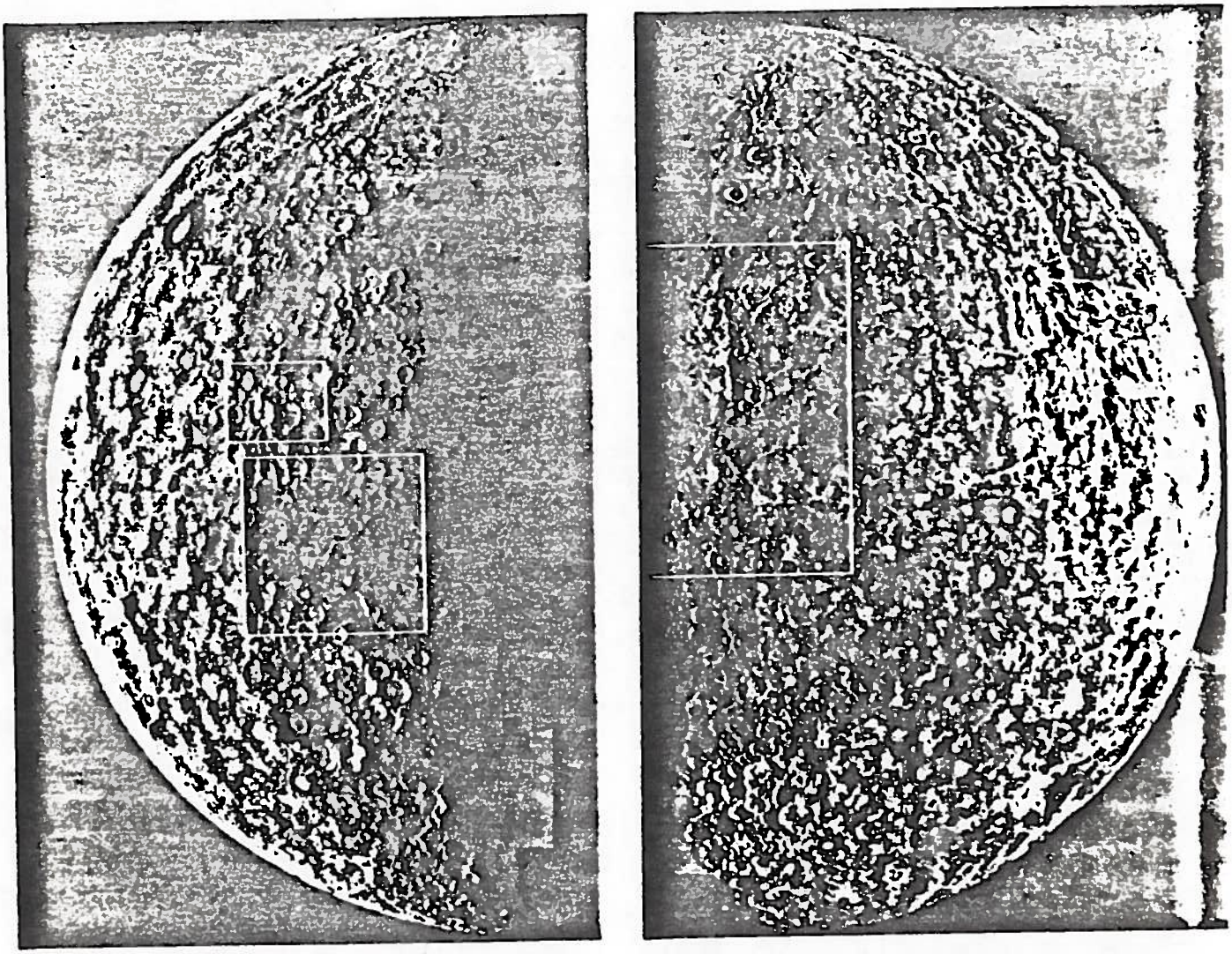

TWO HEMISPHERES OF MERCURY, each approximately half in shadow, were photographed during *Mariner 10*'s first encounter with the planet in March of last year. The mosaic of high-resolution pictures at the left shows the "incoming" hemisphere: the hemisphere visible as the spacecraft approached the planet, before sweeping behind its dark side. The evening terminator, the shadow line at the right, lies near 10 degrees west longitude. Since *Mariner* on the opposite page. The area within the lower rectangle appears enlarged on page 62. The mosaic at the right shows the "outgoing" hemisphere of Mercury, the hemisphere visible as *Mariner 10* "looked back" after passing behind the dark side of the planet. The spacecraft is now viewing Mercury from a point about 20 degrees north of the equator. The morning terminator, the shadow line at the left, lies near 190 degrees west longitude. The large impact structure named the Caloris Basin, comparable to the Imbrium Ba-

alous thermal emission from the dark half must indicate the presence of an atmosphere capable of transporting heat from the day side to the night side.

In 1965 Rolf B. Dyce and Gordon H. Pettengill carefully measured the differences in frequency among returning radar pulses beamed at the edges of Mercury from the Arecibo Observatory. They concluded that the planet did not rotate synchronously around the sun but instead had a rotation period of 59 ± 5 days in the direct sense (in the same sense as the earth's rotation). They did not, however, mention in the scientific publication of their results that this finding would explain the "anomalous" heat emission from the dark side of the planet. Even a year later a comprehensive review article was devoted to the putative atmosphere of Mercury and its presumed role in the transport of heat.

Why a 59-day rotation period? Giuseppe Colombo, an Italian dynamicist with a long interest in Mercury, quickly recognized that a period of 59 days stood in relation to the 88-day period of the Mercurian year about in the ratio 2 : 3. Colombo conjectured that Mercury's rotation period is, in fact, precisely 58.65 days, which means that the planet would rotate exactly three times while circling the sun twice, thereby exhibiting the phenomenon of spin-orbit coupling. The conjecture has been fully confirmed not only by further radar observations but also by the photographs from *Mariner 10*.

It is extremely improbable that Mercury exhibits spin-orbit coupling simply by coincidence. It is more likely that tidal interaction with the sun has removed angular momentum and slowed the planet sufficiently from a higher original rate of spin to trap it into the present resonant period. Such a theory was quickly developed by Peter Goldreich and Stanton J. Peale and by Colombo and Irwin I. Shapiro.

The success of the *Mariner 10* mission depended on a three-body interaction calling for an assist from Venus. The spacecraft initially followed a course that took it close to the intervening planet, where its trajectory was perturbed toward the orbit of Mercury. In this way an entirely different orbit around the sun was achieved, an orbit otherwise quite unobtainable with a launch vehicle of the Mariner class. The new orbit carried *Mariner 10*, nearly at perihelion (the point closest to the sun), to an encounter with Mercury when the planet, traveling in its own eccentric orbit, was nearly at aphelion (the point farthest from the sun). An initially unforeseen property of

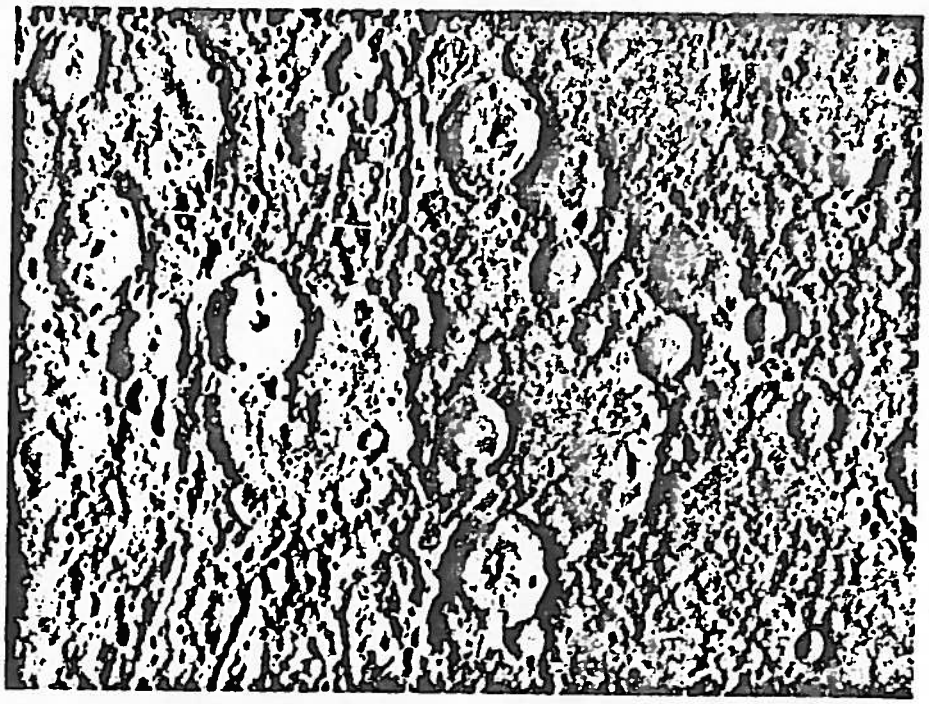

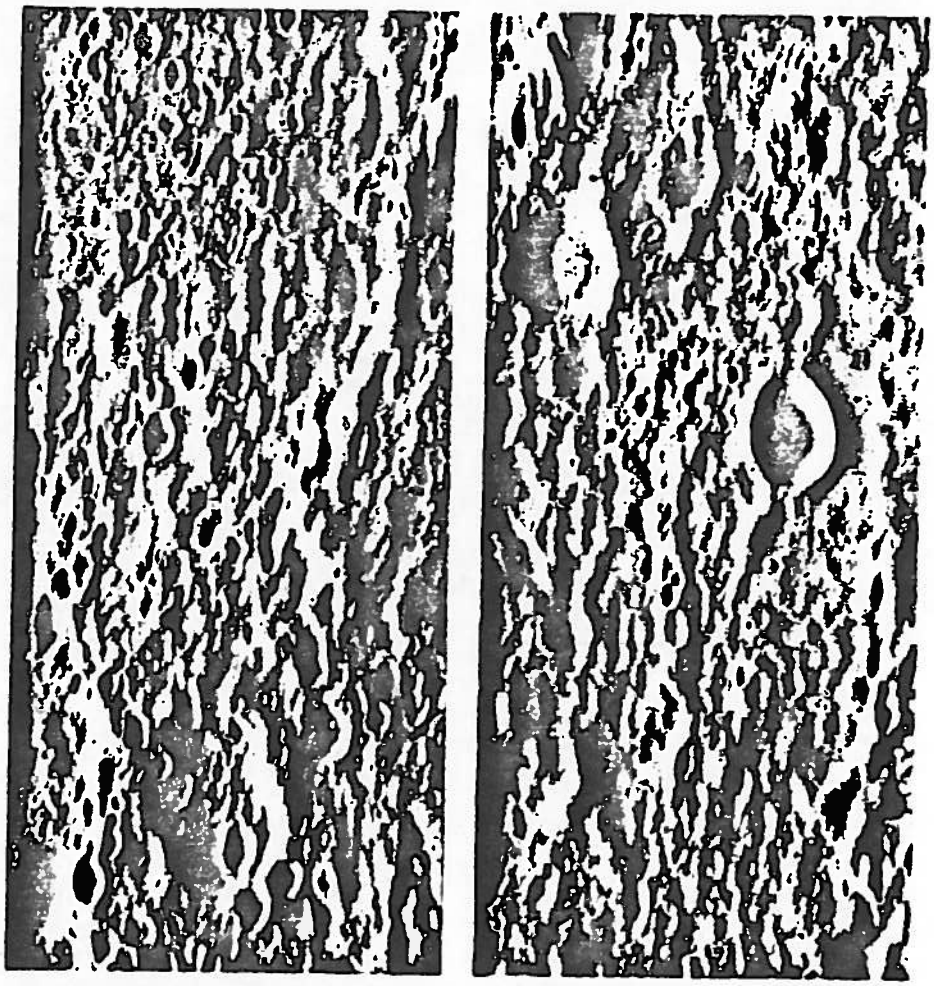

KUIPER CRATER, named for the late Gerard P. Kuiper, who helped to plan the *Mariner 10* photography of Mercury, is shown in the general view (*top*) taken during the first encounter. The white rectangles identify the location of two high-resolution frames (*bottom*) taken during *Mariner 10*'s third encounter with the planet on March 16 of this year. Kuiper Crater, roughly 40 kilometers in diameter, reflects sunlight more strongly than any other feature observed on Mercury. The picture at the top has been computer-enhanced to bring out small-scale features while suppressing most of the variations in reflectivity. The two high-resolution frames show streams of secondary craters produced by material ejected by the impact that created Kuiper Crater. Resolution in these two frames is about 250 meters.

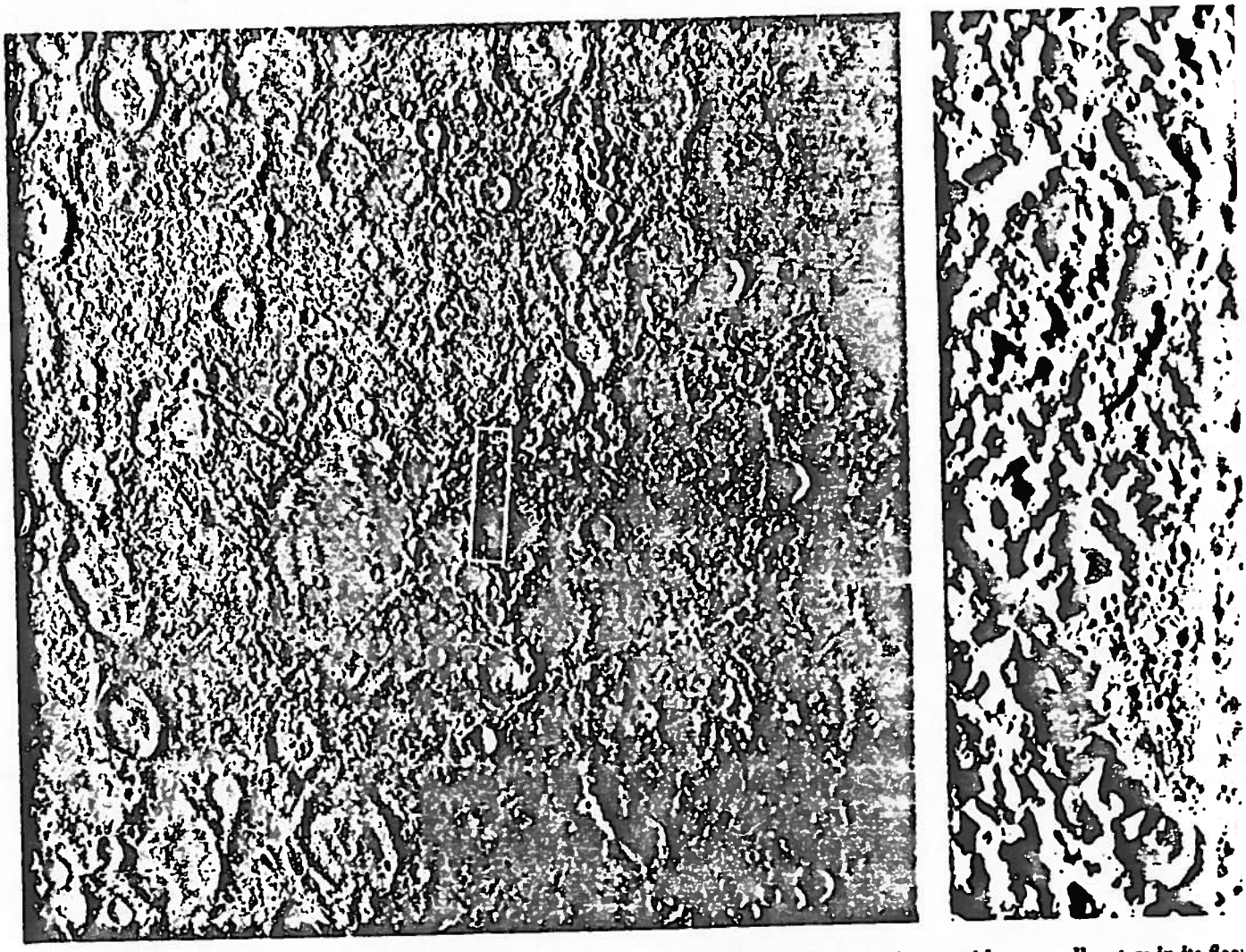

PECULIAR TERRAIN lies southeast of Kuiper Crater and antipodal to the Caloris Basin. The area shown in the picture at the left lies within the lower rectangle in the mosaic at the left on page 60. One hypothesis is that the hilly and lineated terrain shown here was created by the seismic effects of the great impact that created the Caloris Basin on the opposite side of the planet. The large crater near the center of the picture, with two small craters in its floo is about 170 kilometers in diameter. The area within the white re tangle is shown in the high-resolution picture at the right, whic was taken during *Mariner 10*'s third encounter with the plane The picture resolves surface features as small as 450 meters. Th half-visible large crater is approximately 55 kilometers in diamete

this exquisite celestial billiard shot is that *Mariner 10*'s new orbit has a period exactly twice that of Mercury's. As a result *Mariner 10* will continue to return every two Mercurian years to pass Mercury at exactly the same heliocentric longitude. Since Mercury itself spins precisely three times on its own axis in two Mercurian years, the spatial orientation and surface illumination of the planet at each encounter with *Mariner 10* will be exactly the same [*see top illustration on page 66*]. Thus Mercury, the sun and the spacecraft are dynamically in a state of triple resonance.

Mercury has the harshest surface environment of any planet in the solar system. When Mercury is at perihelion, it receives 10 times as much solar energy per unit of surface area as the moon. Noontime temperatures at the K., and in the dark hemisphere the surface cools radiatively to less than 100 degrees. Furthermore, "noontime" lasts a long time at Mercury's perihelion because of the coupling of the planet's rotation with the period of its eccentric orbit. An observer on Mercury at perihelion would see the sun slow to a complete halt in its motion across the sky and then move slightly in a retrograde direction (westward through the constellations) for eight days [*see bottom illustration on page 66*]. The reason is that the orbital angular velocity exceeds the spin angular velocity near perihelion. Moreover, the areas subjected to the longer period of solar radiation at perihelion are always near the same longitudes: 0 degrees and 180 degrees. The longitudes 90 degrees and 270 degrees receive their maximum solar irradiation at aphelion. As a result the 0-degree and a half times more solar radiation over than the meridians 90 degrees aw from them. Hence even though Mc cury's spin axis is probably perpendic lar to the plane of the planet's orbit, that there would be no seasonal var tions with latitude as there are on t earth and on Mars, the spin-orbit co pling of Mercury gives rise to a seaso variation in temperature with longitud

30. Another interesting property of M cury is that in its equatorial regi the subsurface temperatures are alw above the freezing point of water a in the polar regions the subsurface te peratures are well below freezing. contrast, liquid water of internal ori cannot reach the surface of the moor Mars (except through volcanic activ because the subsurface temperatures everywhere below freezing for a de of many kilometers. In view of the la

solar radiation and the potential for a latitudinal variation in chemical weathering conceivably associated with the occasional release of subsurface water, one might expect to perceive some characteristic effects on the surface at appropriate geographic locations on the planet. Actually we have been surprised to find no such effects either in radar maps made from the earth or in the photographs sent back by *Mariner 10*.

The illuminated surface observed by *Mariner 10* as it first approached Mercury is dominated by craters and basins, creating a landscape that could easily be mistaken for parts of the moon. There are, however, significant differences. The heavily cratered regions of Mercury exhibit conspicuous plains, or relatively smooth areas, between the craters and the basins, whereas the highlands of the moon generally show densely packed and overlapping craters. The intercrater plains appear in many cases to predate the formation of most of Mercury's large impact craters. The surface of Mercury is also unlike the surface of the moon in that it is not saturated with large craters having diameters between 20 and 50 kilometers.

One factor contributing to the difference in surface appearance between Mercury and the moon has been suggested by Donald E. Gault of the National Aeronautics and Space Administration. He points out that since on the surface of Mercury the force of gravity is twice that on the moon, material ejected from a primary impact crater on Mercury will cover an area only a sixth as large as the area covered on the moon for an impact crater of the same size. On Mercury secondary impact craters are much more closely clustered around primary craters than they are on the moon. As a result the topographic record of early events may be better preserved on Mercury than it is on the moon, where ejecta from the most recent impact basins has blanketed much of the earlier surface.

Another important difference between the heavily cratered regions of Mercury and those of the moon is the ubiquitous presence on Mercury of shallowly scalloped cliffs running for hundreds of kilometers. The structure of these features, termed lobate scarps, suggests they resulted from an early period of crustal shortening on a global scale. Such features are not conspicuous on the moon or on Mars. On the contrary, on those two lower-density bodies one sees tectonic evidence of crustal stretching. Robert G. Strom of the University of

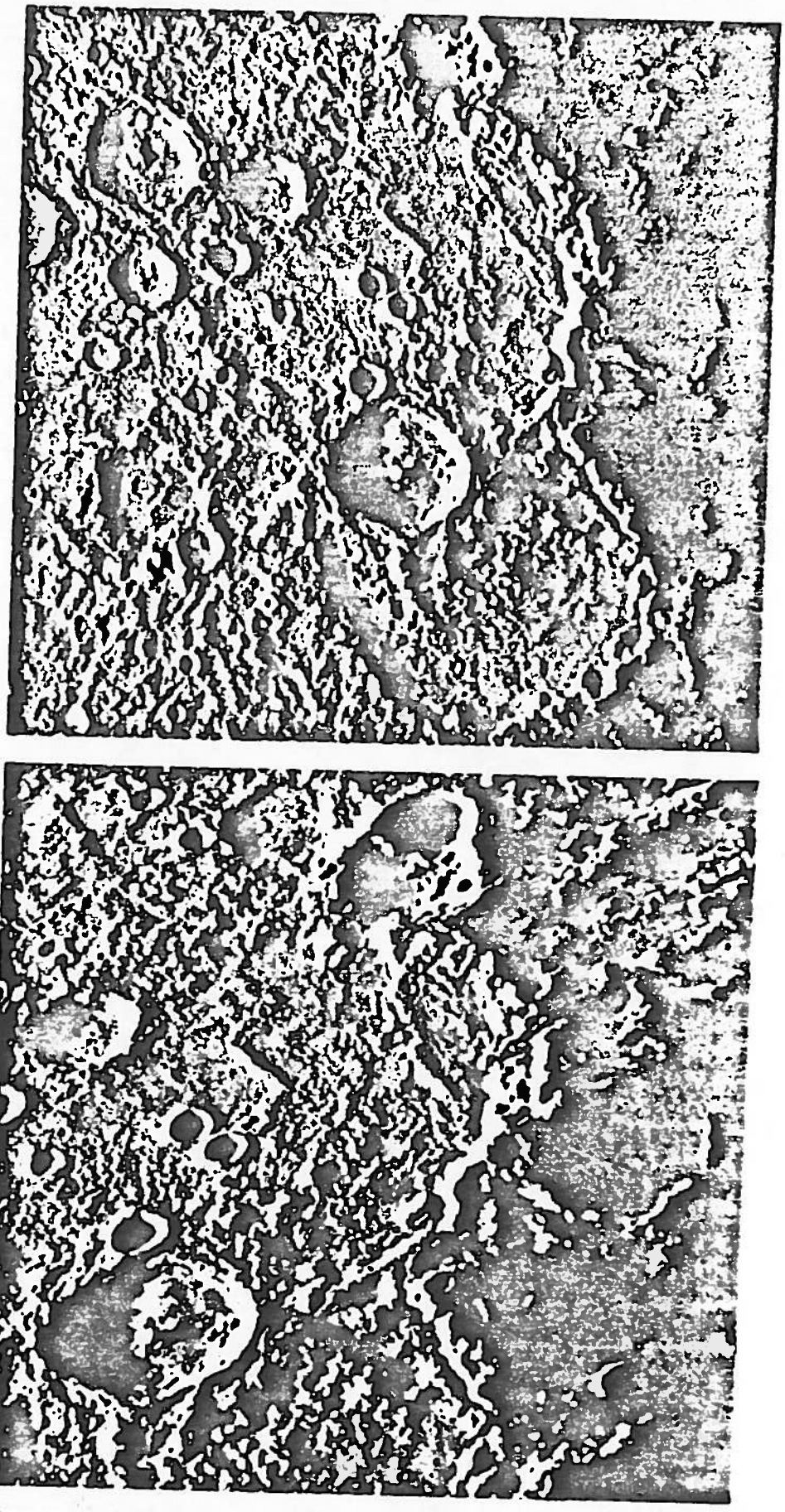

VIEWS TAKEN 176 DAYS APART by *Mariner 10* on its first encounter (*top*) and on its second encounter (*bottom*) show that the angle of solar illumination in each case is virtually identical, thereby supporting earlier evidence that Mercury rotates on its axis exactly three times while going around the sun twice. The planet's orbital period is 88 days and its rotation period is 58.65 days. Bottom picture shows a smaller area and is more distorted than top picture because it was taken closer to the planet and at a more oblique angle.

Arizona and others have speculated that the lobate scarps of Mercury are the result of a long period of crustal shortening produced by the slow cooling and contraction of Mercury's large iron core. In any case the very existence of large, well-preserved craters on Mercury, which are probably three or four billion years old, is evidence that there has been no planetwide melting or earthlike migration of crustal plates since that time. Furthermore, the evident lack of surface erosion rules out any tangible atmosphere for Mercury as far back as the time when the craters were made. In contrast the surface of Mars illustrates clearly how even a tenuous atmosphere quickly blankets and modifies the appearance of large craters, notably removing the initially conspicuous bright "rays" of ejecta that radiate from them.

While the television cameras of *Mariner 10* were revealing the ancient cratered terrain of Mercury, the magnetometer, the plasma probe and the charged-particle detector aboard the spacecraft were recording an interaction with the "wind" of charged particles from the sun that was much stronger than had been anticipated. The track of *Mariner 10* had been calculated so that the spacecraft would pass the dark side of the planet on its initial encounter; in that way the instruments would be able to investigate the wake left by Mercury in the solar wind [*see bottom illustration on page 67*]. A close passage in the wake of a planet provides the least ambiguous observational path for a flyby, particularly to test for the presence of anything resembling an earthlike magnetic field.

On the first flyby, when *Mariner 10* passed about 700 kilometers above the surface of Mercury, the appropriate instruments detected a weak magnetic field and a generally earthlike interaction with the solar wind. In order to get more definitive observations the spacecraft was targeted to make its third pass still closer to the surface (327 kilometers) on a track that carried it closer to the north pole. The third flyby confirmed the strength and orientation of the magnetic field that had been predicted by Norman F. Ness of NASA on the basis of the first flyby. Mercury evidently has a dipole magnetic field approximately aligned with the planet's spin axis. The strength of the field ranges from 350 to 700 gammas at the surface, or about 1 percent of the strength of the earth's surface magnetic field. Mercury's field is far stronger than the field found at either Venus or Mars, and a planetwide internal mechanism seems to be required for its generation. In addition Mercury is surrounded by a very thin envelope of helium gas, suggesting that the planet's magnetic field entraps helium nuclei from the solar wind and possibly from surface emanations as well.

The existence of a seemingly earthlike magnetic field on Mercury certainly provides independent evidence for a chemically differentiated planet with an iron core. Pictures acquired on the second

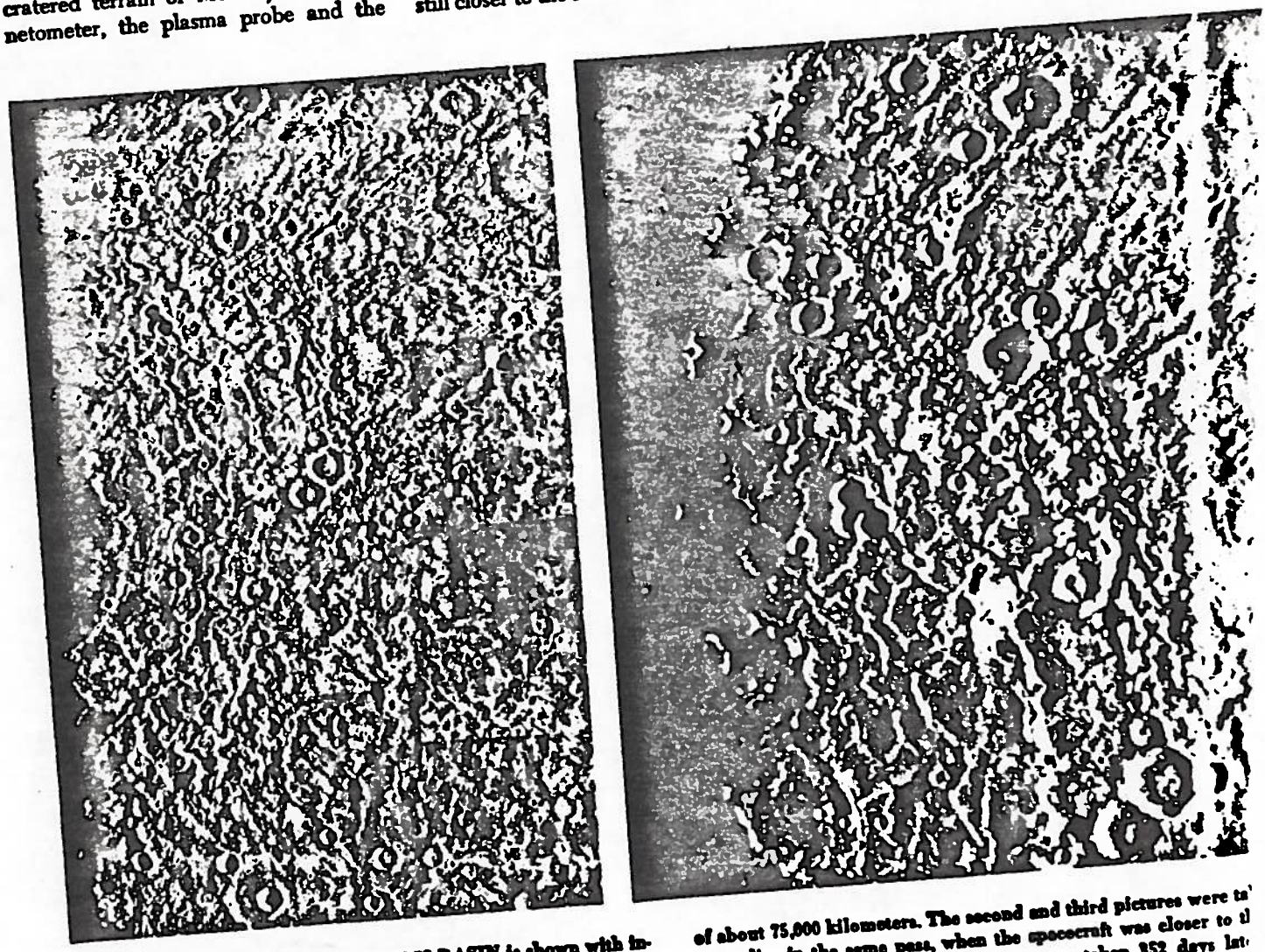

CRINKLED FLOOR OF THE CALORIS BASIN is shown with in- … sequence of five pictures across these two … of about 75,000 kilometers. The second and third pictures were ta… en earlier in the same pass, when the spacecraft was closer to t… planet. The fourth and fifth pictures were taken 352 days lat… … third close approach to Mercury af…

flyby, last September, showed that the lobate scarps seen in the first series of pictures continue across the south-polar region. Pictures from the first and second passes also show that small, steep-walled craters near the two poles have areas that are permanently shaded from the sun and thus constitute enduring "cold traps" for whatever volatile substances may have been released intermittently over Mercury's history. Those sites might be an exciting objective for close inspection in the 21st century.

The "outgoing" hemisphere of the planet photographed by *Mariner 10* as it "looked back" after its close approach exhibits a configuration of surface features totally different from those presented by the "incoming" hemisphere [*see illustration on page 60*]. The outgoing hemisphere shows large areas of relatively smooth plains that are clearly younger than most of the heavily cratered terrain visible in the incoming hemisphere. In addition there is a 1,400-kilometer basin left from a gigantic impact comparable to the one that gave rise to the Imbrium Basin on the moon. This prominent Mercurian feature, named the Caloris Basin because of its equatorial location near the "hot" 180-degree longitude of Mercury, is, like the Imbrium Basin, entirely filled with smooth plains material.

Other plains, less cratered and deformed, extend eastward and northward for thousands of kilometers. The *Mariner 10* television team has concluded that the temporal sequence of these plains, their variation in reflectivity and color, their size relations and their geographic association all point to a widespread episode of volcanism that followed the end of the period of heavy bombardment. The resolution provided by the pictures does not, however, reveal the surface morphology clearly enough to unambiguously identify the origin of the plains.

The situation is reminiscent of the debate about the origin of the smooth plains on the moon before the Apollo missions. It appears that some of the lunar plains were created by gigantic impacts rather than by volcanism. Hence the possibility remains that the material covering the Mercurian plains consists of massive sheets of ejecta from huge impacts, conceivably located on the hemisphere of Mercury that was in shadow during the three *Mariner 10* encounters. Whatever the origin of the plains, the fact that they have not been crumpled by internal activity and have not been modified by atmospheric erosion or deposition testifies to the remarkable quiescence of Mercury since the plains were made. Indeed, the overall similarity in the sequence of events that shaped the surface of Mercury and the moon is extraordinary and, to me, surprising, considering how very different the internal constitution of the two bodies must be.

A preliminary surface history of Mercury can be divided into five major sequences of events, each generally similar to those that shaped the moon. First,

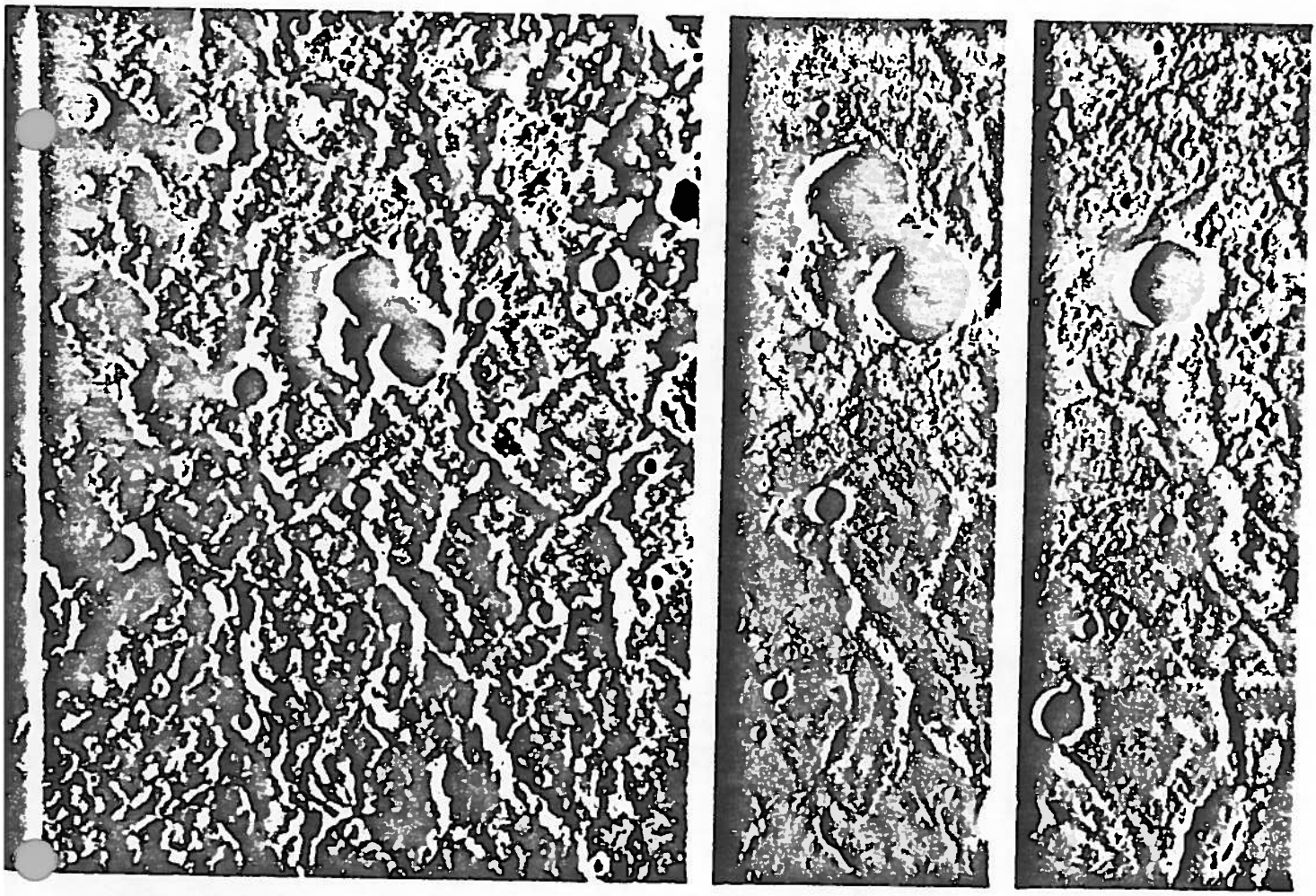

completing two trips around the sun on its own 176-day orbit. The fractures that are visible in the floor of the Caloris Basin vary in width from about eight kilometers down to about 450 meters, the limit of photographic resolution. The largest crater in the fifth picture, which was taken at a distance of 20,000 kilometers above the surface of the planet, is about 12.5 kilometers in diameter. Each of the two young craters in the prominent cluster of three craters that is seen in the other pictures is about 35 kilometers in diameter.

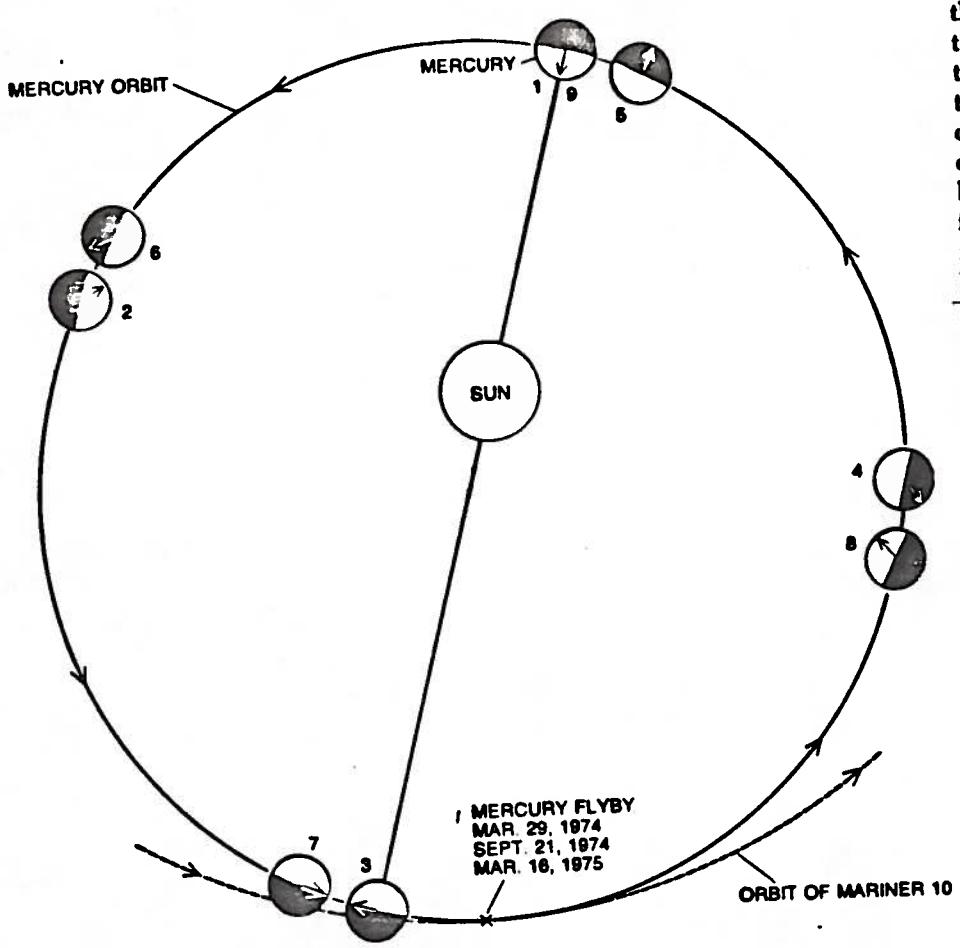

PHENOMENON OF SPIN-ORBIT COUPLING is what has locked Mercury's rotation period and orbital period in the ratio of two to three. In this diagram of Mercury's orbit the fixed arrow points toward one of the planet's two hot subsolar points, that is, the points on the equator that lie directly under the sun at alternate perihelions. The numbers give the sequential position of the planet in its orbit during two of its revolutions around the sun. *Mariner 10*'s encounters with Mercury take place at the point that is marked with an X.

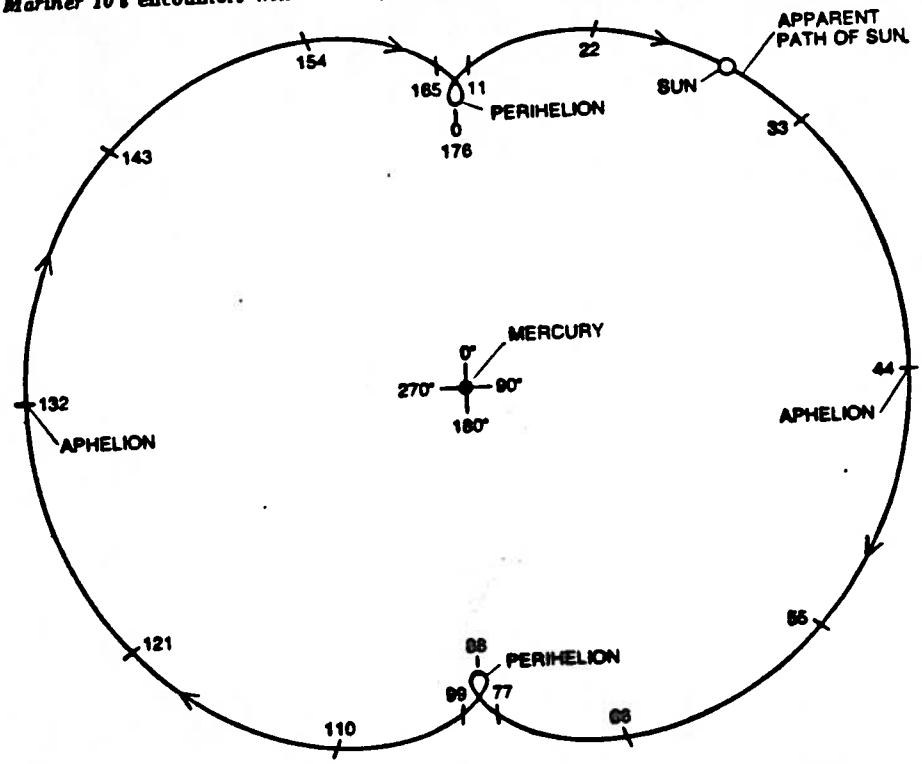

ORBIT AS SEEN FROM MERCURY appears to execute a loop at perihelion. Apparent position of the planet is marked off in 11-day inter-

the absence of recognizable volcanic, tectonic or atmospheric modification of the large old craters on Mercury implies that the mass of the planet was chemically fractionated into a large iron core enclosed by a thin silicate mantle well before any of the oldest craters were formed. Any atmosphere on Mercury must have escaped quite early or was never formed. The heat required for the chemical separation of iron and silicate phases on a global scale must also have dissipated early enough for the outer layers to become sufficiently rigid to maintain the topographic relief of the large old impact craters up to the present time.

In the second major epoch, following the initial period of accumulation and chemical segregation, Mercury must have gone through at least one period of crater obliteration, possibly through early volcanism, if we are to account for the absence of topographic scars of the accretion process. The smoothed surface, surviving in the plains between craters, records not only the terminal phase of heavy bombardment but also the global shrinking of the crust represented by the lobate scarps.

The third and most sharply delineated of the five major subdivisions of Mercury's surface history came toward the end of the heavy bombardment with the large Caloris Basin impact, seemingly the counterpart of the lunar impact that created the Imbrium Basin. The Mercurian collision gave rise both to the Caloris Basin and to the mountainous terrain surrounding it and extended areas of ejecta and sculpturing of the older surface. In addition, approximately antipodal to the Caloris Basin there is a peculiar lineated and hilly terrain, which Gault and Peter Schultz speculate may have been thrown up by the focusing of seismic energy from the Caloris Basin impact on the opposite side of the planet.

During the fourth phase, some time after the Caloris Basin impact, broad plains were created, probably as a result of widespread volcanism similar to the activity that gave rise to the lunar maria, or "seas." Bruce W. Hapke of the University of Pittsburgh argues that the colormetric and photometric evidence from *Mariner 10*, combined with previous telescopic results, suggest that the surface rocks on Mercury may be somewhat less rich in iron and certainly less rich in titanium than the rocks found on the maria of the moon, thus explaining the absence on Mercury of the sharp contrast in brightness levels between the

During the fifth phase of the surface history of Mercury, extending to the present time, little has happened other than a light peppering of impacts, many of which show conspicuous rays. The distribution of impact craters on the Mercurian plains is remarkably similar to the distribution both on the maria of the moon and on some of the oldest smooth plains of Mars. The similarity of impact-cratering rates on Mercury, the moon and Mars over the past three billion years or so came as a surprise to many, considering the great differences in the three bodies' distance from the sun and therefore the differences in the probability of their encountering interplanetary debris from the asteroid belt (which has long been thought to be the principal source of the impacting objects).

Thus *Mariner 10* has clearly established that the exterior of Mercury resembles the moon not just in topography but more surprisingly in surface history. And yet the interior constitution of Mercury appears to be more earthlike than that of any of the other planets. The paradoxical circumstance of Mercury's moonlike exterior and earthlike interior raises important questions not only about Mercury but also about the history and nature of the entire inner part of the solar system. Were the bombarding objects whose impacts are recorded on the surface of Mercury from the same family of objects that bombarded the moon as recently as four billion years ago? Or did each of the inner planets, including the moon, pass through separate periods of late bombardment that overlapped only slightly, if they overlapped at all, and in each case ceased abruptly and independently?

The *Mariner 10* pictures suggest to me and to Newell J. Trask, Jr., of the U.S. Geological Survey that the last great bombardment of Mercury, culminating with the Caloris Basin impact, may not have been part of a steadily decreasing flux of interplanetary debris but could have resulted from a discrete terminal episode of bombardment. George W. Wetherill of the University of California at Los Angeles considers it plausible that the bombarding objects involved in such an early discrete episode could have originated with a single object perturbed to pass near the earth or Venus from an initial orbit beyond Jupiter. Tidal disruptions on the earth or Venus might then conceivably have created a shower of bombarding objects

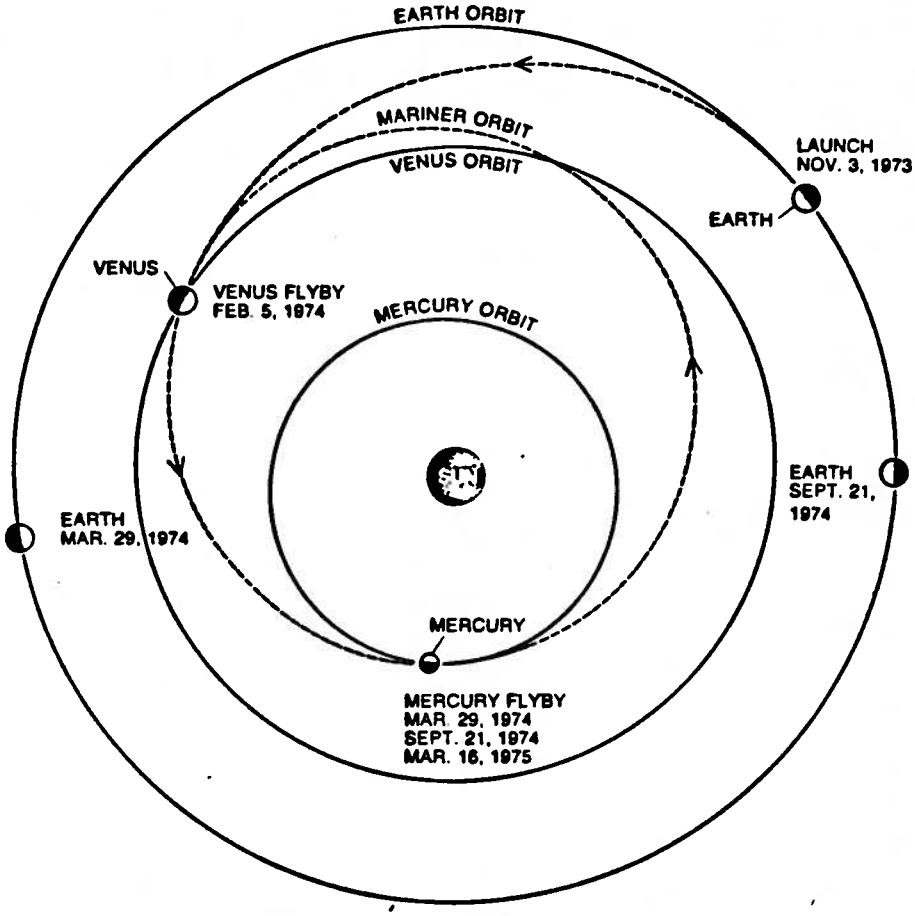

TRAJECTORY OF MARINER 10 was chosen so that the spacecraft was deflected toward Mercury by a precisely timed encounter with Venus three months after leaving the earth. It is as a result of this deflection that the orbit of *Mariner 10* takes it to the vicinity of Mercury every 176 days, or once every two Mercurian years. It was this happy choice of orbital characteristics that enabled *Mariner 10* to achieve three operational encounters with its target.

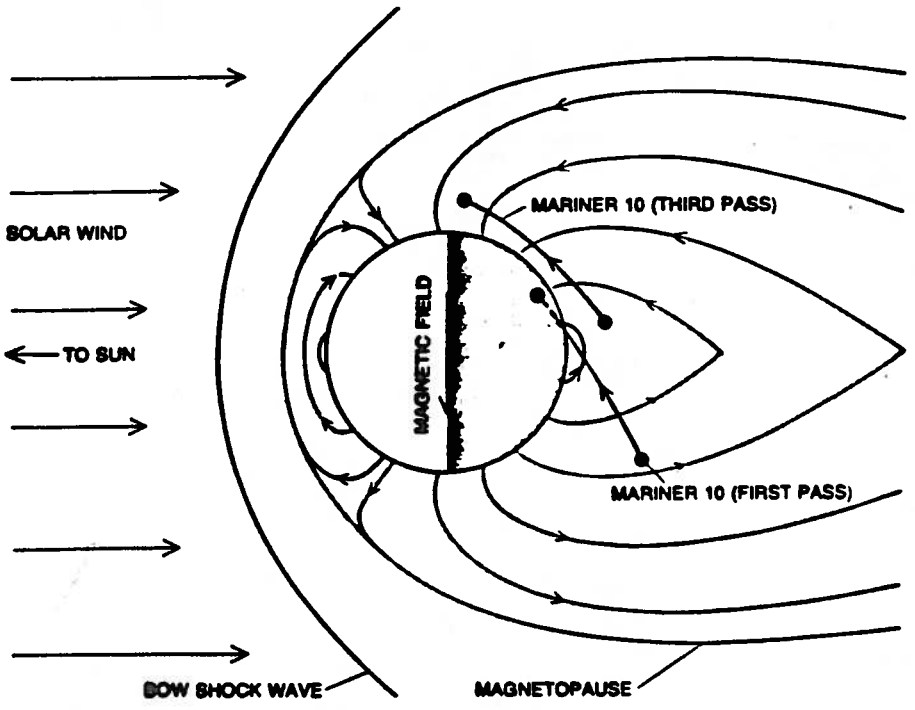

MAGNETIC FIELD OF MERCURY, detected in *Mariner 10*'s first encounter, was fully confirmed in the third encounter, when the spacecraft was targeted to pass closer to the north pole of the planet. The black dots indicate in planar projection when *Mariner 10* entered and

planets. Such a concept would be consistent with recent controversial proposals that the moon was subjected to a similar terminal episodic bombardment about four billion years ago.

On the other hand, if the observed topography was created by a continuously declining bombardment of Mercury, the evidence may have been abruptly and effectively erased by an episode of enhanced crater obliteration. Hence the appearance of an episodic bombardment of the planet may be an illusion. The debate now developing over the early history of the inner solar system is reminiscent of an earlier debate between uniformitarians and catastrophists over the causes of the earth's geological features. There the uniformitarians won.

That Mercury has a dipole magnetic field aligned with its spin axis, very similar to the earth's field although weaker, is to me particularly unexpected. Granted that Mercury probably has a large iron core, the rotation of the planet is nevertheless so slow at present that before *Mariner 10*'s encounter with the planet no one thought that a Mercurian field might be generated by a fluid-dynamo mechanism of the type postulated for the earth (in which the field arises from electric currents associated with fluid motions in the core of the spinning earth). And what about Venus, which presumably has a larger and hotter core than Mercury's and yet does not exhibit a significant planetary magnetic field? Furthermore, if there are fluid motions within the Mercurian core capable of generating the observed magnetic field, the core motions or the associated heat flow have not led to any recognizable deformations of the planet's surface layers.

A quite different explanation for the planet's field is that it is a fossil field of some kind that has persisted from a remote epoch. It seems unlikely, however, that in the billions of years since the hypothetical fossil field was created the temperature within the appropriate portion of Mercury's interior never rose above the Curie point (the temperature at which a substance loses its magnetism). Still a third possibility is that the field has somehow been induced as a result of Mercury's continued interaction with the solar wind. Preliminary examination of this concept suggests that such a field would not exhibit symmetry around the rotation axis.

Perhaps the Mercurian magnetic field arises from causes still unimagined. Or perhaps we shall have to gain a deeper understanding of the mechanism of the earth's own field in order to explain how that mechanism could be reduced to the Mercurian scale. Whatever the outcome, it is fortunate that there is another magnetic field among the inner planets with which to compare and contrast the field of the earth. Further study of Mercury's field, as well as photographic mapping of the still unobserved hemisphere of the planet, would be a major objective of any orbiting satellite of Mercury.

Mariner 10's mission to Mercury has completed the reconnaissance of the inner solar system and has further demonstrated that planetary exploration is full of surprises. The findings of *Mariner 10*, combined with the testimony of the lunar samples brought back by the Apollo astronauts, have made possible an enormous extension of knowledge and inference about Mercury. Out of the new observations is emerging a richer and more unified picture of the origin and evolution of all the planets, including our own.

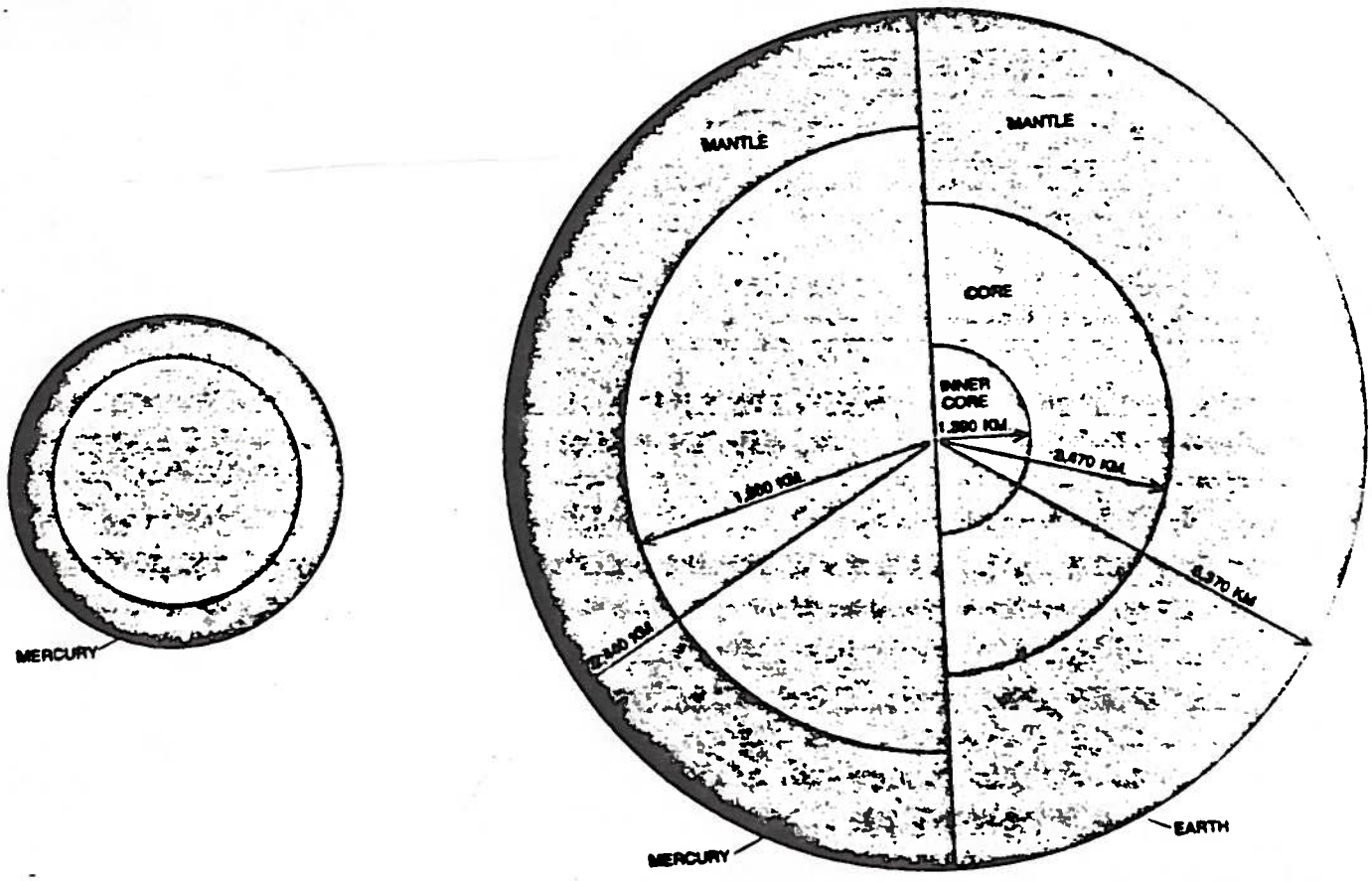

CUTAWAY VIEWS OF MERCURY AND THE EARTH, which are scaled to have the same outside diameter, show how much larg- iron core is thought to be compared with earth's core. relation to the earth is shown by the small disk at the left. Mercury's iron core evidently contains 80 percent of the planet's mass. Therefore the iron core must have a radius of at least 1,800 kilometers, which would make core alone slightly larger than the earth's moon.

Science News: Vol. 105

The Strange and Cratered World of Mercury

Craters, hills and valleys: A moonlike surface on a not-so-moonlike planet. Width of areas shown is about 100 miles.

Until last week, the majority of planetologists felt, with good reason, that Mercury was a pretty nothing planet. No atmosphere (the solar wind would blow it away), no magnetic field (the planet's slow rotation would not create the dynamo effect necessary to sustain one), no ionosphere (no magnetic field to trap the ionized particles), no moons. All in all a dull world.

Now it is "strange," "startling," "spooky," and "fascinating," all thanks to a few days of observations by Mariner 10.

The first spacecraft ever to fly by Mercury has taken close-up photos that reveal a heavily cratered surface and transmitted reams of surprising data that invalidates many of the theories about the sun's nearest and smallest planet.

"The thing that surprised me most," says Bruce Murray of the California Institute of Technology, leader of the huge team analyzing Mariner's photos of Mercury, "is that it looks just like the moon." Yet the planet is too dense to be like the moon through and through, one of the few earth-based estimates that Mariner confirmed. The spacecraft precisely pinned down the ratio of the sun's mass to that of Mercury as 6,023,600 to 1 (recent earth-based calculations have contained uncertainties as great as 50,000 to 1).

Mercury's "bright spot" turned out to be this crater within a crater. Astronomers propose naming it for the late planetologist Gerard P. Kuiper.

"If it were really like the moon in terms of the mare flows and the whole business that goes with that," says Murray, "that's a chemical statement . . . that is very inconsistent with the bulk density of Mercury." But in fact Mercury seems to embody just such an inconsistency: a lightweight, moon-like surface enclosing a heavy, earth-style center. Says Murray, "It could easily have a large iron core."

Finding out just how much of the planet is core will take weeks or months of computer analysis of the subtlest changes in the spacecraft's path. The resemblances to earth's moon, on the other hand, are readily apparent. The entire surface is pocked with crater upon crater, like the bleak highlands of the moon. Some are young enough —perhaps tens of millions of years— that dust or the darkening effects of the solar wind have not had a chance to hide the light-colored rays left by material blasted outward during the craters' formation. But the exciting ones are the old craters. Murray believes they may be relics of the planet's

origin, well over 4 billion years ago, since there are traces of no planetwide events since then that could have covered them up. There are a few piled up cliffs, or scarps, but none of the vast fissures or mountain ranges that characterize the past of the moon.

Yet there is more to the lunar resemblance, including vast smooth areas like the maria and level-floored craters filled in by some still-not-identified process. This fine material, in fact, may be Mercury's most moonlike part, blanketing the planet in a remarkably even layer perhaps a few centimeters deep with "almost no exposed rocks." So says David Morrison of the University of Hawaii, whose readings of infrared emissions suggest a surface layer with moonishly low thermal conductivity, the same high porosity and other similar features. An astronaut walking on Mercury, he says, would leave footprints very much like those on the moon.

One of the jobs of Morrison's experiment was to measure the planet's widely ranging surface temperatures. Daytime readings, measurable from earth, get as high as 800 degrees F., depending on Mercury's distance from the sun. A Mercurian night, however, is 88 days long, giving the surface plenty of time to cool off. As Mariner 10 crossed the planet's terminator, or twilight zone, the temperature fell from about 370 degrees above zero to 200 degrees below zero in only a few hundred kilometers on the surface, then kept on dropping to about 280 below. This gives Mercury a temperature range of more than 1,000 degrees F., by far, says Morrison, the widest in the solar system.

A major surprise was the discovery that the supposedly airless world has an atmosphere. Harvard astronomer Edward Reeves has privately reported signs of one in data from Skylab, recorded when Mercury passed in front of the sun, but the idea seemed so unlikely that he is said to have been discouraged from publishing his findings. The atmosphere is extremely thin, less than one hundred-billionth as dense as earth's, says Michael B. McElroy, also of Harvard, but is indisputably there. The major element is helium, measured out to as far as about 300 miles from the planet, possibly delivered by the solar wind. Another source may be the decay of radioactive materials within the planet. This, according to McElroy, could mean that Mercury has as much uranium and thorium in its crust as does earth.

Other gases include argon, another decay product, neon from the solar wind, and possibly xenon. Conspicuously absent, except for a possible trace near the surface, was hydrogen, which was earlier reported as "extensive" by Soviet astronomer Nikolai Kozyrev.

The most significant discovery about the atmosphere, says A. Lyle Broadfoot of Kitt Peak National Observatory, was the existence of a helium "tail," streaming out from Mercury in a direction away from the sun. It was significant because shaping the tail was another unexpected Mercury feature, a magnetic field.

Norman Ness of NASA's Goddard Space Flight Center was another who expected the planet to have, at least to his magnetometers, a lunar look. It didn't. "It has turned out that Mercury is not at all like the moon." About 20 minutes before the spacecraft reached its closest distance to Mercury (about 466 miles), there were very clear signs of a bow shock, a shock front formed by the solar wind ricocheting off the planet's enveloping magnetic field, of which the moon has little or none.

Mercury's magnetic field it seems, is not completely enveloping. It is so weak—as little as a thousandth as strong as earth's—that the minute push of the solar wind perhaps does not even let the field lines close on the side away from the sun. This would mean that trapped charged particles stream continuously off into space, and that the surprisingly abundant high-energy electrons reported by University of Chicago's John Simpson must be continuously replenished by some mysteriously potent source.

Another mystery is the source of the magnetic field, since the slow rotation of Mercury virtually eliminates the dynamo theory. "The sweeping of interplanetary field lines past the planet," suggests Ness, "may generate an electrical current flow in the planet, and/or a possible weak ionosphere, then generates the magnetic field observed."

The ionosphere, sought directly by H. Taylor Howard of Stanford, did not appear in the earliest analysis of Mariner's data. But the same analysis failed to detect the atmosphere, which is a million times too thin for it, so an extremely weak ionosphere has not been ruled out.

A burst of excitement was generated at the possibility of what would have been one of Mariner's major accomplishments: the discovery of a moon of Mercury. The signs, sudden brightening of the ultraviolet emissions recorded by Broadfoot's spectrometer, appeared repeatedly to the accompaniment of growing excitement. The culprit, however, after checks and counterchecks, seemed at last to have been a star, lined up against phenomenal odds to look in repeated observations as though it were a captured orbiting object.

With flawless—if occasionally misleading—data pouring in from the spacecraft, it came as a shock when engineers at the Jet Propulsion Laboratory in Pasadena discovered that the spacecraft was having some problems. About 30 hours after Mariner 10 passed its point of closest approach to Mercury, one of its two solar panels suddenly began drawing excess power, and the temperature in one equipment compartment shot up about 30 degrees. No data were lost, no experiment suffered, but the heat continued to rush upward, possibly from a short circuit. As the heat rose, optimism fell about the spacecraft's chances of surviving until September when it is scheduled to come around again for its second meeting with Mercury. □

NASA

Mariner view of Mercury's southwest quadrant four hours before closest approach.

equivalent to two eggs a day. The remaining group did not receive supplements.

The pigs were fed these diets with or without supplements for eight months, then were slaughtered. The levels of cholesterol in their blood and the amount of cholesterol in their aortas (the artery that takes blood from the heart and distributes it throughout the body) were measured. The degree of hardening of the arteries was also determined.

The pigs fed the margarine fat had the highest cholesterol levels and the greatest degree of hardening of the arteries. The aortas of seven out of twelve (58.3 percent) of the pigs fed the oil had bumps in their arteries (the first symptoms of hardening of the arteries); bumps for the rest of the pigs appeared in only 14 percent of them. The next group with the most hardening of the arteries were pigs fed the mixture of fat and sugar, but the figures dropped markedly. Only three out of twelve had aortas that showed hardening. No elevation in total blood levels of fat or cholesterol was noted in the pigs fed the basic diet or the basic diet supplemented with crystalline cholesterol, powdered egg yolk or powdered whole egg. Aorta damage was also less than for the other groups.

"No explanation," Kummerow admits, "is presently apparent for the observation that a significantly higher percentage of raised lesions was noted in the aorta from swine fed trans [altered] fat as compared to those fed saturated fats or a dietary source of cholesterol. That the addition of cholesterol to the diet of rabbits increases their plasma cholesterol level is well known. However, such an elevated effect has not been observed in swine. Therefore, swine seem closer than rabbits to human subjects in their response to a source of dietary cholesterol."

What these findings mean for the public, Kummerow says, is that margarine that contains trans-fatty acids is more likely to cause hardening of the arteries than are cholesterol-rich animal fats, such as butter, or cholesterol-rich foods, such as eggs. Some American margarines have been found to contain as much as 36 percent trans-fatty acids. Canadian and European margarines prepared from hydrogenated fish oil and rapeseed oil contain an even higher level of trans fats.

"We can't say which margarines are worse and which are better because the trans content is varied from time to time," he says. "However it is possible to provide trans-free margarine to American consumers. One large international firm is providing such a margarine to their customers in Europe; they should also do so for their customers in the United States." □

Blow up: Removing the people mover

Such a deal! For only $13.4 million I can get you the perfect people mover. It will have 3.2 miles of elevated guideway on which 90 fully computerized, 21-passenger capsules will efficiently whisk people to and from their destinations at the push of a button.

The Federal Urban Mass Transportation Administration (UMTA) bought this spiel in 1969 when enthusiasm ran high for alternate modes of mass transportation. It proceeded to spend $57 million on a prototype people mover.

Where was the money spent? In New York where construction of the Second Avenue subway could serve millions of people? No. The people mover was built in Morgantown, W. Va., on the campus of West Virginia University. This happens to be in the home district of Rep. Harley O. Staggers (D-W. Va.) who, as chairman of the House Commerce Committee, has a lot to say about the Department of Transportation's budget.

After five years of engineering delays, cost overruns, politicking and assorted red tape, all the Transportation Administration has to show for its money is 2.2 miles of track, five test vehicles and three, instead of six, stations. Now, the Government is thinking about blowing up the whole mess.

Why does anyone want to dynamite the people mover? Because it will cost at least another $50 million to complete the system that was supposed to be carrying passengers in 1972. Three weeks before the 1972 election, Mrs. Edward F. Cox, the President's daughter, dedicated the system with much fanfare as a shining example of the Administration's progress in mass transportation. Shortly thereafter, the Administration imposed a one-year moratorium on major work on the system.

UMTA has recently tried to divest itself of this white elephant. It tried to give it to the University of West Virginia but the university doesn't want it. As it stands, the people mover has too little track and too few stations and cars to be of any practical use on the campus. The portion that is completed probably will not work properly because of engineering short cuts and, even if it does, the university does not have the money to operate it.

Engineers are now trying to properly estimate the cost of destroying the people mover. □

Mercury: Revising the textbooks?

Just as Jupiter seems to provide back-looking planetologists with an atmosphere that reflects the earliest days of the solar system, Mercury may be offering them a surface that still shows traces of its formative years. If this is true, there is just a chance that Mercury may rewrite the textbooks on the way in which the planets were born.

From the reams of data collected by Mariner 10, two findings are the keys to what could be one of the most important discoveries since earth-spawned space probes began visiting other worlds. One is the observation that Mercury has an outer layer of lightweight, moonlike material, which, because of the planet's high overall density, argues for a heavy iron core (SN: 4/6/74, p. 220). The other is the possibility, suggested by Bruce Murray of the California Institute of Technology, that much of Mercury's original surface is still showing.

The ranking theory of how planets evolve has long been that they condensed from concentrations in a primordial gas cloud. Then, once they had accreted, or come together, but while still in a largely liquid state, the heavy elements such as iron sank to the center while lighter ones rose to the top. This sorting process is known as differentiation.

The alternative posed by Mercury is iffy at best, but it contradicts such a fundamental part of planetology that it could be foolhardy to reject it out of hand, though even Murray points out that Mariner 10's data merely provide some justification for considering the alternative.

The idea is beguilingly simple: If Mercury is a differentiated planet with its original surface still on top, perhaps the differentiation took place as it formed instead of afterward. Otherwise the original surface would presumably have been plowed under.

The critical factor is whether much of the surface photographed by Mariner 10 is indeed original. There are definite signs of lava flows suggesting volcanic activity, and long, not-too-twisted cliffs and fissures pointing to a planet with at least a somewhat active history. But, says Murray, there are no signs of substantial atmospheric erosion or of worldwide crustal shifts like the plate tectonics of earth. Perhaps some original surface does remain. In fact, because the radioactive elements that provide much of a planet's internal heating are more likely to end up among the rocks at the top than among

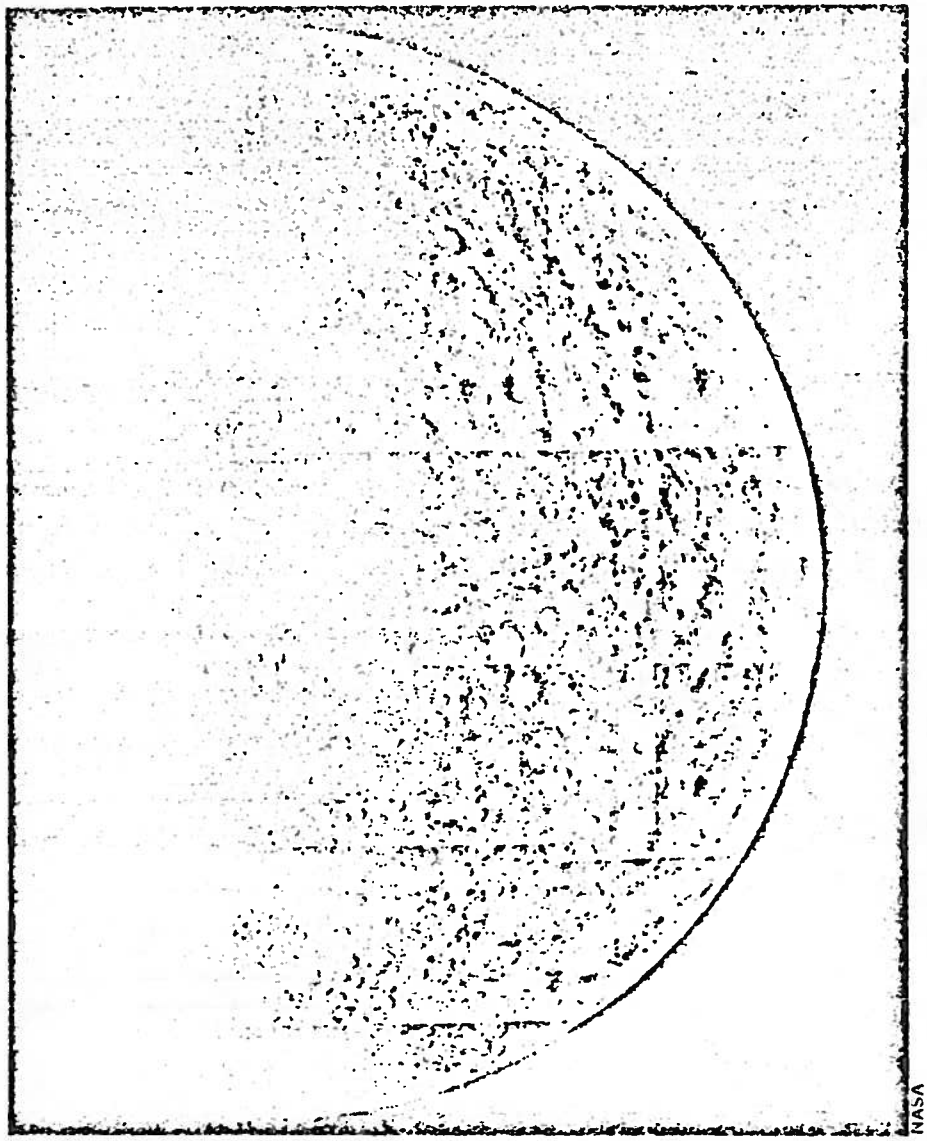

Mariner's outbound view shows smooth, moonlike maria and huge meteorite scars.

Cliff scars Mercury's fossil landscape.

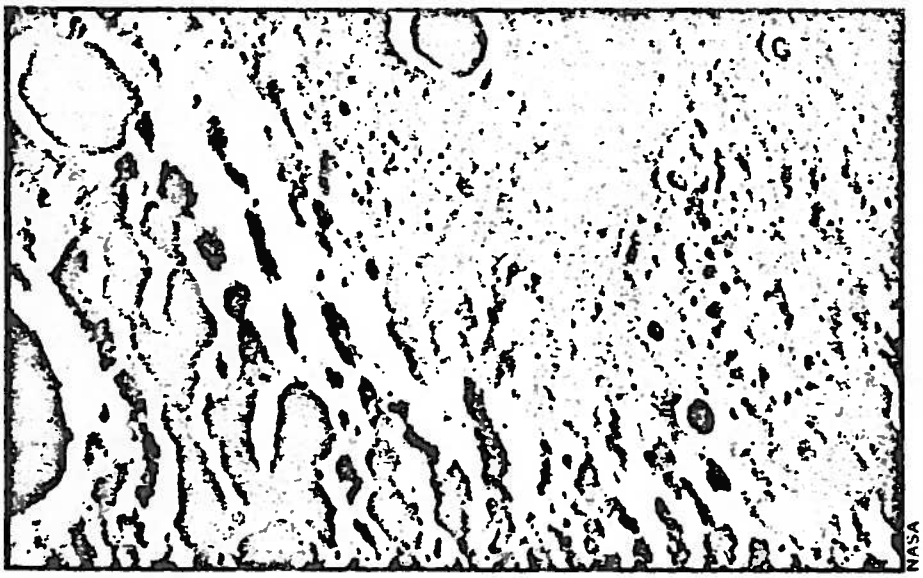

Small events such as lava flows, rather than global cataclysms, appear the norm.

the metals underneath, it is conceivable that a planet that had its iron core from birth might have fewer deep energy sources, so that its volcanic events might be smaller and less surface wrenching.

The newcomer is tempting, but the old standby theory has some logic on its side too. Mercury certainly has a moonlike look, acknowledges John O'Keefe of NASA's Goddard Space Flight Center, and radar measurements of the dielectric strength of the surface suggest similarly iron-free rocks. But if there is no iron, where did it go? The elements that came together to form Mercury and the other planets were in a gaseous state at the time, and, says O'Keefe, it is far more difficult to separate light and heavy elements as gases than as molten liquids. Since iron was there at the beginning, it must have disappeared from the surface afterward, by differentiation.

As theorists take sides, the Mariner 10 scientists live in growing frustration as a demanding schedule of scientific conferences keeps them busy presenting their data rather than staying in their laboratories analyzing it. Furthermore, Mariner's findings may have to suffice for a long time, since NASA's next Mercury flight is not scheduled until 1987. □

Science News: Vol. 106

Thom invented catastrophes in order to explain the discontinuous processes. Thom's theory builds on the results of 300 years' research into the manner in which continuously changing causes produce continuously changing results. But Thom succeeded in showing how continuously changing causes may produce results that exhibit dramatic discontinuities, or in his terminology, catastrophes.

There is more to the theory, of course, than pictures of folded sheets of paper. Scientists have long recognized that when two or more causative agents vary independently (temperature and pressure in the atmosphere, for example, or hostility and fear in animal behavior) the totality of all possible results can be represented conveniently by a surface with as many dimensions as the number of causative agents. Such surfaces are called manifolds and are the objects studied by differential topologists.

In developing his theory of catastrophes, Thom showed first how a manifold with an appropriate pleat can explain observed instances in which continuous causes produce catastrophic consequences. He then went on to classify all possible pleats in manifolds of low dimensions—thus providing scientists with a relatively small number of models for catastrophic phenomena together with a general proof that these models are the only possible ones. It is this latter point, contained in Thom's basic theorem on the classification of elementary catastrophes, that forms the core of the theory.

Thom showed that under certain specific but quite general circumstances, any singularity of a function on a manifold is equivalent to one of a few basic types called "elementary catastrophes." In a two-dimensional manifold (representing two interacting causes) there are just two possible types of catastrophes —a fold-catastrophe which may occur at the boundary of the manifold, and a cusp-catastrophe caused by a pleat on the surface of the manifold.

In 3, 4 and 5 dimensional manifolds there are, respectively, 5, 7 and 11 possible elementary catastrophes. Since these cases are quite difficult to visualize and interpret, Zeeman's Warwick colleagues Tom Poston and Ted Woodcock have developed computer graphics to illustrate the higher dimensional catastrophes.

One curious feature of Thom's classification theorem is that when the number of dimensions (the number of causative factors) reaches 6, the number of possible elementary catastrophes becomes infinite. As the number of dimensions increases, so does the space available in the manifold. Eventually the manifold contains enough room for the elementary catastrophes to evolve continuously from one to another. □

Mariner 10 returns to Mercury

Since March 29, when Mariner 10 flew by the planet Mercury, Mariner has almost completed a full journey around the sun, while Mercury has been around almost twice. On Sept. 21, spacecraft and planet will meet once again, although a mishap aboard the probe last week has strained the chances of a third encounter in the spring.

Unlike the first flyby, the September meeting will take place along Mercury's brilliantly sunlit side (SN: 7/6/74, p. 9), which will both enable photography of the south polar region of the planet and trim the spacecraft's trajectory for a third pass next March. The probe is expected to pass slightly less than 48,000 kilometers from the planet, much farther out than the 689 kilometers that separated them last March, but it should increase photo coverage of the sunlit side to 60 percent, as well as providing better viewing angles of areas already photographed. The only other of Mariner's instruments to scan the planet during the encounter will be an ultraviolet airglow detector seeking traces of hydrogen, helium, oxygen, neon and carbon in the thin atmosphere.

What worries flight controllers at Jet Propulsion Laboratory in Pasadena is that the spacecraft may run out of gas before it can come around a third time. Last Wednesday, an uncontrolled oscillation in the circuit that stabilizes Mariner on its roll axis caused the stabilizing jets to expend 0.54 pounds of the remaining 1.8 pounds of control gas. This should not affect the upcoming encounter, but will make things tight for the spring meeting. A previously developed solution involving orienting the spacecraft in a certain position (SN: 5/18/74, p. 319) was only partially applicable this time, and although a flight official estimates that next year's encounter could be accomplished on as little as 0.8 pounds of gas, a "strict conservation strategy" will be in force all the way. □

Searching out typos by computer

First newspapers and printing houses used computer tape to eliminate hand typesetting. Then they put in cathode ray terminals to eliminate hand copy-editing in the newsroom and hooked these to the computer tape operation. Now, Bell Labs of Murray Hill, N.J., has developed a way to computerize the proofreading operation and hook up all three.

By using standard medium-sized computers—found with increasing frequency in the publishing business—a 100-page book or a complete newspaper could now be proofread for misspellings and typographical errors in about three minutes. Two Bell researchers, Robert Morris and Lorinda L. Cherry, developed a special computer program to carry out this function for the Bell system's own extensive writing mill of in-house books, pamphlets and technical reports.

The system is fairly simple. The text is entered directly into the computer, either through a teletype machine or a cathode ray terminal (a television screen on which words appear as the author writes on a keyboard.) The computer then rapidly breaks each word into all of the possible two- and three-letter combinations and compiles them into a table of common word segments used in the article. It stores this in its memory—and one second has passed by. The computer then rescans the entire document and compares each wrong whole word to the table and assigns to each an "index of peculiarity." Two seconds. Then the computer prints out a list of the peculiar words in the order of their peculiarity, with the strangest one at the top—three seconds.

Bell Labs

Cathode ray screen shows word list and computer-assigned index of peculiarity.

The author or proofreader now has a list of words to check for corrections, but does not know or need to know how many times each appeared or where they appeared in the text. He instructs the computer to correct each word wherever it appears, sends the document through one more time, and is finished.

The computer program will not catch punctuation or semantic errors, but should cut total proofreading time tremendously, a Bell spokesman says, and should be useful to large publishing concerns with electronic equipment. □

Mercury: Scarps, massive impact craters and a compressed core

Mariner 10 view of south polar region of Mercury: Very much a world of its own.

Less than six months after Mariner 10 became earth's first emissary to Mercury, it also became the second. Passing less than 48,000 kilometers from the planet on Sept. 21, the spacecraft confirmed the finding of its initial visit: that Mercury, far from being a dull, run-of-the-mill ball of rock, is very much a world of its own.

Following a space trek of more than 560 million kilometers, including a full trip around the sun since last March's Mercury encounter, Mariner swooped this time between the planet and the sun, dipping low to photograph the never-before-seen south pole. In addition, its cameras scanned across the full expanse of the southern sunlit face, providing images to link the incoming and outgoing pictures gathered during the previous darkside pass. "We now have a very good topographic and geologic tie," says Robert Strom of the University of Arizona, "between the two sides of the planet."

Establishing such continuity is important not only for mapping and other general studies but also for learning about the planet's regional characteristics. Mars, for example, appeared to Mariners 6 and 7 as a world completely dominated by seemingly endless fields of meteor impact craters—until Mariner 9, after waiting out a month-long dust storm, revealed a series of huge volcanic basins, a vast canyon that would span the United States and apparent erosion features looking for all the world like ancient dry riverbeds. By the same token the Soviet Lunik 3 surprised scientists by revealing the far greater concentrations of craters on the far side of the moon.

Mercury has its own special features—huge scarps, or cliffs, thrust upward by irresistible compression of the planet either the moon or Mars. Planetologists have been awaiting Mariner's revisit to find out whether the scarps are only an occasional phenomenon or exist over most of the surface of this world that otherwise seems strangely to lack any signs of planetwide geologic activity. More than half of the planet is still unphotographed, but enough has now been seen that Strom feels confident in saying of the scarps, "they are global in scope."

But, do they evenly cover the surface, or do they give Mercury a puzzling asymmetry, a difference between one face and the other, such as is found on Mars, the moon, even the earth? The real answer must wait until computers can assemble the photographs into montages covering vast areas of the surface, but there are signs of asymmetries even in preliminary viewings. Smooth, volcanically filled in plains, for example, seem to exist more around the newly seen south pole than at lower latitudes, according to NASA's Donald B. Gault, a member of the huge team of experimenters studying the photographs. If the scarps' detailed distribution is not yet known, the fact that they at least seem to occur generally across the planet nonetheless offers some insight into the nature of Mercury. The compression that caused them, says California Institute of Technology's Bruce Murray, leader of the TV team, is a likely consequence of the shrinking of the planet's core, probably an iron one, creating wrinkles like those that form on a deflating balloon.

The core, says Strom, is probably a big one. Mercury's overall density of 5.45 (almost that of earth) and lightweight, apparently nonmetallic crust, suggests that the core may include as much as 70 percent of the planet's mass, percent of its volume. Earth's core, by comparison, accounts for less than a sixth of the volume of the planet.

But among all the scarps, plains and craters, there is one feature on Mercury that stands out, one of the greatest single markings on any world yet studied by man: the titanic Caloris Basin. Discovered during the first flyby, the giant crater is some 1,300 miles across, straddling the Mercurian twilight zone about 30 degrees north of the equator. Gault says the gargantuan object that produced it smote the planet with a trillion times the energy that created gigantic Meteor Crater in Arizona. And possibly coupled with it is another striking feature.

The TV team calls it "the weird terrain." Hilly, corrugated, raked with grooves, yet mysteriously smooth between the rough spots, the peculiar marking has been seen only in one area of Mercury—a part directly through the planet from Caloris Basin. Researchers have searched the preliminary versions of the second-encounter photos for more, but so far to no avail. Similar terrain has been found on earth's moon, but again, only opposite two of the largest lunar basins, Mare Imbrium and Mare Orientale.

Gault theorizes that the unusual landscape could have been produced by shockwaves resounding all the way through the planet from the impact that caused the basin, possibly reverberating along the channel between the core and crust. It is also possible, but unlikely, he says, that it is a volcanic feature, born of internal forces rather than a world-shaking blow. The most exotic proposal is that the impact that formed Caloris ejected material so violently that it flew around the planet in all directions, finally touching down 180 degrees away. Surveyors, Lunar Orbiters, and Apollos have failed to explain the lunar patches, however, so Mercury's weird terrain may remain unexplained for some time.

One of the biggest surprises about the first flyby was the discovery that Mercury makes its presence felt in the space around it. A magnetic field was weak but present where none was expected, and the spacecraft reported the equally unanticipated presence of rich streams of high-energy electrons flowing along the field lines. Prior to the second encounter, Mariner scientists were even more certain that they would find nothing; the spacecraft at its closest would be more than 60 times farther from the planet than it was the first time. It is still too early to be sure—Norman Ness of NASA has just started looking at his magnetometer data—but plasma researcher Al Lazarus of Massachusetts Institute of Technology reports fluctuating streams of the same high-energy

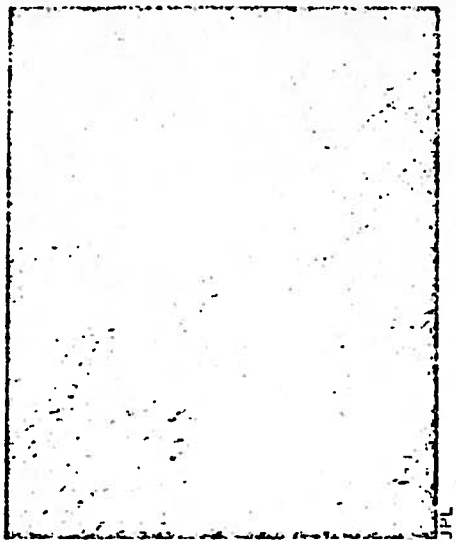

Scarp runs 185 miles across surface.

sun side of Mercury. If, as it appears at first glance, the planet's influence is present there, it may show up in the magnetic field as well. The main goal of the second encounter, however, was the pictures. Next March, the third and final pass, on the planet's darkside again, will be largely devoted to the infrared, ultraviolet and other instruments, looking from as close as 2,360 kilometers. There is some concern about whether Mariner's reserve of control gas is adequate for the journey—"I think it'll have some of the element of 'the Perils of Pauline,'" says Project Manager Gene Giberson—but officials are cautiously optimistic. "As far as I'm concerned," says Program Manager William Cunningham, "we're on our way to 'Mercury 3' right now." □

'Jupiter effect': Mixed reaction

The planets of the solar system are moving surely and inevitably toward a configuration that happens only once in 179 years. In 1982 there will come a moment when all the planets are in line with each other on the same side of the sun.

A newly published book, *The Jupiter Effect* by John Gribbin and Stephen Plagemann (New York: Walker and Co., 1974), foresees disastrous effects for that planetary imbalance. Gribbin and Plagemann predict increased seismic activity in the years around 1982 and specifically a major earthquake for the Los Angeles area.

Due to stories about it in the past two weeks by United Press International and Newsweek, the Jupiter effect theory is getting considerable public attention, including a formal query from a U.S. Senator. But the theory is receiving, at best, mixed reviews by scientists.

The two authors propose this chain of events: The planets exert tidal forces on the sun, and with all planets lined up on the same side of the sun such forces reach a maximum. The maximum force triggers an overabundance of sunspots. More sunspots mean more solar particles reaching the earth's upper atmosphere. The particles trigger unusual movements of large air masses. These movements affect the earth's rate

The Colombo Connection: How Mariner was brought back

"Looking back on things like this, you kind of kick yourself," says Joseph G. Beerer, "but sometimes you just can't see the forest for the trees." He wasn't the only one. In 1970, Beerer was the trajectory analyst helping to plan Mariner 10's flight past Venus and Mercury. His gentle self-chastisement is for his failure to realize the significance of a number buried in a computer printout on his desk, showing that Mariner could easily be aimed to pass close to Mercury two, three, and a virtually infinite number of times. And almost for free.

The math was easy. It would almost inevitably have occurred to someone sooner or later. As it happened the brainstorm was that of Italian astrophysicist Giuseppe Colombo, whose work in 1966 had helped to explain the newly discovered 3:2 ratio between Mercury's rotational and orbital periods.

Early in February of 1970, a group of scientists met at the California Institute of Technology to discuss Mercury, including the upcoming flyby. The launch date had already been chosen to minimize the energy required for the flight, and an arrival date had been picked to give a proper lighting angle for photography on the single visit that was then planned. Mission officials had also decided because of some of the experiments to aim for the planet's "dual-occultation zone," a region where Mercury would block both the earth and the sun from the spacecraft's view. Even with these stipulations, however, there was a range of available aiming points, each of which would take Mariner 10 into a different solar orbit after leaving Mercury.

It was at this meeting that Colombo tugged on the jacket of Caltech's Bruce Murray, who would be Mariner's chief picture analyst, and exclaimed, "The spacecraft will return! The spacecraft will return!" Queried by Murray, Colombo pointed out that among the range of possible post-Mercury solar orbits there seemed to be one with a period of 176 days, exactly twice the 88-day period of the planet. Couldn't this orbit be fine-tuned so that every two trips around the sun Mercury would find the spacecraft waiting for it?

Murray asked Beerer to find out. Sure enough, already on Beerer's desk was a computer listing of alternatives including one in which Mariner would move around the sun an average of 2.04 degrees per day. Divided into the number of days in a year, it came out just right for repeated encounters—extra flybys for free.

Well, not quite. A few changes had to be made in the spacecraft design, and time was short since the contracts with the builder (Boeing) had to be signed that autumn. Valves were adapted from Apollo so that Mariner's engine could be restarted the required number of times. Pioneer contributed a larger tank to hold an increased amount of control gas. Solar panels had to be made movable for better cooling, and an antenna was pivoted so that it could aim at earth while the spacecraft was behind the sun between encounters.

And it all had to be done while adding neither cost nor weight. Fortunately (and atypically), Mariner 10 came in about $750,000 under budget, thanks largely to its NASA project, program and spacecraft managers, respectively, Gene Giberson, William Cunningham and John Casani, and the spacecraft program manager at Boeing, Edward Czarnecki. The weight miraculously took care of itself: The conservatively rated Atlas-Centaur rocket turned out to be able to handle the load.

The cost of keeping data analysts and others around for the second encounter had added only about two percent to Mariner 10's $98 million budget, with another 1.7 percent for "Mercury 3" next March 16, but that comes out of more recent budgets. Altogether, the Colombo Connection, with Beerer, Giberson, Cunningham and colleagues, has been one of the better investments in NASA's planetary research program. □

Science News: Vol. 107

Planetology: Mercury and magnetism

Martians and Mercurians met on Monday, along with a few representatives of earth's moon. On Tuesday, the Venusians appeared, as did the asteroid and meteorite people. The Jovians had the next day to themselves, followed on Thursday by the Saturn, Uranus, Neptune and satellite delegations, leaving Friday for factions otherwise unheard from.

For the planet people it was the event of the year: the annual meeting of the American Astronomical Society's Division for Planetary Sciences. From as far away as Hawaii they came, to congregate at Columbia, Md., for the one occasion at which ranking U.S. experts on the entire solar system (except for the sun itself—that's another division) can compare results, propound and shoot down theories, and generally talk the shop of other worlds.

In 1969 when the division was established by a committee including such noted researchers as Lewis Branscomb, Gordon Pettengill and Carl Sagan, only two planets—Mars and Venus—and earth's moon had been visited by man-made spacecraft. Most studies were, and still are, done from earth. Even so, planetologists are fully aware of the unique value of a close look, and last year's meeting in California was a standing-room-only affair, thanks largely to hot-off-the-computer data on Venus and Mercury from Mariner 10 and on Jupiter from Pioneer 10 (as well as Skylab's observations of Comet Kohoutek). Interest in the planets has grown so rapidly, according to one attendee, that the present 260 members of the Division for Planetary Sciences outnumbers the entire AAS at the time the division was formed.

One of the most interested these days is Norman Ness of the Laboratory for Extraterrestrial Physics at the NASA Goddard Space Flight Center in Greenbelt, Md. In charge of the twin magnetometers aboard Mariner 10, he was amazed as were most of his colleagues when the spacecraft's first encounter with Mercury last March 29 revealed the "absolutely unanticipated" presence of a substantial magnetic field. The second encounter, on Sept. 24, was primarily for photography and was too far away for good magnetic field measurements. But there's one more chance: a third and final pass coming up on March 16—even closer than the first one. Although other instruments will be operating in addition to Ness' magnetometers, "this," says an official at the Jet Propulsion Laboratory in California, from which the spacecraft is being controlled, "is Norman's show."

be the last visit to the solar system's innermost planet in many years. So intriguing are the possibilities of this final flyby, and so high is the interest in the data already in hand from the first two, that the First International Colloquium on Mercury has been scheduled to meet at Pasadena in June.

Since Mariner 10's initial revelation, Ness has been at work making what he could out of his surprising data. His basic conclusion, and the most significant one for future studies of Mercury, is that the magnetic field is a real one, internal to the planet, rather than a vague interloper poured on from the outside by the solar wind. The most compelling evidence for this is that while both approaching and leaving the planet, Mariner 10 reported the presence of a clear "bow shock," like the wake around the bow of a boat, where the million-mile-an-hour flow of the solar wind was being pushed aside not by Mercury itself, but by its magnetic influence. Furthermore, says Ness, it seems likely that the field is caused by an "active dynamo mechanism"—electric currents moving around the planet within its metallic core. Previously it was assumed that such a dynamo requires a rapidly rotating planet, which Mercury is decidedly not.

The heavy metallic core, however, seems decidedly present. Mercury seems to be made of such lightweight, moon-like stuff on the outside that its large mass (confirmed by its bending effect on Mariner's trajectory) must signal a truly ponderous interior. Ness estimates, in fact, that the core may be as much as 70 percent of the radius of the planet and that 60 to 70 percent of its mass is iron—fine stuff for a dynamo.

The strength of the field seems to be about 350 gammas at the equator. The

field is, not surprisingly, dipole shaped, like the doughnut-shaped field around a bar magnet. However, Ness says, it is either tilted by about 7 degrees from the axis of rotation of the planet (less than the field of either earth or Jupiter), or it is something more complicated than a simple dipole. The upcoming encounter with Mariner 10 ought to help determine that. Besides simply providing more "data points," the final flyby should occur barely 500 kilometers from the planet, about 200 kilometers closer than the one that revealed the field in the first place. This should put the probe in a region where the field is about twice as strong as it was where it was first measured, so that fine details should be more visible.

The biggest question for "Mercury-3" will be whether there is really a dynamo effect in Mercury, or whether instead the field is due to a large mass of permanently magnetized materials. If there is a dynamo, what makes the currents that run it—convection currents from internal heating or precession of the core's axis within the planet? If, as seems likely, there is such a core, how did it evolve?

There are many such questions at the gathering of the planet people. Norman Ness, however, may be closer than most of his colleagues to a few of his answers. □

Marine models will aid future research

"Boy, have we got models for you!" This statement, made last week by a marine biologist, sums up the feelings of many researchers in marine biology and predicts what they see as a changing emphasis in biomedical research. Researchers from several fields met last week in Washington at a marine biomedical conference sponsored by the National Institute of Environmental Health Sciences to discuss this changing emphasis, and agreed that marine animals will play an increasing role in environmental and biomedical research.

Many researchers have in recent years focused on complex mammalian systems in their study of disease

closer their research animals are to humans, the more meaningful will be the application of their results. But, says Stewart G. Wolf of the University of Texas at Galveston, a phylogenetically simpler organism might yield more information than a complex mammal. "We now know that understanding the body's regulation of chemicals is the key to the secret of understanding disease. The question has gone from what happens to how does it happen." We must consider, he says, "the possibility of looking at human disease by turning to phylogenetically earlier periods where systems are simpler, but the biochemical

Mercury's Magnetism Is Its Own

"Unquestionably," says Norman Ness. "Unequivocally," says James Dunne. Surviving a knuckle-whitening last-minute cliff-hanger, the crippled Mariner 10 spacecraft this week revealed that the magnetic field of Mercury, a complete surprise when the probe first detected it a year ago, is definitely the planet's own, intrinsic to Mercury, rather than something generated from outside by some complex interaction with the solar wind.

Mariner barely lasted long enough to tell the tale. From the very day of its Nov. 3, 1973, launching, when balky heaters threatened to let its two TV cameras freeze solid, the probe was assaulted with a seemingly endless succession of woes. The most recent was a severe tracking problem that threatened to wipe out this week's third encounter with only two days to go. More than any other planetary mission on record, in fact, Mariner 10 has brought out the best in its human crews, who have staved off innumerable potential tragedies to convert ever-looming disasters into a two-planet, four-encounter triumph.

The third and final encounter with Mercury (which was so down-to-the-wire that Mariner will probably run out of control gas by the end of this week) was originally no more than a promising bonus, made possible by an accident of celestial mechanics. But the discovery of Mercury's magnetic field during the first encounter last March 29 gave new importance to the third visit (the second pass, on Sept. 24, was too far from the planet to help). In this third pass Mariner skimmed by only 323 kilometers from the newly intriguing world. The earth's much more powerful magnetic field, points out Ness, of the Goddard Space Flight Center, blocks the solar wind at a distance equal to about 15 times earth's radius. Mercury's little field, however, forms its solar wind shock wave less than half a Mercury radius out from the planet's surface; in other words, the planet itself occupies most of its magnetosphere, making a close flyby a necessity.

It would have paid off even if it had only answered the one big question. But besides showing that the field is intrinsic, says Ness, the data from the final pass may also have made it possible to shed some light on why it is there at all. One possibility is that Mercury is composed in part of permanently magnetized rock, but this, Ness points out, "requires a very special sequence of events occurring during the formation and evolution of the planet." Even so, he says, a comparison with Apollo lunar samples suggests that a 300- to 600-kilometer-thick crustal shell with similar magnetization could account for the observed field strength. The more likely source, he implies, is an active "dynamo" of spinning electric currents within Mercury's iron-rich core. Detailed studies of the first and third encounters should help. But the dynamo idea "faces some difficulties because we are uncertain about the exact structure" of Mercury's interior.

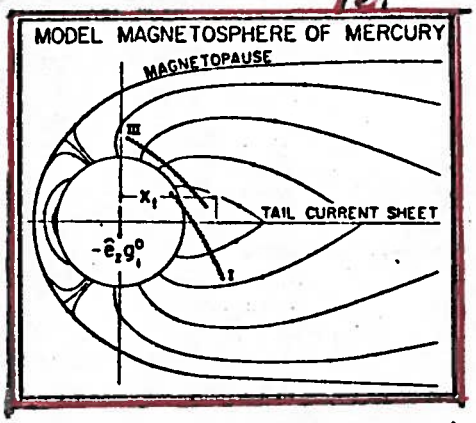

The surface is better known, thanks not only to Mariner 10 but to ground-based work as well. T. B. McCord and F. Vilas of Massachusetts Institute of Technology reported as long ago as 1972 that the surface was moon-like, basaltic, rich in iron and titanium and partially smoothed by the effects of "shock weathering." Last month, Rob Landau of the University of California added the finding, from thermal polarization studies, that the surface may be loosely packed on a scale of centimeters or meters but that the loose particle seemed to be composed of smalle structures that are compact on th scale of microns.

One particularly important contribu tion of the close flyby, points ou Clayne Yates of JPL is in the form c evidence showing that one character istic of Mercury, notably its charged particle populations, can be reasonabl compared with the earth's. Electro fluxes, for example, show similar dis tributions around both worlds given th different scales of their magnetic field says Yates. Occasional bursts of charge particles originating in Mercury's mag netic tail, adds University of Chicago John Simpson, also resemble the earthy counterparts. Such data coul become important if it becomes neces sary to rework ideas about the earth such as the out-of-hand assumption tha it is earth's rapid rotation that make possible its magnetic field, in the ligh of new insights into slowly turning Mer cury.

Mariner 10 data will keep research ers going for a long time; they'll hav to, since the National Aeronautics an Space Administration has no presen plans to return to Mercury before th late 1980's. But the team that made all possible is already fast fading fron view. Project scientist James Dunn and project manager Gene Gibbersor for example, are even now at work o the 1978 ocean-monitoring satellit called SEASAT. The 110-person comple ment of flight controllers was down t about 35 before the final encounter and, says Dunne, "Viking [the upcom ing Mars-landing mission] is swarmin all over the control area now, kickin us out."

Helios makes closest pass to sun

Last Sept. 21 during its second encounter with Mercury, Mariner 10 reached within 68,314,000 kilometers of the sun. Not even Venus probes had previously come as close to the sun as 100 million kilometers, but now all previous record keeping has become academic. Less than a month ago, on Feb. 25, the German-built solar probe called Helios (SN: 8/3/74, p. 74) smashed Mariner 10's record, and last Saturday it reached its own closest point, some 46,291,060 kilometers from earth's home star.

At such proximity, about 30 percent of the earth's mean distance from the sun, water would have long since boile away. Lead would melt. At perihelion Helios was bathed in 11 times as muc solar energy as ever reaches earth' atmosphere, and the temperature hov ered around 700 degrees F.

Yet the hardy spacecraft is surviving In fact, says Gilbert Ousley who man ages the U.S. side of the predominantl German project from NASA's Goddar Space Flight Center in Maryland, "i works better in space than it did o the ground." So exhaustive an effor went into developing the craft th officials at the German Space Opera tions Center near Munich referred t

Science News

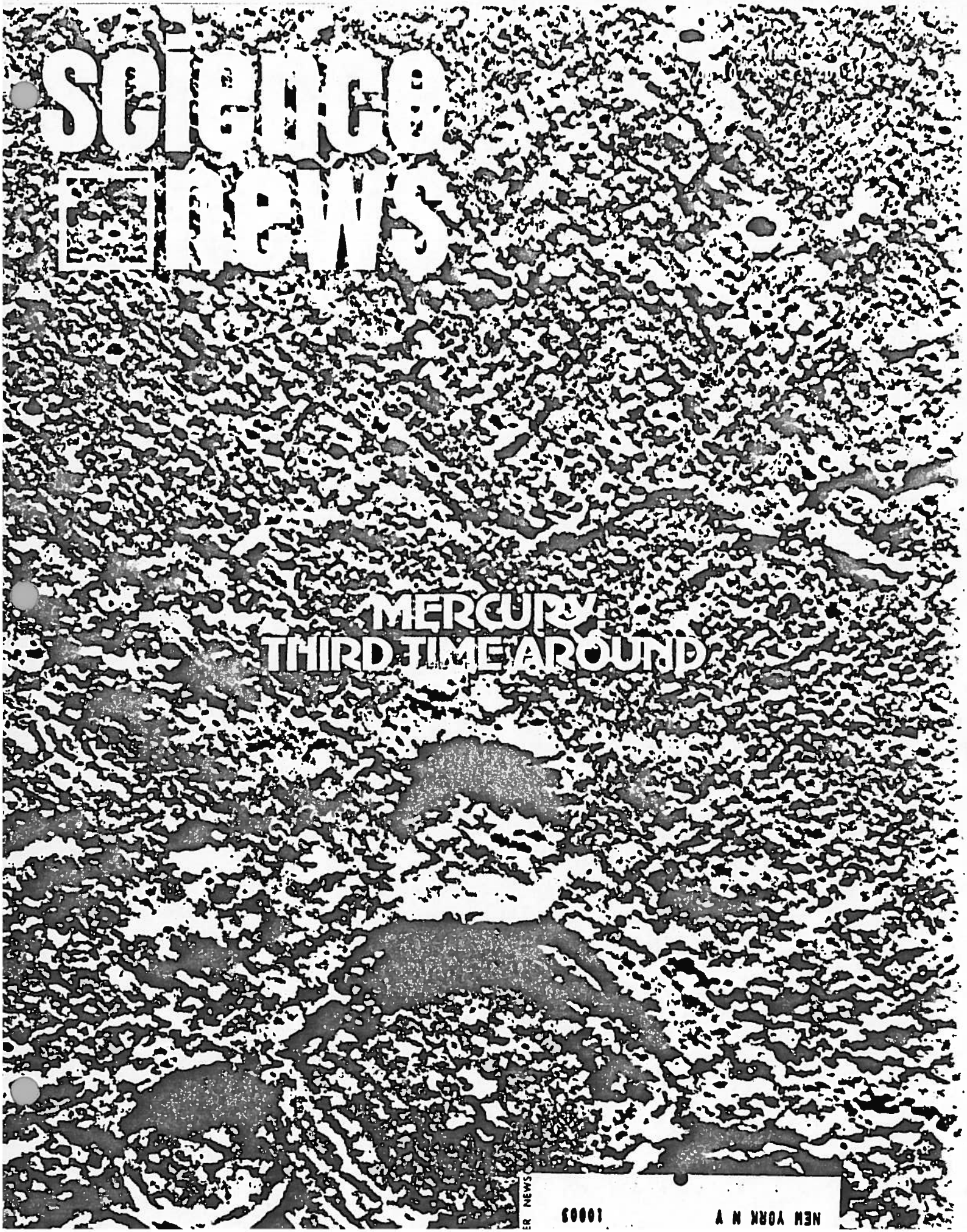

MERCURY: THIRD TIME AROUND

Science® News

A Science Service Publication
Vol. 107/March 29, 1975/No. 13
Incorporating Science News Letter

Of the Week

Research Notes

Articles

Departments

COVER: Mercury, photographed March 17 by Mariner 10 as the spacecraft sped away from its third and last controlled encounter with the planet, shows obvious similarities with the moon. But even with a relatively coarse resolution of about 518 meters (the photo was taken from 18,600 kilometers away), greater secondary cratering effects are visible, due to Mercury's higher gravity. Such comparisons, a change from the rock-at-a-time approach of past years, were a feature of the sixth Lunar Science Conference in Houston last week. See p. 205. (Photo: NASA)

Subscription Department
231 West Center Street
Marion, Ohio 43302

Subscription rate: 1 yr., $10; 2 yrs., $18; 3 yrs., $25. (Add $2 a year for Canada and Mexico. $3 for all other countries.) Change of address: Four to six weeks' notice is required. Please state exactly how magazine is to be addressed. Include zip code.

Printed in U.S.A. Second class postage paid at Washington, D.C. Established as Science News Letter in mimeograph form March 13, 1922. Title registered as trademark U.S. and Canadian Patent Offices.

Published every Saturday by SCIENCE SERVICE, Inc., 1719 N St., N.W., Washington, D.C. 20036. (202-785-2255). Cable SCIENSERV.

To the Editor

AMA and physicians' assistants

The last sentence of Joan Arehart-Treichel's "Off the Beat" article titled "What we can learn from Chinese medicine" (SN: 3/1/75, p. 141) showed an insight into the American Medical Association that has been slow in coming. The sentence states, "Until now the AMA has taken a dim view of physicians' assistants and midwives, largely because they appear to threaten the structure and power of physicians."

Eventually people will come to realize that two of our largest unions, the American Medical Association and the American Dental Association, do not always have the best interests of the general public in mind when they make decisions among themselves which affect all of us.

Robert L. Berger, D.D.S.
Port St. Lucie, Fla.

The concluding sentence of Joan Arehart-Treichel's article "What we can learn from Chinese medicine" was particularly misleading to your readers and not at all reflective of the American Medical Association's leadership in promoting effective use of potential manpower.

In December 1970 the House of Delegates of the American Medical Association adopted the following policy statement: "that state legislatures be urged to amend state medical practice acts to remove any barriers to increase delegation of tasks to allied health personnel by physicians." The intent of this policy is to obtain medical practice acts which would codify the physician's recognized right to delegate patient care functions to competent personnel in a manner consistent with the patient's welfare and would also codify the right of the one who accepts the delegated responsibility to participate in the practice of medicine.

The following December (1971), the House of Delegates of the American Medical Association adopted the "Essentials of an Approved Educational Program for the Assistant to the Primary Care Physician," which identifies minimum accreditation standards for an educational program. The accreditation process is conducted under the auspices of the AMA's Council on Medical Education in collaboration with the American Academy of Family Physicians, the American Academy of Pediatrics, the American Academy of Physicians' Assistants, the American College of Physicians, and the American Society of Internal Medicine. These four medical specialty organizations represent a significant portion of the practicing primary care physicians throughout the nation.

Since the accreditation effort was initiated in May, 1973, 69 applications have been received, 49 programs have been accredited and 96 on-site evaluations have been conducted.

In addition, as a result of substantial initiative on the part of the American Medical Association, a National Commission on Physician's Assistant Certification was established in November 1974. The initial certification examination was administered nationally in December 1973 and offered again in December 1974.

I believe Ms. Arehart-Treichel would find of interest the recent study completed by Ms. Eva Cohen et al of the Office of Regional Activities and Continuing Education, Yale University School of Medicine. The study was published in two volumes in October 1974 under the title "An Evaluation of Policy Related Research on New and Expanded Roles of Health Workers."

L. M. Detmer, Assistant Director
Joint Review Committee on Educational Programs for the Assistant to the Primary Care Physician
American Medical Association
Chicago, Ill.

The last half of your article, which is concerned with the contributions of the ill-trained barefoot doctor and the partially trained physician's assistant is hardly the quality of medicine that the citizens of this country should expect and I doubt it is what you would settle for.

One of the big problems in our country today is getting our citizens to utilize the medical knowledge and facilities that we at the present time have. I agree we should have more physicians until every man has his needs fulfilled, but we should not reach this goal by the acceptance of inferior quality.

The motive that you described to the American Medical Association as to why they object to the support of physicians' assistants and midwives is most unfair and short-sighted. The insistence upon quality is perhaps a unique expression in American society, but it is a motivating factor in the medical profession. For those who cannot understand this attitude, I can only ask for their indulgence.

S. A. Wills, M. D., F.A.C.S.
Decatur, Ga.

Address communications to Editor, Science News, 1719 N Street, N.W. Washington, D.C. 20036

Mariner 10 Pictures of Mercury: First Results

Abstract. *Mercury has a heavily cratered surface containing basins up to at ast 1300 kilometers diameter flooded with mare-like material. Many features e ely similar to those on the moon, but significant structural differences ist. Major chemical differentiation before termination of accretion is implied.*

Mariner 10 began photographing ercury on 23 March 1974, from a tance of 5,400,000 km. Intermittent ture taking continued daily until 28 arch when nearly continuous photo- aphic operations were initiated to lude the period of closest encounter 29 March. Periodic photographic erations continued until 3 April when probe was 3,500,000 km past Mer- ry. More than 2000 television frames re transmitted from the twin high-resolution cameras previously described (*1*).

As a consequence of the great public interest in closeup pictures of this previously unexplored planet, we think it is desirable, even at this early time, to present a very brief description and preliminary interpretation of those images initially available in hard copy. An extensive preliminary report is planned after the entire data set has been examined; it will accompany reports on the six other experiments aboard Mariner 10 to appear in this journal.

The major landforms on Mercury observed by Mariner 10 are basins, craters, scarps, ridges, and plains (Fig. 1). Morphologically these features strongly resemble analogous landforms on the moon. Where the plains are absent, overlapping craters and basins form rugged terrain. The plains materials have many of the characteristics of the lunar maria and have been cratered to approximately the same degree. This twofold division of the surface morphology of Mercury is strikingly similar to that on the moon.

The largest basin observed so far on Mercury is centered at ~ 195°W,30°N (Fig. 2) and has many of the characteristics of the lunar Imbrium basin.

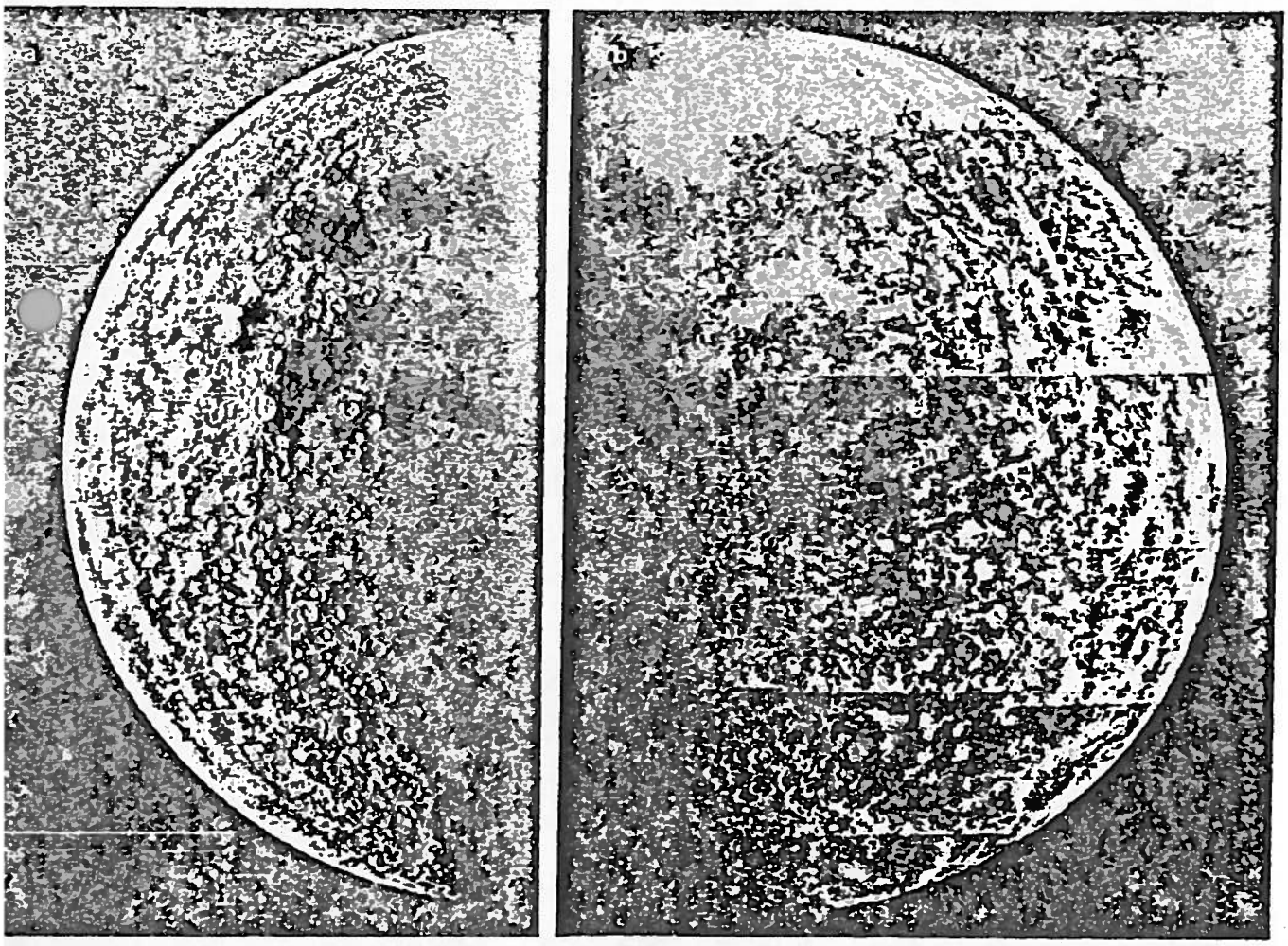

1. (a) Photomosaic of Mercury made from nine computer-enhanced pictures taken at 234,000 km, 6 hours before closest proach to the planet. North is at the top and the sun's illumination is from the left. The evening terminator is at about 20°W gitude and the bright limb is at 110°W longitude. This part of Mercury is heavily cratered, the craters ranging in size up to ost 200 km. Apparently the freshest craters are those with bright rays, for example, the bright crater (diameter about 40) ar the center of the picture. This picture and (b) show the whole of the illuminated portion of the planet; adjoining a along the bright limb of both pictures. (b) Twelve computer-enhanced pictures taken at 210,000 km 5½ hours after sest approach form this photomosaic. Half of a 1300-km multiringed basin appears near the center of the disk on the termina- . The inner portion and parts of the surrounding area are relatively poorly cratered plains materials similar in aspect to the ar mare units. Several craters with bright rays are evident; a bright ray pattern, which appears to connect several young craters, ms a smooth hyperbolic curve. The north pole is at the top and the equator extends from left to right about two-thirds of the y down the photo. The bright limb is at 110°W and the terminator is at 200°W.

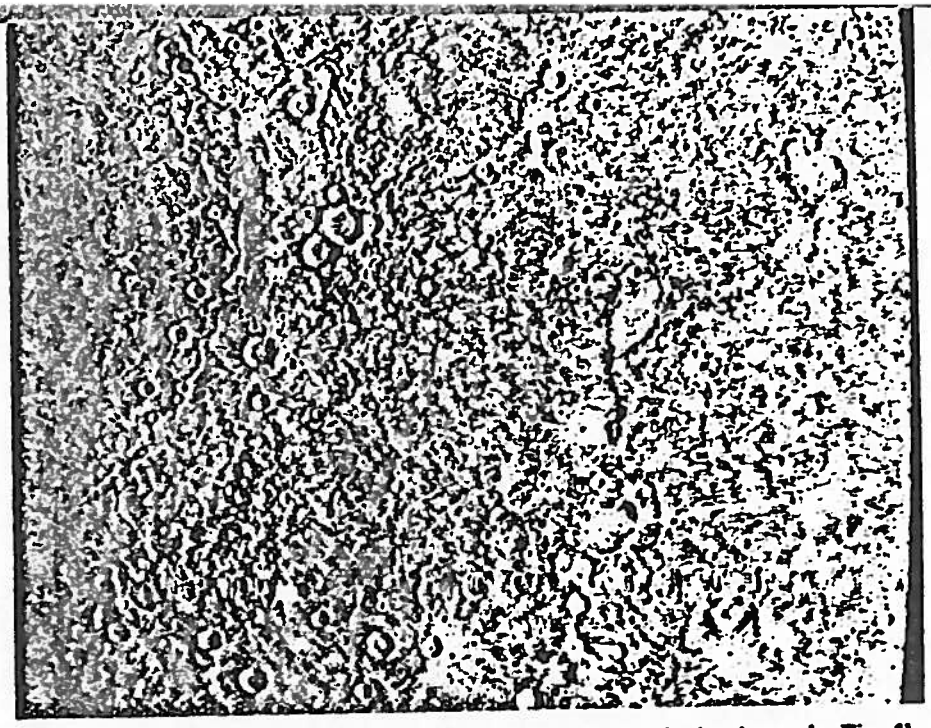

Fig. 2. Close-up view of one-half of the 1300-km circular basin shown in Fig. 1b. The other half is hidden beyond the terminator to the left. Hills and valleys extend in a radial fashion outward from the main ring. Interior of the large basin is completely flooded by plains materials; adjacent lowlands are also partially flooded, and superimposed on the plains are bowl-shaped craters. Wrinkle ridges are abundant on the plains materials. The area shown is 1600 km from the top to the bottom of the picture. The sun's illumination is from the right. Blurred lines extending across the picture near the bottom are missing data lines that have been filled in by the computer.

Numerous smaller basins also are evident, grading from sharply defined to barely discernible; some have two concentric rings. Craters range in size downward from the dimensions of basins (Fig. 3, a and b) to the limits of detectability on the highest-resolution photographs (Fig. 3c). Extensive ray systems are present around some bright craters. The plains materials have filled and embayed the larger basins and adjacent lowlands (Fig. 2). Smooth material morphologically like lunar mare in some cases fills ancient craters without evidence of external origin (Fig. 4). As on the moon, a local source of volcanic material is suggested. Numerous wrinkle ridges similar to those on the lunar maria have formed within the plains (Figs. 2 and 3c). A volcanic origin for much of this material is implied.

Prominent structural features on Mercury include irregular scarps which are up to 1 km high, extend for hundreds of kilometers, and cut across large craters and intercrater areas (Fig. 3a). Similar features are absent on the

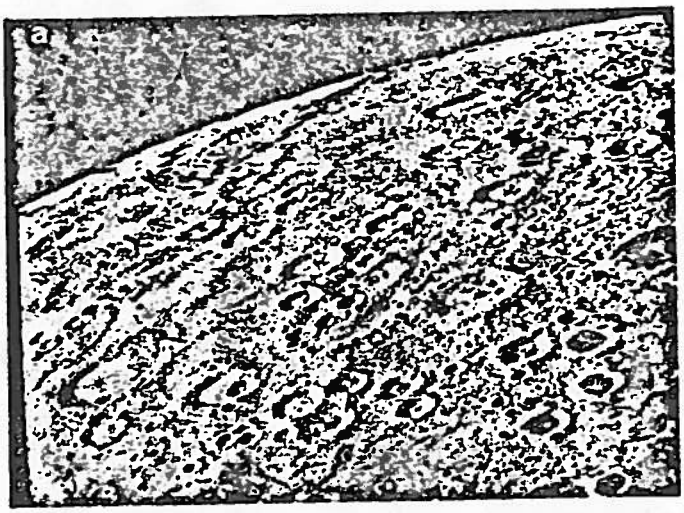

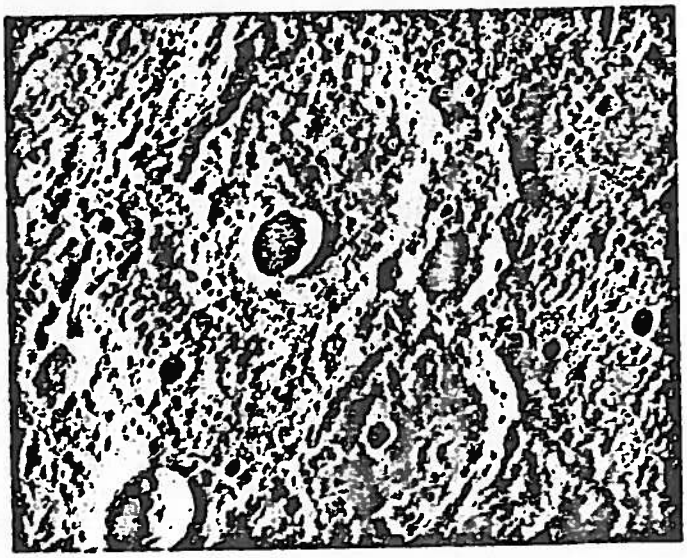

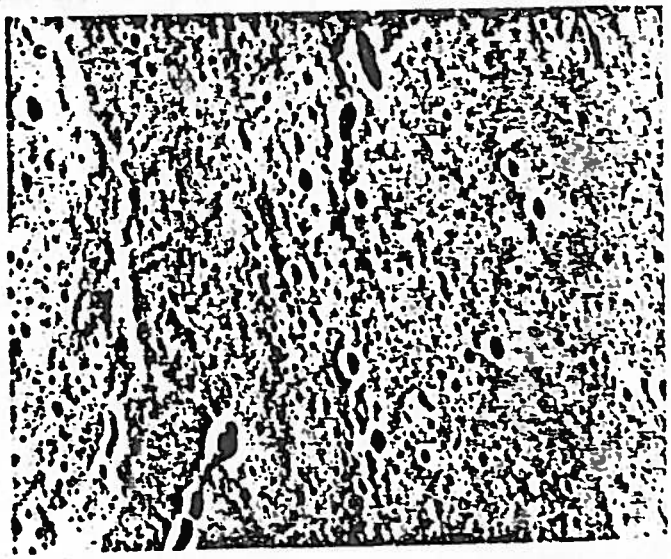

Fig. 3. (a) View of Mercury's northern limb taken from 77,800 km. A prominent east-facing scarp (also seen near the northern limb in Fig. 1a) extends from the limb southward for hundreds of kilometers. The "tear" in the limb was caused by a loss of data. The area shown is about 580 km wide. (b) Closeup view taken from 19,370 km, revealing several old craters of intermediate size with a smaller sharp crater about 12 km in diameter. The rims of these older craters have been denuded by smaller craters, many having the characteristics of secondary impact craters. The area shown is 122 by 145 km. (c) High-resolution photograph taken from 7342 km shortly after encounter, showing plains materials at 25°N latitude and 161°W longitude. Both primary and secondary impact craters can be recognized, the secondary craters being less circular and often forming clusters and chains. The largest craters are about 2 km across. Low scarps and hills on the left are similar to wrinkle ridges on the lunar maria. The continuum of crater morphologies and other analogies indicate that lunar-like erosion has occurred on Mercury. The area shown is 55 by 46 km.

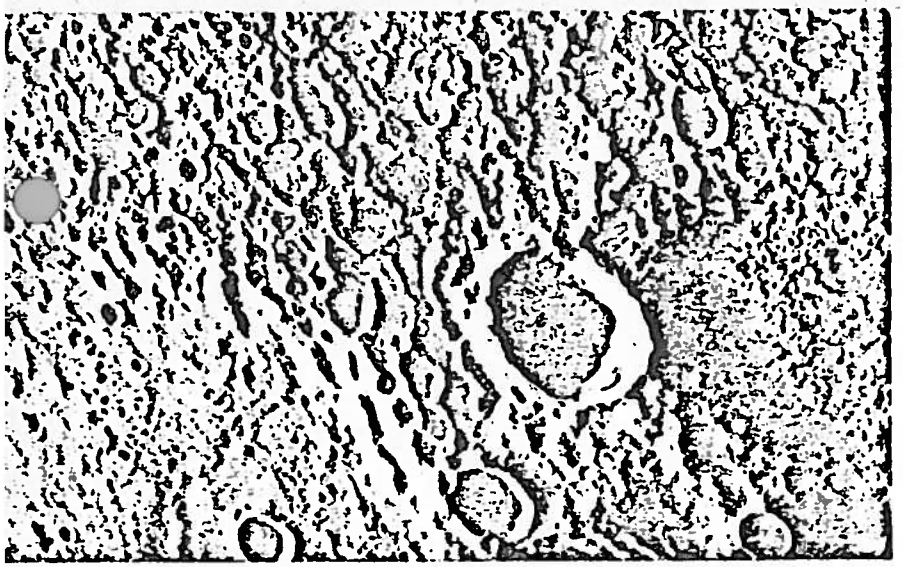

g. 4. The long shadows in this picture taken near the terminator help to bring it the roughness of this heavily cratered terrain. The large sharp crater to the right id below the center of the frame is about 25 km across. Part of a 100-km, flat-floored ater can be seen in the lower left corner. The flat floor apparently results from bsequent filling by plains material. The lobate scarp on the floor suggests a volnic origin for this material. The smoothness and lack of continuous cratering is dicative of younger age than the surrounding terrain, which is peppered by craters, any of which may be of secondary impact origin.

oon. In addition, the paucity of raight rilles and graben on Mercury ggests a major difference in structral style between Mercury and the oon. No features suggestive of either rth-like plate tectonics or large-scale nsional faulting in the crust have en recognized so far.

The Mariner 10 photographs of ercury, combined with previous studs of the terrestrial planets, suggest ur preliminary conclusions.

1) Extensive flooding by rock materials at least grossly similar to those of e lunar maria has occurred on Mercury. The large horizontal scale of such atures implies a silicate composition lensity ~3) for the entire outer reons of the planet, not just the upper ntimeters or meters as is indicated rectly by remote optical, infrared, id radio measurements. Yet the mean anetary density of 5.5 g/cm^3 requires at very much denser material must cur at depth, very probably in the rm of a large iron core. Thus Mercury is a chemically differentiated anet.

2) The heavily cratered surfaces on ercury record the final periods of avy impact bombardment at Mercury. We consider it likely that those ndscapes include at least some topoal features which have survived om the end of tangible accretion (*2*). nce planetwide melting would have stroyed such topographic features, ercury's major chemical differentiaon must have taken place before the d of accretion there. Similarly, there can have been no tangible atmosphere, primitive or secondary, about Mercury since those topographic features formed, because eolian processes would have modified them, as on Mars. An early speculation by Kuiper that Mercury's high density might reflect an extraordinary erosion of surface material by anomalous solar activity likewise is not confirmed.

3) In the half of the planet observed by Mariner 10, Mercury, like the moon, seems to exhibit a hemispherically nonuniform distribution of flooded basins. If this impression is valid, previous explanations of the near-side/far-side dichotomy of the moon which involve processes peculiar to the presence of the earth may require reevaluation.

4) Mare-like surfaces now have been formed on the moon, Mars, and Mercury which show a surprising similarity in accumulated impacts, although only those of the moon have been dated radiometrically. The impacting objects traditionally have been regarded as asteroids or comets. A strong decrease in flux between Mars and Mercury had generally been expected. Yet, barring extraordinary coincidence in both age and local fluxes, no strong dependence on heliocentric distance in postaccretion impact flux is suggested by the Mariner 10 pictures. The Mercury results may lend support to the recent speculation of Soderblom *et al.* (*3*) that the impact flux histories of Mars and the moon (and, by inference, Mercury) have been rather similar.

These preliminary conclusions carry important suggestions concerning the origin and evolution of the terrestrial planets. Widespread cratering and basin formation dating back to the final stages of accretion may be common to their early history. Major chemical differentiation well before the end of accretion is suggested for Mercury; perhaps this is a significant clue to the origin of other objects in the inner solar system. The Mariner 10 flyby of Mercury ultimately may contribute significantly to the understanding of the early history of our own planet.

BRUCE C. MURRAY
California Institute of Technology, Pasadena 91109

MICHAEL J. S. BELTON
Kitt Peak National Observatory, Tucson, Arizona 85726

G. EDWARD DANIELSON
Jet Propulsion Laboratory, Pasadena, California 91103

MERTON E. DAVIES
Rand Corporation, Santa Monica, California 90401

DONALD GAULT
Ames Research Center, Moffett Field, California 94035

BRUCE HAPKE
University of Pittsburgh, Pittsburgh, Pennsylvania 15260

BRIAN O'LEARY
Hampshire College, Amherst, Massachusetts 01002

ROBERT G. STROM
University of Arizona, Tucson 85726

VERNER SUOMI
University of Wisconsin, Madison 53706

NEWELL TRASK
U.S. Geological Survey, Reston, Virginia 22092

References and Notes

1. B. C. Murray *et al.*, *Science* **183**, 1307 (1974).
2. We recognize that petrographic, chemical, and isotopic analyses of returned lunar samples may indicate a heavy bombardment shortly after what otherwise might be regarded as the end of accretion. We do not feel this uncertainty about the end of lunar accretion seriously detracts from the force of our conclusions about Mercury.
3. L. A. Soderblom, R. A. West, B. M. Herman, T. J. Kriedler, C. D. Condit, *Icarus*, in press.

4. The return of closeup television pictures from Mercury is a remarkable accomplishment reflecting the skills and perseverance of many at Jet Propulsion Laboratory, California Institute of Technology (Caltech), Boeing, and NASA headquarters. In the initial scientific interpretation we have benefited from the aid of our television team associates, Audoin Dollfus of l'Observatoire de Paris, James Anderson of Caltech, and especially John Guest of the University of London Observatory. Robert P. Sharp and Arden L. Albee of Caltech provided valuable criticism of the manuscript. Contribution No. 2464 of the Division of Geological and Planetary Sciences, California Institute of Technology.

9 April 1974

Reports

Mariner 10 Mercury Encounter

Abstract. *Mariner 10's closest approach to Mercury on 29 March 1974 occurred on the dark side of the planet at a range of approximately 700 kilometers. The spacecraft trajectory passed through the shadows of both the sun and Earth. Experiments conducted included magnetic fields, plasma and charged particle studies of the solar wind interaction region, television photography, extreme ultraviolet spectroscopy of the atmosphere, the detection of infrared thermal radiation from the surface, and a dual-frequency radio occultation in search of an ionosphere.*

Mariner 10 encountered Mercury on 29 March 1974 after a flight of 146 days (Fig. 1). The exploration of Mercury was the primary objective of the mission and the basis for the selection of the Mariner 10 experiment complement. It was desired to grossly characterize several of the important properties of this little-known planet, particularly to determine the nature of its surface morphology; whether an atmosphere is present, and, if so, the constituents; its interaction with the solar wind; and a ement of its mass and radius. In recognition of the important information it contains concerning a planet's bulk properties, the study of the interaction between Mercury and the solar wind was given a high scientific priority, with the result that a dark-side passage was selected for the flyby. An aim point within the solar occulation zone also made possible a sensitive search for a tenuous neutral atmosphere by observation of the extinction of solar extreme ultraviolet radiation and a favorable groundtrack for studying the infrared thermal emission of the surface from midafternoon to midmorning, local time. Passage through the region wherein Earth is occulted by Mercury as viewed from the spacecraft was desired for the conduct of a dual-frequency (X- and S-band) radio occultation probe in search of an ionosphere and for the radius measurement. The flyby trajectory was not optimal for the classic tool of the exploratory spacecraft, imaging, but the provision of two telescopes (focal h, 1.5 m) capable of 100-m resoon at a range of 5000 km resulted in a very satisfactory television experiment. A second extreme ultraviolet spectrometer, designed to detect resonance scattering emissions of H, He, O, C, Ne, and Ar, was mounted on the scan platform, sharing its positioning control with the television experiment.

The Mariner 10 spacecraft and its flight through Venus encounter has been described by Dunne (*1*). After the Venus encounter operations, spacecraft activity lapsed into a normal cruise mode with continuous collection of data on magnetic fields, plasma, and charged particles at 2450 bits per second. On 16 March 1974 at 1155 G.M.T., a third trajectory correction maneuver (TCM) was carried out, moving the flyby point at Mercury from a miss distance of some 10^4 km on the bright side to the desired dual occultation target point. The Mercury flyby geometry is shown in Figs. 2 and 3.

The closest approach occurred at 2046 G.M.T. on 29 March; the closest approach distance was 703 km relative to the surface, based on a Mercury radius of 2439 km. The spacecraft velocity relative to Mercury was 11.13 km sec^{-1}, and the distances to Earth and the sun were 148.6×10^6 and 69.7×10^6 km, respectively. Solar occultation entry and exit times were 2042 and 2049 G.M.T., respectively. Corresponding times for Earth occultation were 2048 and 2059 G.M.T. The sun-Earth-probe angle at closest approach was 27°.

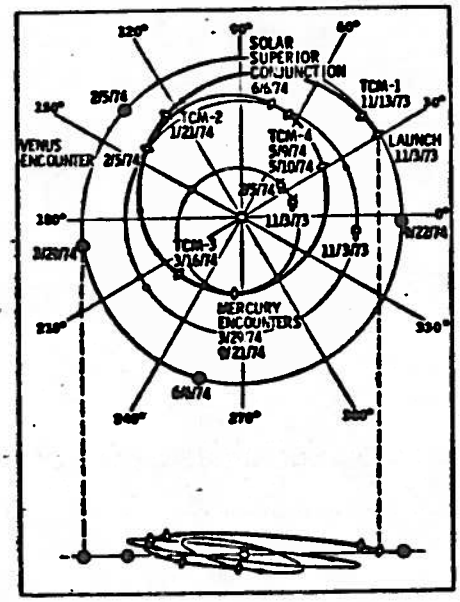

Fig. 1. Overview of the trajectory of the Mariner 10 mission, showing the relative position of the spacecraft, Earth, Venus, and Mercury at the times of significant events. Verticle exaggeration is approximately 3 to 1 in the lower view.

The Mercury encounter sequence extended from 23 March, when the first television pictures were obtained at a range of some 5.3×10^6 km, to 2 April, approximately 4 days after closest approach (CA). During the early phases of the encounter sequence, operations were confined to about an hour of picture-taking per day, using the spacecraft tape recorder, with interleaved extreme ultraviolet airglow spectrometer scans and spacecraft motion-driven drifts through the planet's atmosphere. This cyclic pattern was accelerated as the spacecraft closed rapidly with the planet, becoming a 1½-hour cycle starting at a range of about 750,000 km (16 hours prior to CA). From this time until some 16 hours past encounter, all science sequence commands were issued by the spacecraft's central computer and sequencer (CC & S), which had been programmed to do so before the start of the ground-commanded far encounter sequence on 23 March. The transmission of full-resolution pictures at 117.6 kilobits per second started 3 hours, 33 minutes, prior to encounter, continuing until 4 hours, 15 minutes, past CA. This high data rate, which increased high-resolution (< 2.7 km) coverage by approximately a factor of 4, was made possible by the installation of special low-noise masers (*2*) on the 64-m antennas at Deep Space Station (DSS) 14 (Goldstone, California) and DSS 43 (Tidbinbilla, Australia). Near CA, from 28 minutes before until 8 minutes after, imaging was interrupted, and high-resolution extreme ultraviolet airglow spectrometer scans were obtained in search of Ar, the heaviest of the gases for which the experiment was designed and therefore the smallest in scale height.

During this interval, a range point was obtained at X-band for the celestial mechanics experiment. This was accomplished by means of a rapid uplink transfer between Goldstone DSS 12

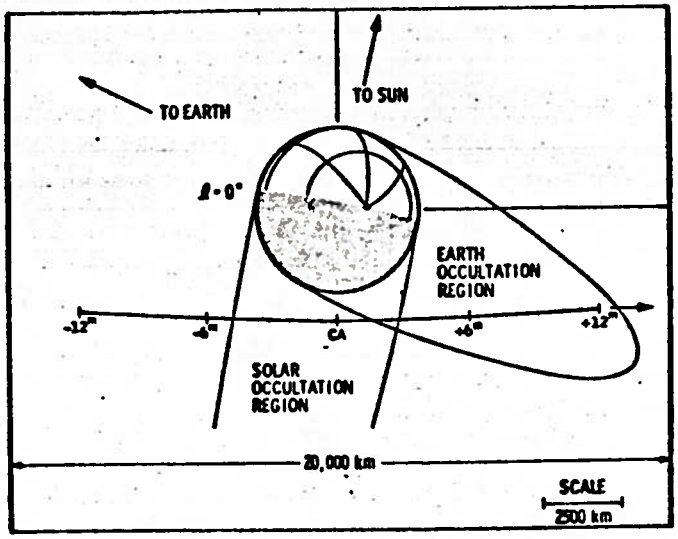

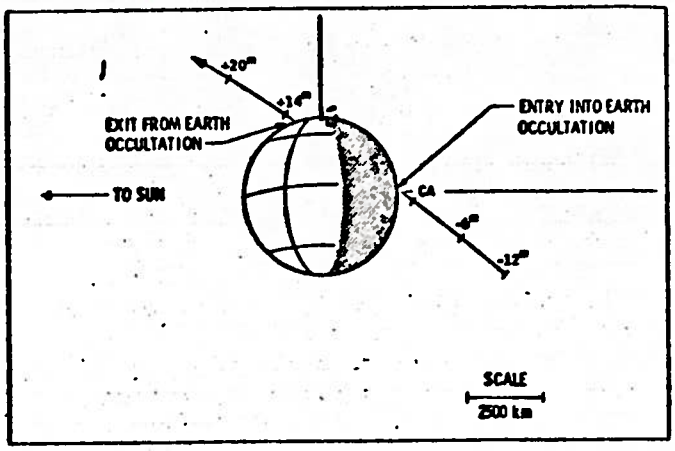

Fig. 2 (left). Mercury close flyby geometry, viewed from the trajectory north pole. Fig. 3 (right). Mercury encounter as viewed from Earth, showing Earth occultation immersion and emersion.

(26-m antenna, 10-kw transmitter) and Goldstone DSS 14; DSS 12 had been maintaining uplink for command purposes in order that DSS 14 could be operated in a "listen only" mode to receive the high rate imaging. The 100-km DSS 14 transmitter was required to provide an adequate signal-to-noise ratio in the received spacecraft carrier and its superimposed range code. The forward beam of the infrared radiometer (IRR) intersected Mercury's surface at 2022 G.M.T., leaving at 2044 G.M.T. The IRR mode-2 command (aft beam, planet; forward beam, reference) was sent by the CC & S at that time; 1 minute later, the aft beam intersected the surface, continuing measurement until crossing the far limb at 2057 G.M.T.

Data obtained during passage through Earth occultation was recorded on the spacecraft tape recorder and played back several times starting at 16 hours after encounter. With the exception of this playback, the outgoing sequence mirrored the incoming one but was terminated after an imaging search for a Mercury satellite conducted at encounter plus 4 days.

After Mercury encounter operations, the spacecraft was returned to its cruise state for the long voyage around the sun and back to Mercury. A TCM was conducted on 9–10 May to allow a reencounter with Mercury on 21 September 1974 between 2100 and 2200 G.M.T.

The scientific results obtained at Mercury are of significant planetological interest. The distinctly nonlunar solar wind interaction region characterized by the existence of a planetary magnetic field and structured streams of accelerated electrons and protons is as exciting as it was unexpected. Whether that field is induced or intrinsic, its implications with respect to the internal constitution of the planet may be profound. The existence of extensive areas of terrain morphologically similar to the lunar mare material, combined with the planet's high density and the apparently primordial character of the surface in general, leads to important speculations concerning the nature of processes which occurred early in Mercury's history, the understanding of which may lead to modifications in theories dealing with the formation and subsequent evolution of the terrestrial planets. It should be remembered, however, that Mariner 10 has given us but a brief glimpse of Mercury, raising, as do most initial ventures in planetary exploration, many more questions than it has answered. But the questions now have a sharper focus, and their answers a clearer place in the hierarchy of solar system studies.

JAMES A. DUNNE
Jet Propulsion Laboratory,
California Institute of Technology,
Pasadena 91103

References and Notes

1. J. A. Dunne, *Science* 183, 1289 (1973). The Mariner 10 launch time which was reported to be 0245 on 2 November 1973 was in fact 0545 on 3 November.
2. R. C. Clauss and E. R. Wiebe, *Jet Propulsion Lab. Tech. Rep. 32-1516 XIX* (1974), p. 93.
3. I thank J. Y. Pedigo of the Jet Propulsion Laboratory (JPL) for assistance in the preparation of figures and manuscript and D. G. Rea and J. B. Jones of JPL for critical review and comment. This report represents one aspect of research carried out by JPL under NASA contract NAS 7-100.

31 May 1974

Preliminary Infrared Radiometry of the Night Side of Mercury from Mariner 10

Abstract. *The infrared radiometer on Mariner 10 measured the thermal emission from the planet with a spatial resolution element as small as 40 kilometers in a broad wavelength band centered at 45 micrometers. The minimum brightness temperature (near local midnight) in these near-equatorial scans was 100°K. Along the track observed, the temperature declined steadily from local sunset to near midnight, behaving as would be expected for a homogeneous, porous material with a thermal inertia of 0.0017 cal cm^{-2} sec$^{-1/2}$ °K^{-1}, a value only slightly larger than that of the moon. From near midnight to dawn, however, the temperature fluctuated over a range of about 10°K, implying the presence of regions having thermal inertia as high as 0.003 cal cm^{-2} sec$^{-1/2}$ °K^{-1}.*

The average thermophysical properties of the upper few centimeters of the Mercurian soil can be inferred from measurements of the cooling curve of the surface during the night. The night temperatures are sensitive primarily to a single parameter, the thermal inertia $(K\rho c)^{1/2}$ of the soil (I), which in turn depends primarily on the porosity of the soil. Temperature fluctuations

und a mean cooling curve ("thermal
s") also provide a sensitive
ans of identifying inhomogeneities
the structure of surface materials
, for instance, to exposures of rock
an otherwise powdery surface. The
ared radiometer experiment on
riner 10 was designed to measure
surface brightness temperature
ng a near-equatorial track from mid-
rnoon across the night side to mid-
rning, local time. In this preliminary
ort we will discuss only the data
n the night side—19 hours to 05
rs, local time.

The radiometer is essentially the
ie as that flown on Mariners 6, 7,
9 (*2*), but with modifications as
essary to accept radiation in the
spectral bands from approximately
o 14 μm and 35 to 55 μm. The
iometer was fixed relative to the
ecraft and gave two scans of
rcury, first by the "forward" beam,
ch traversed the evening side of the
et, and then by the "aft" beam,
ch traversed the morning side. The
ervations discussed in this report,
ns they do near the lower end
th emperature range of the radi-
ter, were all made with the long-
e (45-μm) channel. The field of
v was 1.1°, providing a maximum
ar resolution of 90 km for the for-
d beam and 40 km for the aft
m. At the minimum temperature
sured, ~ 100°K, the temperature
lution was limited by the digitiza-
interval, which corresponded to
≃ 0.5°K.

t the time of the flyby, Mercury
near aphelion and the longitude
he sunset terminator was 9°, where
origin of longitudes is the so-called
t meridian," one of the two meri-
s that alternately face the sun at
helion (*3*). The forward beam
sed the evening terminator at a lati-
: of −21°, swept gradually north-
d to achieve its highest linear re-
tion near 23 hours local time at a
ude of −12°, and left the planet
r 02 hours local time.

he track of the aft beam was
llel to and slightly north of the
ard beam, but close enough that
e is substantial overlap in the
ace areas observed between longi-
s 310° and 250°. The highest re-
tion of the aft beam was near 250°
out local time 02 hours) and at lati-
: + 5°. The aft beam crossed the
ning terminator at + 22° latitude.
the time of this writing, final

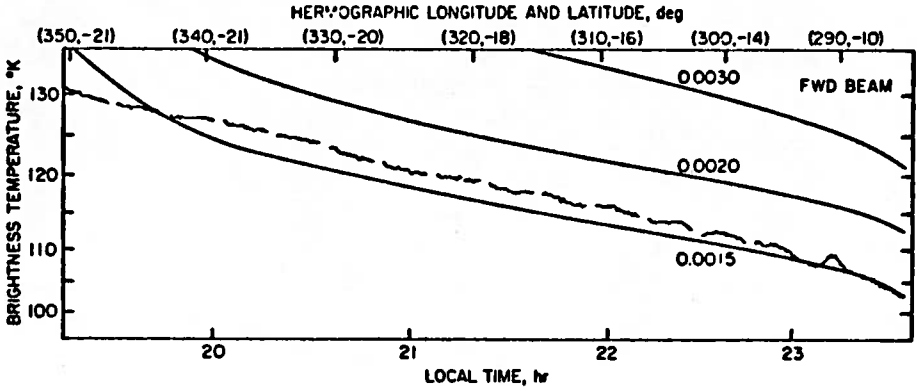

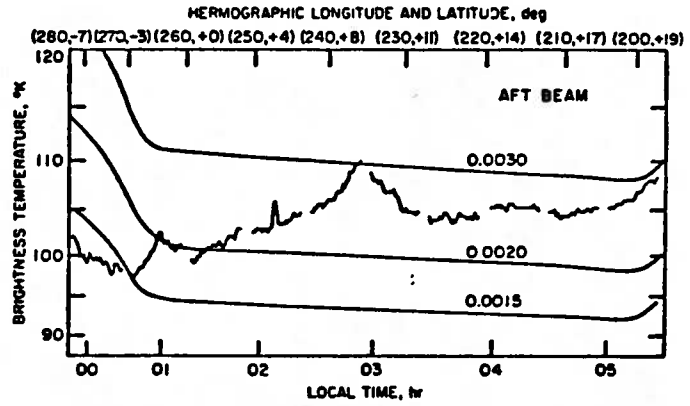

Fig. 1 (top) Brightness temperatures of Mercury at 45 μm obtained from the trace of the forward beam. The plot is linear in 45-μm intensity and in spacecraft time. The ordinate is labeled in brightness temperature and the abscissa in local time and in hermographic longitude and latitude. Three model curves, as described in the text, are labeled by their thermal inertias. The data gaps are due to 6.0 seconds of calibration each 42 seconds. Fig. 2 (bottom). Same as Fig. 1, but for the observation with the aft beam.

received, and all coordinates given must be considered preliminary.

Figure 1 illustrates the forward beam observations from before 20 hours local time to shortly before local midnight. The plot is linear in the recorded intensity of the 45-μm radiation and in the spacecraft time, although the figure is labeled in units of brightness temperature and of hermographic (Mercurian) time and longitude. The region of precipitous decline in temperature immediately following sunset ends just before the start of the plot. The temperatures along this trace decline smoothly from 130° to 105°K, exactly as would be expected for a homogeneous material with low thermal conductivity. The predictions of three calculated homogeneous models that differ only in the thermal inertia are also illustrated (*4*, *5*). The observed cooling curve for this part of Mercury corresponds to a thermal inertia of 0.0017 and suggests that the minimum, predawn temperature will be ~ 90°K. Only one large thermal anomaly, with an amplitude of ~ 3°K, is conspicuous (near longitude 290°). On the scale of the figure, instrumental noise is negligible and the small-scale structure

Figure 2 illustrates the data from the aft beam obtained between 00 and 05 hours local time and plotted on the same scale as Fig. 1. Clearly the areas of Mercury seen in this swath do not exhibit nearly as homogeneous thermal properties as those discussed in the previous paragraph. The brightness temperature reaches a minimum of about 100°K near 00 hours and then rises slowly, with superimposed fluctuations of several degrees, toward the dawn terminator. Both small-scale features (comparable to or smaller than the field of view of the radiometer) and large-scale ones (> 200 km) are evident. A comparison of the observed temperatures with the models illustrated in Fig. 2 shows that the thermal inertia along much of this trace is near 0.0025, while for the largest anomaly the inertia apparently exceeds 0.003.

The data illustrated in these two figures are raw, in the sense that they have not been corrected for possible out-of-field response of the detector or for possible directionality of emissivity of the surface. The model calculations shown in Figs. 1 and 2 have, however, been convolved with the first-order esti-

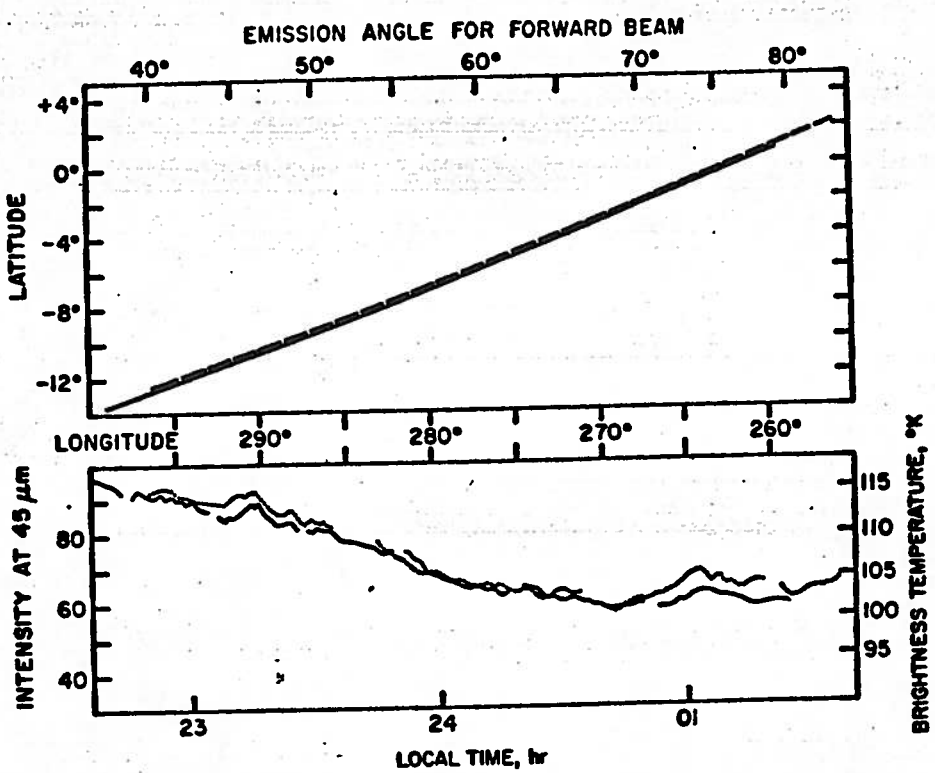

Fig. 3. Data from the region of overlap of the two beams. The upper part of the figure shows the predicted traces of the two beams. The abscissa at the top gives the emission angle as seen by the forward beam; the emission angle for the aft beam is 120° minus that of the forward beam. The temperatures have been corrected for dependence of emissivity on emission angle, as described in the text. The forward beam observations are represented by solid lines in both parts of the figure.

reproduces the onset onto the planet. The rise in temperature seen between 01 and 04 hours is thus certainly not an artifact of scattered radiation from beyond the dawn terminator of Mercury. The rise in the model temperatures of Fig. 1 for local times before ~ 20 hours is, however, an artifact of the field response; more refined fits must be made after refined trajectory data become available.

The dependence of the emissivity on direction can be investigated from the data in the region of overlap of the forward and aft beams. Figure 3 illustrates the observations made with the two beams between longitude 297°, where the emission angle into the aft beam becomes less than 80°, and longitude 258°, where the emission angle into the forward beam first exceeds 80°. The brightness temperatures from the two beams agree to within ± 2°K near longitude 277°, where both view the surface at an emission angle of 60°, demonstrating the equivalence in calibration of the beams. At other places, however, the beam viewing the larger emission angles generally records the lower brightness temperature. The data from the two beams can be brought into agreement if the measured intensity, $I\phi$ is corrected according to the expression:

$$I(\phi) = I(0)\cos^{\beta}(\phi)$$

where ϕ is the emission angle of the infrared radiation, and the exponent $\beta = 0.2 \pm 0.01$. The observations in Fig. 3 have been corrected in this fashion, and the good agreement between the beams in general level and in many of the details of the small-scale variations is evident. Note that the linear resolutions of the two beams are similar near the start of the overlap region, but that near the end the forward beam is observing an area several times greater than that seen by the aft beam.

The thermal inertias determined from the observed brightness temperatures are characteristic of porous fragmented rock or dust similar to the lunar soil. Previous Earth-based observations have also suggested moon-like thermophysical properties for Mercury (*6*), but no definite measurement of any dark-side temperature has been reported. In 1923, Pettit and Nicholson (*7*) reported a tentative detection of thermal radiation from the night side of the planet, suggesting a temperature of the order of 180°K, but subsequently they failed to repeat this detection (*5*, *8*). From 10-μm scans made with the Hale 200-inch telescope several years ago, Murray (*9*) set an upper limit of 150°K to the mean night temperature on the planet. Murdock and Ney (*10*) attempted to separate the radiation emitted from the dark side from that of the illuminated part of the disk on the basis of observed color temperatures over the spectral range 3.75 to 12 μm and concluded that the mean temperature of the night side was 111° ± 3°K. In contrast, the temperatures measured by Mariner 10 near the equator of Mercury suggest that the disk-averaged 12-μm flux from the night side should be smaller by about a factor of 2 than the amount deduced by Murdock and Ney.

There is a substantial literature on microwave radiometry of Mercury (*11*), in which measurements of disk-averaged temperatures originating in material tens of centimeters below the surface have been reported. The amplitudes of the variations in microwave brightness as Mercury rotates define the ratio of electrical to thermal skin depths, which has a value of 0.9 ± 0.3 at a wavelength of 1 cm (*6*, *11*). The thermal inertia of 0.002 determined from these Mariner 10 observations corresponds to a thermal skin depth of $22/\rho$ cm, where ρ is the mean density in the upper subsurface. The electrical skin depth for microwaves is then given by $20\lambda/\rho$, where λ is the wavelength in centimeters. This quantity is, in turn, a function of dielectric constant [known from radar studies to be $\epsilon \simeq 2.9$ (*6*)] and the electrical loss tangent. Thus, we can obtain not only the basic thermal parameter of the soil but also the basic electrical parameter, the loss tangent divided by the density. This value is $\tan\Delta/\rho = 0.005 \pm 0.001$, in excellent agreement with laboratory measurements of dry silicate rock powders (*12*).

The Mariner 10 radiometer observations of the night side of Mercury are consistent with the presence of a moon-like layer of insulating silicate dust constituting at least the upper tens of centimeters of the soil. The spatial variations in the thermophysical properties of this layer, as seen in these two scans across the planet, are considerable, however, suggesting large-scale regions of enhanced thermal conductivity. These could be either areas

which the soil is more compacted
s in which there are boulders
outcroppings of rock that are not
nketed by dust. In the absence of
ages of the regions of Mercury ob-
ved by the radiometer, we cannot
nment on possible relationships be-
en the thermal structure and sur-
e morphology.

S. C. CHASE
ta Barbara Research Center,
leta, California 93017

E. D. MINER
Propulsion Laboratory,
lifornia Institute of Technology,
adena 91103

D. MORRISON
itute for Astronomy, University
Hawaii, Honolulu 96822

G. MÜNCH
G. NEUGEBAUER, M. SCHROEDER
lifornia Institute of Technology,
adena 91109

References and Notes

The thermal inertia is the square root of the product of the thermal conductivity (K) and the heat capacity per unit volume (ρc). In this report we express this parameter in the familiar units of cal cm^{-2} sec$^{-1/2}$ °K^{-1}; the numbers can be converted to S.I. units of cm^{-2} sec$^{-1/2}$ °K^{-1} by multiplying by 4.2×10^7 erg/cal.
S. C. Chase, *Appl. Opt.* **8**, 639 (1969).
The maximum temperature expected, near noon on the equator, was 560°K at the time of the Mariner 10 encounter. The substantial variations in the maximum temperatures with hermographic longitude that result from the high eccentricity of the orbit of Mercury are not expected to affect the nighttime temperatures significantly.
The models assume a homogeneous material with temperature-independent thermal properties and a plane-parallel geometry. The method of calculation is described by D. Morrison *Smithson. Astrophys. Obs. Spec. Rep. No.* 192 (1969) and (5)]. As shown in these references, the existence of temperature-dependent thermal properties has little effect on calculated surface temperatures.
D. Morrison, *Space Sci. Rev.* **11**, 271 (1970). For a general review of Earth-based studies of the thermophysics of Mercury, see Morrison (3).
E. Pettit and S. B. Nicholson, *Publ. Astron. Soc. Pac.* **35**, 194 (1923). For additional discussion see Soter (8) and Morrison (5).
S. L. Soter, *Science* **153**, 1112 (1966).
B. C. Murray, *Trans. Am. Geophys. Union* **48**, 148 (1967).
T. L. Murdock and E. P. Ney, *Science* **170**, 535 (1970).
The ratio of skin depths is determined primarily by the observations at 3.3 mm by E. E. Epstein, M. M. Dworetsky, W. G. Fogarty, J. W. Montgomery, and R. C. Cooley [*Radio Sci.* **5**, 401 (1970)] and at 3.75 cm by G. J. Klein (*ibid.*, p. 397). More recent microwave measurements are reported in D. Morrison and M. J. Klein, *Astrophys. J.* **160**, 325 (1970); B. L. Ulich, J. R. Cogdell, J. H. Davis, *Icarus* **19**, 59 (1973); F. H. Briggs and F. D. Drake, *Astrophys. J.* **182**, 601 (1973); and G. N. Cuzzi, *ibid.*, in press.
G. J. Campbell and J. Ulrichs, *J. Geophys. Res.* **74**, 5867 (1969).
We thank the entire Mariner team, both at the Propulsion Laboratory and at Santa Barbara Research Center, for making the mission successful. We thank J. Bennett for help with the data analysis, J. Engel for his work as leader of the radiometry group at SBRC, and T. Clarke for his work as instrument engineer.

Observations at Mercury Encounter by the Plasma Science Experiment on Mariner 10

16.

Abstract. A fully developed bow shock and magnetosheath were observed near Mercury, providing unambiguous evidence for a strong interaction between Mercury and the solar wind. Inside the sheath there is a distinct region analogous to the magnetosphere or magnetotail of Earth, populated by electrons with lower density and higher temperature than the electrons observed in the solar wind or magnetosheath. At the time of encounter, conditions were such that a perpendicular shock was observed on the inbound leg and a parallel shock was observed on the outbound leg of the trajectory, and energetic plasma electron events were detected upstream from the outbound shock crossing. The interaction is most likely not atmospheric, but the data clearly indicate that the obstacle to solar wind flow is magnetic, either intrinsic or induced. The particle fluxes and energy spectra showed large variations while the spacecraft was inside the magnetosphere, and these variations could be either spatial or temporal.

An unexpectedly strong interaction between the solar wind and Mercury was detected by the plasma science experiment (PSE) when Mariner 10 encountered Mercury on 29 March 1974. Before this encounter, the interaction was generally thought to resemble that of the moon, where the solar wind impinges directly on the surface. Planets, such as Earth and Jupiter, having strong magnetic fields, hold the solar wind off from the surface and deflect its flow around a cavity larger than the planet itself. Results from Mariner 5 and Mariner 10 have indicated that at Venus the solar wind is deflected by a well-developed ionosphere. Mercury presents to the solar wind an obstacle more analogous to Earth than to the moon or Venus.

This report presents preliminary results from the rearward-looking (antisolar) electrostatic analyzer which forms part of the plasma science experiment on Mariner 10. This experiment, a cooperative effort by groups from the Massachusetts Institute of Technology (MIT), the Los Alamos Scientific Laboratory (LASL), the Goddard Space Flight Center, and the University of California at Los Angeles, has been described previously (*1*) in connection with the encounter of Mariner 10 with Venus. These first measurements of plasma electrons in the vicinity of Mercury clearly show the presence of a bow shock and sheath region, resulting from deflection of the solar wind around the planet, enclosing a region which we tentatively identify as a "magnetosphere," containing a population of electrons whose properties differ from those in the surrounding medium, even though we cannot conclude whether they are trapped.

The data on which this interpretation

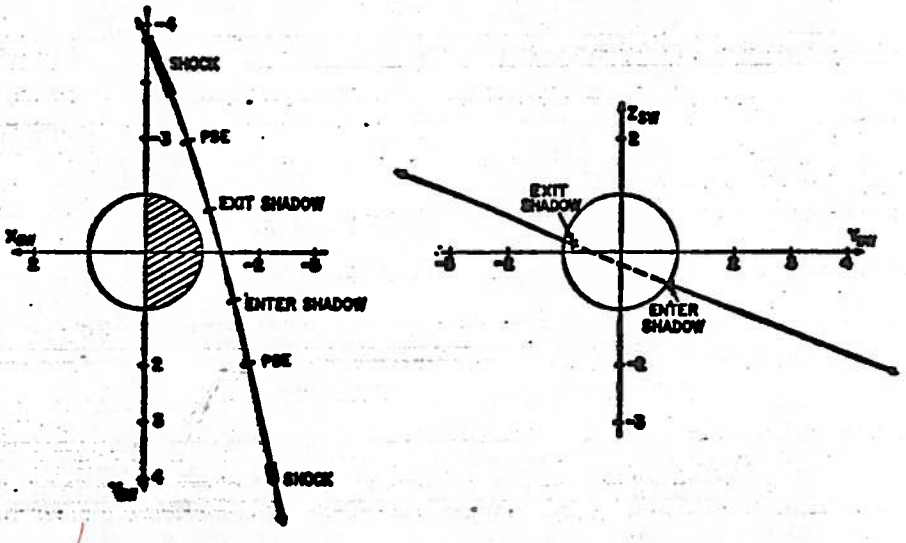

Fig. 1. The trajectory of Mariner 10 at the time of encounter with Mercury. Distances are in planetary radii, and the X_{SW} axis points in the antisolar wind direction taken to be 3° to the west of the sun. The Z_{SW} axis is to the north in the right-hand coordi-

is based consist of measurements of electron spectra taken every 6 seconds throughout the period of encounter. Each spectrum is composed of 15 differential flux measurements, each made in 0.4 second; the energy channels are logarithmically spaced between 13.4 and 687 ev with a fractional width in energy of 6.6 percent. The fan-shaped field of view of the instrument scans at a rate of 1° per second through an arc of 120° centered on a direction in the ecliptic plane 6.5° east of the spacecraft-sun line. The field of view is ± 3.5° in the scan plane and ± 13.5° perpendicular to that plane. The spacecraft passed on the dark side of the planet, along a trajectory shown in Fig. 1.

Prior to the encounter, the instrument measured typical interplanetary solar wind electron spectra, illustrated by spectrum 1 of Fig. 2. The spectra were similar in form to those taken near 1 A.U. (astronomical unit) having separate low-energy ("core") and high-energy ("halo") components which were both approximately Maxwellian in form and characterized by temperatures of 1.5×10^5 °K and 6×10^5 °K, respectively (*2*).

Figure 3 shows fluxes at 13.4, 71, and 389 ev and the electron density and pressure as a function of time for the period between 2000 and 2200 U.T. Earth-received time (ERT). A scale with the events referred to the time of closest approach is given at the bottom of Fig. 3, and the U.T. of spacecraft observation is given across the top. The density n and pressure P are defined in terms of the velocity distribution function, f, as follows:

$$n = \frac{4\pi}{\Delta\Omega} \int f \, d\bar{v}$$

$$P = 2\pi \frac{m}{\Delta\Omega} \int f \bar{v}^2 \, d\bar{v}$$

where $\Delta\Omega$ is the solid angle of acceptance of the detector; the integrations have been carried out numerically over the whole energy range of the detector, and extrapolation from 13.4 ev to zero has been made assuming a Maxwellian form for the distribution function. Modulation of the derived density and pressure by the solar wind flow velocity has not been removed; this modulation is less pronounced after encounter than before because of increased magnetic activity. The peak values of the scan modulation of the density and pressure are the most representative of ambient conditions.

From the variation with scan angle of electron flux at 13.4 ev at a time some 20 minutes before the spacecraft encountered the bow shock, we have determined a solar wind velocity of 630 ± 40 km sec^{-1}, and a mean flow direction in a frame moving with the planet of $3 \pm 6°$ from the west of the sun. The results of the MIT plasma experiments on Explorer 47 and Explorer 50 at 1 A.U. indicate bulk speeds, corrected for propagation and corotation, which corroborate this value. The preencounter conditions are $n = 17 \pm 2$ cm^{-3} and a ram pressure $\rho v^2 = 1.1 \times 10^{-7}$ dyne cm^{-2}.

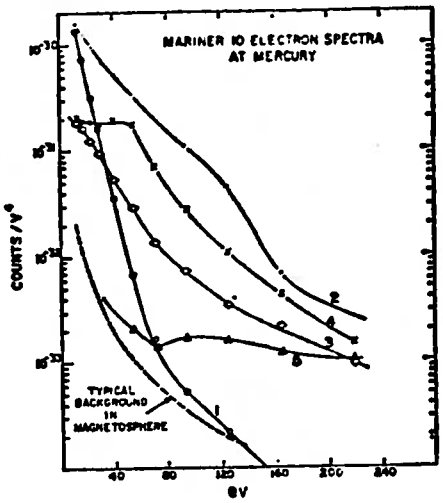

Fig. 2. Electron spectra at various times, given in the text, during the encounter. Spectrum 1 was taken in the interplanetary medium before the spacecraft reached the bow shock; spectrum 2 was taken in the magnetosheath; spectra 3 and 4 were taken in the magnetosphere; and spectrum 5 was taken between energetic particle events B and C, just before the spacecraft reentered the magnetosheath. A typical background as observed in the magnetosphere is shown; the background in the interplanetary medium is several times lower.

We now describe the events illustrated in Fig. 3. On the incoming leg of the trajectory, the bow shock was traversed three times within 1 minute, beginning at −19 minutes, 38 ± 6 seconds and ending at −18 minutes, 49 ± 6 seconds, in agreement with the corresponding magnetometer observations (*3*) to within the resolution of the electron spectrometer. This thin shock structure closely resembles Earth's bow shock observed by an electron detector when the interplanetary magnetic field is approximately perpendicular to the direction of the shock normal ("perpendicular" shock) (*2*). Across the discontinuity there was a density change of approximately two times and a temperature change of approximately three times, in satisfactory agreement with observations of density and temperature jumps by electron detectors that have traversed Earth's bow shock at comparable locations (*2*).

After the shock traversals, we observed a region analogous to Earth's magnetosheath, where the flux of electrons at, for example, 71 ev, was greatly increased. Spectrum 2 of Fig. 2, taken in this region, does not show the "flat" form at low energies characteristic of electron spectra taken in Earth's magnetosheath (*2*) but does show the large increase of electron flux at moderate energies resulting from "thermalization" behind the shock. In the inner sheath, traversed between −17 and −13 minutes, there was a reduction in flux above about 100 ev which varied with the direction of pointing of the detector. The observations made during that period will be discussed below.

At −10 minutes there was a well-defined change in spectral form (from that shown in Fig. 2 as spectrum 2 to that shown as spectrum 3), accompanied by a drop in density to about 1 cm^{-3}. There was an abrupt increase in electron flux between 200 and 680 ev at this time. Comparing these plasma data with similar observations made near Earth (*4*), we conclude that the spacecraft crossed a boundary analogous to a magnetopause. This interpretation is strengthened by changes in the magnetic field observed at the same time (*3*). Fluctuations in the data limit the accuracy with which the time of crossing can be determined to about 1 minute.

The spacecraft passed into the optical shadow of the planet at −4 minutes, 48 seconds, after which the electron spectra gradually assumed the form of spectrum 4 in Fig. 2, as a result of increasing electron fluxes at all energies. Passage out of the shadow of the planet occurred at +2 minutes, 39 seconds.

A second traversal of the magnetopause boundary occurred at approximately +7 minutes when the density and spectral form became similar to those observed immediately after the shock crossing on the inbound leg of the trajectory. Between +12 and +17 minutes the spacecraft passed through a highly disturbed region, which we interpret as a pulsating ("parallel") shock (*5*). This interpretation is consistent with the nature of the incoming shock, the geometry of the orbit and shock boundary, and the measured direction of the magnetic field before and

the encounter (*3*). In this region plasma properties varied rapidly time, and it is possible that at some of the electron spectra are because of possible large uations during a single measure- sequence. After this shock pas- typical solar wind spectra and parameters were observed; in ad- n, "upstream events" were seen as ated in Fig. 3. These events are itatively similar to those recorded lectron detectors situated upstream Earth's bow shock on magnetic lines intersecting the bow shock Increases in the 71-ev flux before ounter (for example, at −26 min-) appear to be different in nature n those observed after encounter; former coincide with transient de- ises in the interplanetary magnetic l (*3*). The presence of upstream nts is consistent with our interpreta- of the outgoing shock as having allel geometry. We show in Fig. 4 omparison between the observations sented here and observations of a parallel shock at Earth made by the triaxial electron spectrometer on Orbiting Geophysical Observatory, OGO-5, which had a time response similar to that of the instrument used here. The times scale according to which the Mercury data have been plotted has been adjusted by the ratio $[c/(\omega_{pe} V_{sw})_{Earth}]/[c/(\omega_{pe} V_{sw})_{Mercury}]$ to take account of plasma conditions and the speed of the observer, V_{sw}, where c is the speed of light and ω_{pe} is the electron plasma frequency. The similarity between observations at Mercury and Earth is quite striking.

At the times marked on Fig. 3 by the letters A, B, C, and D, the University of Chicago energetic particle experiment (*7*) recorded high-intensity bursts of energetic electrons of short duration. During bursts B and C, energetic protons were also identified. The response of the plasma instrument showed no change in flux or in spectral shape during events A and D. Changes in these quantities did take place during events B and C. After event A, the spectrum was similar to spectrum 4 of Fig. 2. Shortly after event B began (at +1 minute, 31 seconds), the counting rates in our intermediate energy channels fell to the background value, leaving only low rates in the energy channels below 20 ev and in channels above 389 ev. The spectrum then relaxed to the form shown as spectrum 5 in Fig. 2, and retained this shape and approximately the same intensity until +6 minutes, 43 seconds in the middle of event C. After this there were two spectra in which the counting rates at intermediate energies were again reduced to their background values. Then the spacecraft entered the magnetosheath, and the spectrum returned to the form of spectrum 2 of Fig. 2.

Having described the major features of the observations, we now consider features of particular interest in more detail and interpret them in terms of the interaction of Mercury with the solar wind. First, let us consider the possibility that the interaction is with a neutral atmosphere or with an iono-

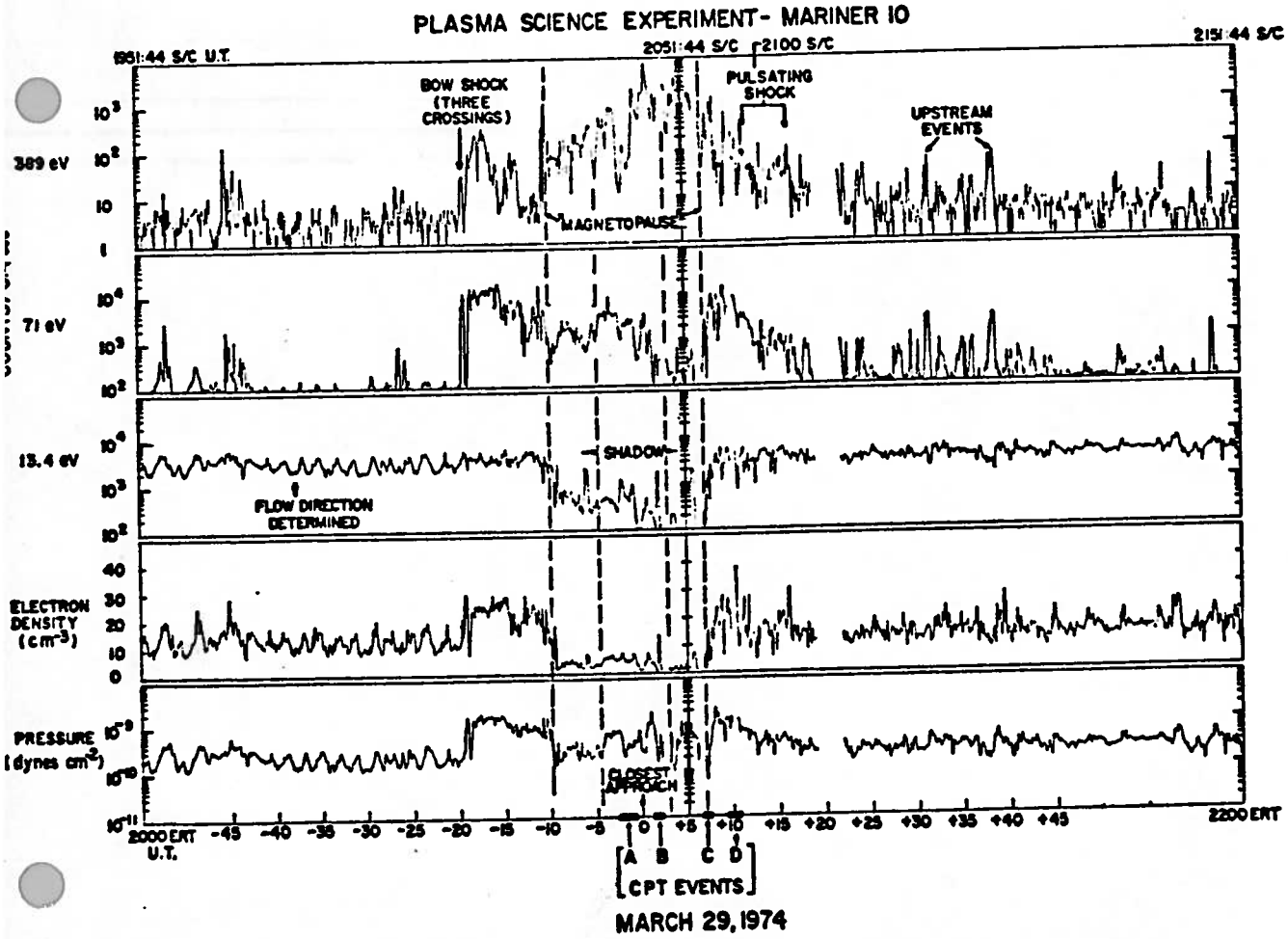

ig. 3. Time plots of the fluxes observed at 389, 71, and 13.4 ev, and the density and pressure deduced from them. The times f events are indicated, and a time scale with zero at the time of closest approach is given along the bottom. The positions of ie boundaries have been assigned on the basis of a consideration of the form of the electron spectrum; CPT, charged particle elescope experiment.

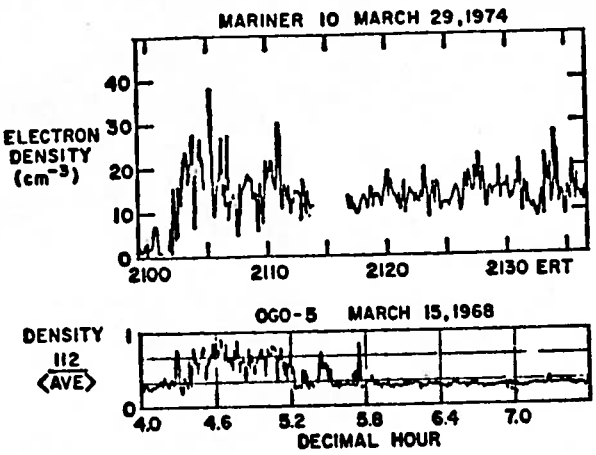

Fig. 4. Observations of a parallel shock made at Earth by OGO-5, compared with the present observations at Mercury. A scaling factor of $[c/(\omega_{pe}V_{sw})_{Earth}]/[c/(\omega_{pe}V_{sw})_{Mercury}]$ has been introduced to compensate for the different environments and spacecraft velocities, V_{sw}, when observing the two shocks. The (112) detector was "looking" toward the traversed shock, as was the Mariner 10 detector after pulsation (outbound) shock crossing.

sphere [as appears to be the case with Venus (*1*)]. The atmosphere of Mercury is thin or "exospheric"; that is, the mean free path for collisions is greater than the atmospheric scale height. The ultraviolet spectrometer experiment (*8*) gives an instrumental background upper limit on the column densities of 3×10^{13} cm^{-2} for neon, 10^{13} cm^{-2} for argon, a measured upper limit of 7×10^{11} cm^{-2} for helium and other column densities with lower values. In addition, an upper limit for the total pressure, P_T, at the terminator, to 2×10^{-9} mbar was inferred from the ultraviolet occultation experiment (*8*). To determine whether the atmosphere alone can stand off the solar wind, we consider the change in the velocity of the wind from its free streaming value, v, to its value v' after it has been slowed down by atmospheric mass addition at the rate $m_i J_i N_i$ (where m_i is the mass, J_i is the ionization rate, and N_i is the column density of the ith atmospheric constituent which behaves as a fluid). For this case, the one-dimensional continuity, momentum, and energy equations give

$$\frac{v}{v'} = \frac{\gamma}{\gamma - 1} \pm \left[\frac{1}{(\gamma - 1)^2} - \frac{\gamma + 1}{\gamma - 1} \sum_i \frac{m_i J_i N_i}{\rho v} \right]^{1/2}$$

where γ is the specific heat ratio and ρ is the solar wind mass density. This equation is consistent with the high-Mach number limit obtained previously (*9*). The plus sign corresponds to the formation of a shock; the minus sign refers to no shock. The maximum mass addition rate preceding the formation of a shock occurs when the argument of the square root vanishes. This fluid equation is realistic only when the ion gyroradius is smaller than the scale of the system, planet plus atmosphere. From the above, we find that the light constituents hydrogen and helium cannot stand off the solar wind. Since the gyroradii for heavier atmospheric ions, >12 atomic mass units, born in the solar wind, are of the order of the scale of the system, a microscopic point of view must be considered. In such cases the time it takes the solar wind to pass through a corresponding scale height is of the order of tenths of seconds while it takes much longer to accelerate heavy ions to the solar wind speed, of the order of tens of seconds for neon and argon. Hence, only a small impulse along the solar wind direction is imparted to heavy atmospheric ions as the wind passes through a scale height above the surface. On this basis we find that the momentum change of the solar wind along X_{sw} is negligible in traversing the maximum argon and neon atmosphere and seems to be small when passing through possible atmospheres limited by P_T. Consequently the solar wind, under this hypothesis, would be expected to strike the surface and be absorbed without forming a shock. However, the upper limits on the neutral gas would permit a strong limb shock (*10*). A limb shock seems to be excluded by the observed locations of the shock crossings, since they occur too far upstream. Therefore, we conclude that the solar wind must be deflected by a magnetic field.

The ionosphere within such a magnetic obstacle appears to be too weak to contribute appreciably to the total pressure. For this to occur a temperature > 10^5 °K would be required, based on the maximum possible ionospheric electron density of 10^3 cm^{-3} obtained from the radio occultation experiment (*11*). Such a temperature is untenably high.

The most likely source of the interaction at Mercury is thus a planetary magnetic field, either intrinsic or induced by the solar wind. It is instructive to consider the simplest possibility and to assume that the magnetic obstacle is a dipolar field. Using a theoretical model (*12*) for the locations of the terrestrial magnetopause and bow shock, we find the corresponding boundary crossings observed at Mercury can be fitted by varying the strength and location of a planetary dipole. In fitting to the model we assume that the dipole axis is perpendicular to the local orbital plane of the spacecraft, and that the Y_{sw}-Z_{sw} trace of the trajectory passes through the origin (Fig. 1). To a good approximation, this plane also contains the solar wind velocity vector, which is along $-X_{sw}$.

Figure 5 shows the result of such a scaling for three cases: case A, using the first inbound shock crossing, the two magnetopause crossings, and a solar wind flow 7° west of the sun; case B, using the last inbound shock crossing, the two magnetopause crossings, and a solar wind flow 7° west of the sun; and case B′, the same as case B but with the solar wind flow 3° west of the sun. For case A, we find that the distance from the center of the planet to the nose of the magnetopause is 1.6 $R_\mathbb{Q}$ and the dipole is located at $X_{sw} = 0.4$ $R_\mathbb{Q}$, $Y_{sw} = 0$, $Z_{sw} = 0$. Corresponding values for case B are as follows: nose distance = 1.25 $R_\mathbb{Q}$, dipole at $X_{sw} = 0.15$ $R_\mathbb{Q}$, $Y_{sw} = 0$, $Z_{sw} = 0$; for case B′ the values are: nose distance = 1.9 $R_\mathbb{Q}$, dipole at $X_{sw} = 0.55$ $R_\mathbb{Q}$, $Y_{sw} = 0$, $Z_{sw} = 0$. If we consider 0° flow, we find that the dipole must be located off the X_{sw} axis with a positive Y_{sw} coordinate. The fits give a range of dipole strengths from 4×10^{-4} to 9×10^{-4} times that of Earth. These dipole model fits clearly demonstrate the impossibility of a unique and accurate determination of the upstream stand-off distance of the magnetopause from the observations made during this single flyby, because of the sensitivity of this quantity to small variations in shock crossing times and flow direction. Furthermore, the dipole may be tilted in a direction different from that assumed, or it may be situated off the X_{sw} axis, or both. A preliminary estimate is that the present experiment can only determine the distance to the magnetopause nose to be less than 2.5 planetocentric radii.

In the above discussion we have not considered the origin of the magneti

ield which causes the plasma interaction observed at Mercury. In general, h[illegible]re three possible sources for the ield: (i) an intrinsic planetary field; (ii) a steady-state induction process (unipolar generator); and (iii) an induction process arising from changes n the direction and magnitude of the ncident magnetic field. Unfortunately, data from the present experiment do not allow an unambiguous choice from among these possibilities. Although the induction processes have been extensively discussed in the literature (*13*), a definitive three-dimensional model is still lacking. For any model which involves an induced magnetic field, some fraction of the incident plasma flow must contact the surface of the planet; hence in this case the nose of the "magnetopause" should coincide with the surface of the planet. Although, in principle, the position of the nose can be calculated from the measured boundary positions and from an adequate theory, as noted above, the measurements reported here lead to large uncertainties in the calculated positions even on the assumption that the theor[illegible]l models were complete. Given th[illegible] experimental and theoretical uncertainties, no definite conclusions can be drawn concerning the origin of the magnetic field.

We consider next some detailed plasma features or events. The fluxes of electrons with energies greater than ~ 100 ev show interesting variations in the inbound magnetosheath, as illustrated by the 389-ev data field in Fig. 3. The flux increases by approximately a factor of 10^2 on crossing the shock and remains high for about 5 minutes. It then decreases to about twice the solar wind value for 1 minute, increases by a factor of 10 for 2 minutes, decreases to slightly greater than the solar wind value for 3 minutes, and remains low until the magnetopause crossing at −10 minutes. These variations might be temporal; however, the two intervals of decreased flux coincide with the times when the scanning angle of the instrument is directed toward the downstream shock (the instrument "looks" farthest from the planet), and the increased flux intervals coincide with [illegible]ning angles directed away from the downstream shock (the instrument "looks" closest to the planet). The variations, therefore, probably represent a directional asymmetry in the particle flux. This could be either a pressure or a streaming anisotropy directed downstream along draped field lines. The second possibility is more likely since the stronger upstream bow shock is a more intense source of electrons than the downstream bow shock.

A different scan modulation of the flux of the > 100-ev electrons was observed by the same instrument in the magnetosheath of Venus, where the highest fluxes were observed at scan directions farthest from the planet. A comparison of the two encounter geometries is given in Fig. 6 in which an inferred draped field line pattern, based on observed upstream magnetometer observations, is shown. In each case the ambient field had approximately the local corotation-spiral direction. At Mercury the maximum flux corresponds to electrons coming away from the upstream bow shock. A similar interpretation could be made for the anisotropy observed at Venus since the flux is a maximum when the instrument is viewing along a field line away from the planet and toward the point where the line crosses the bow shock. However, in the intervals of decreased flux at Venus, the fluxes were much less than the ambient solar wind fluxes, requiring an explanation in terms of an anisotropic electron removal rather than an anisotropic electron source. Figure 6 indicates that removal by interaction with the dayside atmosphere of Venus gives an explanation with the right asymmetery (*1*).

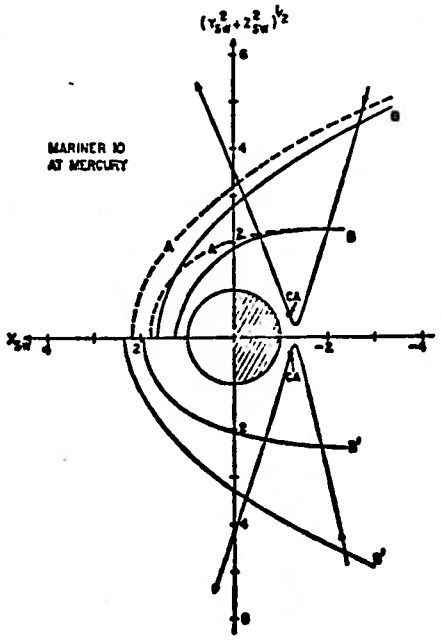

Fig. 5. (Top) The trajectory of Mariner 10, in a coordinate frame moving with the planet for the case of solar wind flow from a direction 7° west of the sun. This flow direction is that of the X_{sw} axis; *A*–*A* and *B*–*B* represent scaled magnetopause and bow shock boundaries, *A* for the incoming bow shock crossing occurring 1 minute before *B*; *CA* is the time of closest approach. (Bottom) *B'*–*B'*, the shock, and magnetopause corresponding to solar wind flow from a direction 3° west of the sun, and the same shock crossing time as *B*.

In the outbound magnetosheath of Mercury variations of the fluxes of energetic electrons also occurred, but these do not coincide with particular scan directions or with the scan period. They are interpreted as due to time-dependent generation by the pulsating shock encountered in the outbound interval. We note the absence at Mercury of intervals with energetic plasma electron fluxes less than ambient solar wind values such as occurred at Venus, and which we interpreted as atmospheric absorption. This absence of absorption is consistent with our earlier conclusion that the atmospheric interaction at Mercury is weak.

The changes in plasma properties observed in the Mercury magnetosphere could be either spatial features or temporal events. A single flyby does not permit a unique interpretation. The combination of highly structured plasma electron data, the magnetic field variations (*3*), and the energetic particle events observed in the magnetosphere suggest that a time-dependent interpretation is a reasonable possibility. If the magnetosphere is either induced or intrinsic, changes in the orientation of the external field can cause dramatic changes in structure. In the case of an induced field, this is obvious since the induced field must change as its driving electric field (equal to $-\bar{V} \times \bar{B}$ or $\partial \bar{B}/\partial t$) changes. For an intrinsic field (Earth's magnetosphere is the best-studied example), we know that rapid time changes occur during events known as substorms. There are some striking similarities between the Mercury observations interpreted as temporal events and substorm phenomenology in the magnetosphere of Earth.

To indicate that a substorm interpretation is a reasonable one to consider, we estimate the possibility of a substorm occurring in the 16 minutes Mariner 10 was in the Mercury magnetosphere, based on a scaling of the magnetosphere of Earth. The relevant time scale is the "convection time" given by the time to cycle all of the magnetic flux, F_t, in the tail under the action of the convection electric potential. The convection electric field varies

from essentially zero when the interplanetary field is oriented antiparallel to the planetary dipole moment to a maximum when the interplanetary field is oriented parallel to the planetary dipole. The maximum potential is approximately $\phi_c = V_{sw} B_{sw} R_{\mathbb{Q}}$, where V_{sw} and B_{sw} are the ambient solar wind speed and field strength and $R_{\mathbb{Q}}$ is the scale size of the magnetosphere. If B_T is the field strength in the tail, the maximum convection electric field gives a minimum cycle time of

$$T_c = F_l/\phi_c \sim \frac{2\pi B_T R_{\mathbb{Q}}}{B_{sw} V_{sw}}$$

For Earth a typical value of T_c is 60 minutes. Scaling to Mercury gives

$$(T_c)_{\mathbb{Q}}/(T_c)_{Earth} = (B_t R_{\mathbb{Q}}/B_{sw})_{\mathbb{Q}} \, (B_{sw}/B_t R_{\mathbb{Q}})_{Earth} \sim 1/50$$

That is, the convection time scale for Mercury is 1/50 that of Earth and is typically between 1 and 2 minutes. Thus, when the external field is oriented to give maximum convection, the substorm time scale for Mercury is approximately 1 or 2 minutes. If the plasma, field, and energetic particle events that began near −2 minutes are Mercury-variety substorms, they begin $\sim 4T_c$ before the spacecraft emerged from the magnetosphere. A consistent interpretation requires a change in external field orientation while the spacecraft was in the magnetosphere. This interpretation will be presented elsewhere (*14*).

The following conclusions may be drawn from the data presented here:

1) A fully developed bow shock and magnetosheath were observed near Mercury. These features provide unambiguous evidence for a strong interaction between Mercury and the solar wind.

2) Inside the magnetosheath there is a distinct region analogous to the magnetosphere or magnetotail of Earth. This region is populated by electrons with lower density and higher temperature than the electrons observed in the solar wind or magnetosheath.

3) The solar wind ram pressure, ρv^2, corresponds to a stagnation pressure equivalent to a magnetic field strength of 170 gammas.

4) The interaction is most likely not an atmospheric or ionospheric one. The assumption of an interaction with an intrinsic magnetic dipole requires a dipole strength approximately in the range 4×10^{-4} to 9×10^{-4} times that of Earth. The data do not preclude an interaction with an induced magnetic field.

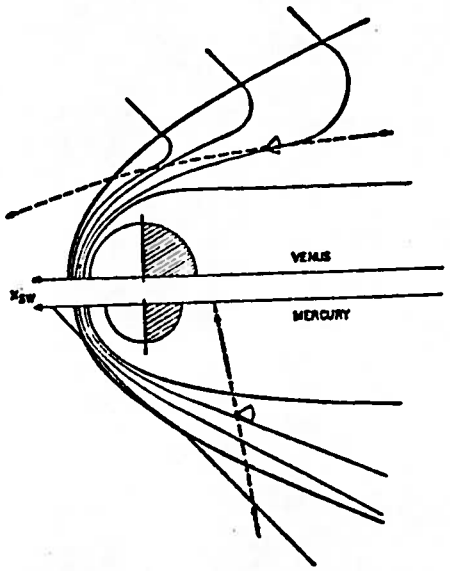

Fig. 6. A sketch of the trajectories of Mariner 10 (not to scale), in the vicinity of Venus and Mercury, and the directions of scanning of the instrument with respect to the likely magnetic field geometry.

5) The particle fluxes and the energy spectra show large variations while the spacecraft is inside the region we have called the magnetosphere. The variations could be either spatial or temporal in nature. It is possible that temporal events similar to substorms on Earth have been observed at Mercury.

6) At the time of observations, conditions were such that a perpendicular shock was observed on the inbound leg and a parallel shock was observed on the outbound leg of the trajectory. Energetic plasma electron events were observed upstream from the outbound shock crossing.

Appendix. In our analysis we have assumed that the spacecraft potential is negligible. In this section we discuss briefly the basis for that assumption and point out that there may have been some significant charging of the spacecraft during the period between events A and C.

If the spacecraft were charged positively, electrons would be accelerated toward the sensor and the peak of the electron distribution would be observed rather than the monotonically decreasing interplanetary spectra exemplified by spectrum 2 of Fig. 2 (*15*). Negative charging would move the distribution to lower energies but must be insignificant since both core and halo components were observed in the energy ranges observed for those components near Earth. In addition, the Mariner 10 densities scaled to 1 A.U. are in good agreement with near-Earth interplanetary densities measured by the LASL and MIT plasma experiments on Explorer 47 and Explorer 50.

During encounter, the possibility of charging to a negative potential can be tested by looking for changes in density when the spacecraft enters and leaves the shadow zone; no changes were observed. For the period beginning after energetic particle event A and ending with the magnetosheath reentry, there is a possibility that positive charging of the spacecraft occurred: the shape of spectrum 4 of Fig. 2 could be explained by a spacecraft potential near 50 volts, and the rather strange spectra observed between events B and C (when the counting rates were low at high and low energy but down to background levels for intermediate energies) could be due to a positive potential in the vicinity of a kilovolt. In that case, the high-energy channels would measure the low-energy portion of the shifted spectrum, and the low-energy counts, which are measured when the deflecting voltage is small, could be due to a large flux of higher energy particles striking a deflecting plate and producing spurious counts. We conclude that the only period of time in which spacecraft charging could have affected the measurements was between charged particle telescope (CPT) events A and C, and that during that time the spacecraft could only have charged positively, as noted above.

K. W. OGILVIE
J. D. SCUDDER
Laboratory for Extraterrestrial Physics, NASA Goddard Space Flight Center, Greenbelt, Maryland 20771
R. E. HARTLE
Laboratory for Planetary Atmospheres, NASA Goddard Space Flight Center
G. L. SISCOE
Department of Meteorology, University of California, Los Angeles 90024
H. S. BRIDGE, A. J. LAZARUS
Center for Space Research and Department of Physics, Massachusetts Institute of Technology, Cambridge 02139
J. R. ASBRIDGE, S. J. BAME
University of California Los Alamos Scientific Laboratory, Los Alamos, New Mexico
C. M. YEATES
Jet Propulsion Laboratory, Pasadena, California 91109

References and Notes

H. S. Bridge, A. J. Lazarus, J. D. Scudder, K. W. Ogilvie, R. E. Hartle, J. R. Asbridge, S. J. Bame, W. C. Feldman, G. L. Siscoe, *Science* 183, 1293 (1974).
M. D. Montgomery, J. R. Asbridge, S. J. Bame, *J. Geophys. Res.* 75, 1217 (1970); J. D. Scudder, D. L. Lind, K. W. Ogilvie, *ibid.* 78, 6535 (1973); W. C. Feldman, M. D. Montgomery, J. R. Asbridge, S. J. Bame, H. R. Lewis, paper presented at the 3rd Solar Wind Conference (Asilomar, Calif., 1974).
N. F. Ness, K. W. Behannon, R. P. Lepping, Y. C. Whang, K. H. Schatten, *Science* 185, 151 (1974).
K. W. Ogilvie, J. D. Scudder, M. Sugiura, *J. Geophys. Res.* 76, 3574 (1971); S. J. Bame, J. R. Asbridge, H. E. Felthauser, E. W. Hones, I. B. Strong, *ibid.* 72, 113 (1967).
E. W. Greenstadt, I. M. Green, G. T. Inouye, D. S. Colburn, J. H. Binsack, E. F. Lyon, *Cosmic Electrodyn.* 1, 160 (1970); E. W. Greenstadt, *J. Geophys. Res.* 77, 1729 (1972); D. H. Fairfield, *ibid.* 74, 3541 (1969).
K. A. Anderson, *J. Geophys. Res.* 74, 95 (1969); F. L. Scarf, F. L. Fredricks, L. A. Frank, M. Neugebauer, *ibid.* 78, 3697 (1973); W. C. Feldman, J. R. Asbridge, S. J. Bame, M. D. Montgomery, *ibid.* p. 3697.
J. A. Simpson, J. H. Eraker, J. E. Lamport, P. H. Walpole, *Science* 185, 160 (1974).
A. L. Broadfoot *et al.*, *ibid.*, p. 166.
L. Bierman, B. Brosowski, H. Schmidt, *Solar Phys.* 1, 254 (1967); P. A. Cloutier, M. B. McElroy, F. C. Michael, *J. Geophys. Res.* 74, 6215 (1969); R. E. Hartle, S. J. Bauer, C. S. Wu, *Int. Assoc. Geophys. Aeron. Bull.* 34, 569 (1973).
10. G. L. Siscoe and N. R. Mukherjee, *J. Geophys. Res.* 78, 3961 (1973).
11. H. T. Howard *et al.*, *Science* 185, 179 (1974).
12. J. R. Spreiter, A. L. Summers, A. W. Rizzi, *Planet. Space Sci.* 18, 1281 (1970).
13. C. P. Sonett and D. S. Colburn, *Nature (Lond.)* 216, 340 (1967); A. J. Dessler, in *Atmospheres of Venus and Mars*, J. C. Brandt and M. B. McElroy, Eds. (Gordon & Breach, London, 1968), pp. 241–250; F. S. Johnson and J. E. Midgley, *J. Geophys. Res.* 73, 1523 (1968); J. V. Holweg, *ibid.*, p. 7269; G. Schubert *et al.*, *NASA Tech. Mem. X-62* (1973), p. 227.
14. G. L. Siscoe, K. W. Behannon, R. P. Lepping, N. F. Ness, *Geophys. Res. Lett.*, in press.
15. S. E. deForest, *J. Geophys. Res.* 77, 651 (1972).

16. We thank all those whose work contributed to the success of the experiment and those whose names are listed in (*1*). We also thank members of the magnetometer, energetic particle, and ultraviolet teams on Mariner 10 for extensive discussions and comparisons of experimental results. We are grateful to E. W. Greenstadt for discussions concerning the nature of pulsating shocks, to V. Vasyliunas for discussions of spacecraft charging, and to M. Acuña for assistance in calibration, and to W. C. Feldman for helpful discussions.

29 May 1974 ■

Magnetic Field Observations near Mercury: Preliminary Results from Mariner 10

Abstract. Results are presented from a preliminary analysis of data obtained near Mercury on 29 March 1974 by the NASA-GSFC magnetic field experiment on Mariner 10. Rather unexpectedly, a very well-developed, detached bow shock wave, which develops as the super-Alfvénic solar wind interacts with the planet, has been observed. In addition, a magnetosphere-like region, with maximum field strength of 98 gammas at closest approach (704 kilometers altitude), has been observed, contained within boundaries similar to the terrestrial magnetopause. The obstacle deflecting the solar wind flow is global in size, but the origin of the enhanced magnetic field has not yet been uniquely established. The field may be intrinsic to the planet and distorted by interaction with the solar wind. It may also be associated with a complex induction process whereby the planetary interior-atmosphere-ionosphere interacts with the solar wind flow to generate the observed field by a dynamo action. The complete body of data favors the preliminary conclusion that Mercury has an intrinsic magnetic field. If this is correct, it represents a major scientific discovery in planetary magnetism and will have considerable impact on studies of the origin of the solar system.

Results from a preliminary analysis of "quick-look" data obtained by the NASA-GSFC magnetic field experiment during Mercury encounter on 29 March 1974 are summarized in this report. The purpose of this investigation was to study the magnetic field environment of the planet Mercury and the nature of the solar wind interaction with it. There is substantial evidence in this initial assessment of the results to support the preliminary conclusion that an intrinsic planetary magnetic field exists. Rather unexpectedly, a very well-developed, strong, detached bow shock wave was observed, as well as a magnetosphere-like region in which the field magnitude increased to 98γ at closest approach, 704 km from the planetary surface. This is a factor of 5 greater than the average interplanetary magnetic field strength of 18γ measured outside the Mercurian bow shock.

Scientific interest in Mercury received a major stimulus in 1965 from data provided by radar observations of the planet. It was discovered (*1*) that the planet's rate of rotation was not synchronous with its orbital motion. Explanations for this remarkable result were soon forthcoming (*2*), and a new era in planetary studies began in which coupling of orbital motion and rotation rates was found to be considerably more complex and informative than previously expected.

For some time, it has been acknowledged that Mercury is anomalous among the terrestrial planets, having a remarkably high average density of 5.6 g/cm^3 for its small radius of 2434 km (*3*). Studies of the planet's interior have been hampered both by the inadequacy of available data concerning its shape, size, and mass and by the absence of definitive information concerning its rotational axis and precessional motion. Only recently have attempts been made to study these problems and their significance in the history of the formation of Mercury (*4*).

The atmosphere of Mercury has also been the subject of considerable speculation (*5*), the earlier work being prejudiced by the erroneous assumption of synchronous rotational and orbital periods. Studies incorporating new radar results (*6*) suggested that revision of the traditional concept of a planet devoid of an atmosphere was necessary.

In the absence of any evidence for appreciable rotation of the planet or for a substantial atmosphere, it was thought that Mercury would resemble our own moon in many respects. Taking into account recent observations of microwave emissions and the newly established correct rotation period for the planet, it was suggested strongly that its surface thermophysical characteristics would be rather close to those of the moon (*7*). There was no evidence for any radio emissions from Mercury such as those from Jupiter's radiation belts.

Thus, with the traditional view of geomagneticians that a rapidly rotating planet with some precession were features essential for generation of a planetary magnetic field (*8*), there was little reason to suggest an intrinsic field of Mercury. Some elementary estimates of a planetary magnetic field were made by using simple scaling laws for planetary volumes or rotation rates, or both, but the bases for these studies were rather speculative.

In specific studies related to the solar wind interaction with Mercury, the results depended on the planet's physical characteristics. Figure 1 summarizes four modes of interaction, of which three have been observed in the exploration of the solar system. In model A, a lunar type of interaction

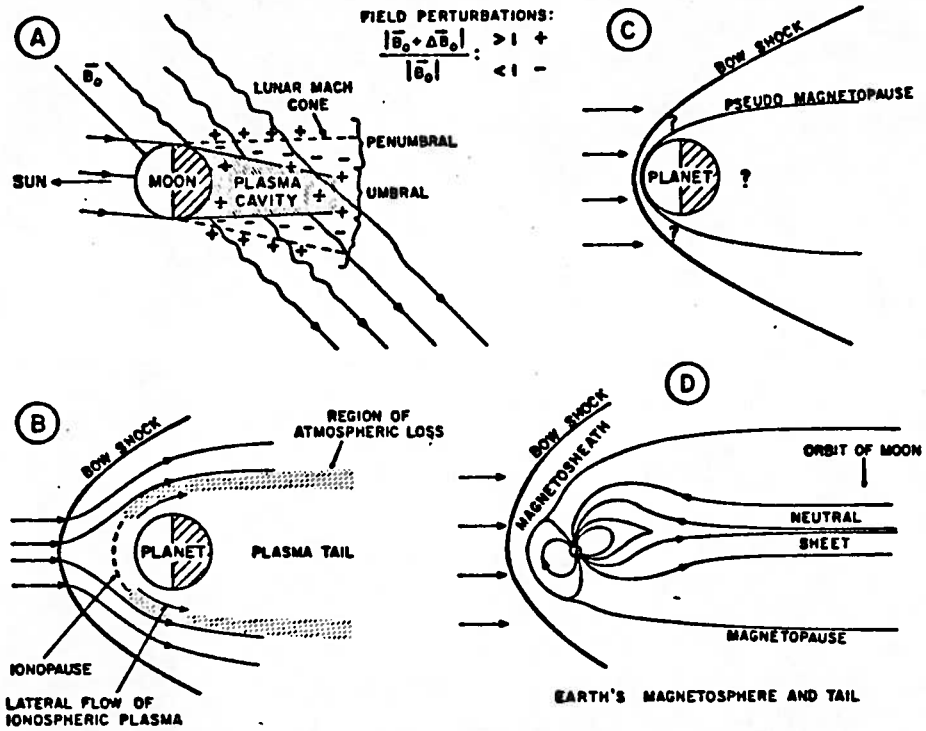

Fig. 1. Four models of the solar wind interaction with an object of planetary size. The weakest interaction, model A, is typified by the moon and occurs in the case of an insufficient intrinsic magnetic field or atmosphere and ionosphere to deflect the solar wind (*9*). In all other models a bow shock develops because of the deflection of super-Alfvénic flow around the planet. The deflection is due to a sufficient atmosphere and ionosphere in model B (*10*); a sufficiently conducting planetary interior in model C; or a sufficient intrinsic planetary magnetic field, as in the case of the earth, in model D.

was proposed (*9*), based on an atmosphere-ionosphere insufficient to deflect the solar wind flow and a planetary interior with electrical conductivity insufficient for induction of a significant secondary magnetic field. In model B, a modest atmosphere-ionosphere was proposed (*10*) and a deflected solar wind flow anticipated, contingent on the specific model of the atmosphere assumed. In this model there was no discussion of the magnetic field in the vicinity of the planet associated with the complex interaction with the magnetized solar wind.

Basic concepts of the induction of a secondary magnetic field were developed in association with studies of the solar wind interaction with the moon (*11*). The secondary magnetic field could be either a steady state field induced by the convective flow of the magnetized solar wind past the planet or a transient field associated with changes in the interplanetary magnetic field as observed at the planet. In the case of the moon, the low electrical conductivity of the surface layer decouples the planet from the solar wind for the steady state interaction mode and only the transient mode of induction is significant. Model C depicts, very qualitatively, a steady state induction mode; the question marks indicate regions where there are critical uncertainties regarding the interaction process and magnetic field topology.

Most authors have assumed that Mercury does not possess a sufficient magnetic field for deflection of solar wind flow. However, for completeness in this discussion and because of the results obtained, we include the solar wind interaction with the earth's magnetic field, model D. Here a substantial magnetosphere is developed which contains permanently trapped energetic particles forming the radiation belts and includes a very well-developed, large magnetic tail extending far downstream away from the sun, much like a comet tail.

Instrumentation. The magnetic field experiment consists of two triaxial fluxgate magnetometers. The dual magnetometer system used on Mariner 10 and its performance characteristics have already been described with the Venus encounter results (*12*). During Mercury encounter, the instrument operated continuously in the high range with each axis covering ±128γ. Vector measurements at intervals of 40 msec with 10-bit precision yielded quantization step sizes of 0.26γ. The root-mean-square noise level of each sensor over the band pass of 0 to 12.5 hertz ranged between 0.03 and 0.06γ, significantly less than the digitization value.

We shall not discuss the instrument further except to remark that, as the spacecraft passed through solar occultation at Mercury, no significant change in the spacecraft magnetic field was noted. This provides experimental in-flight verification of the assumption that the magnetic field of the spacecraft solar array panels was negligible. This solar array feature was designed by appropriate backwiring and tested before the flight, but was not checked at Venus encounter since no solar occultation occurred there. During Mercury encounter, a variable spacecraft magnetic field was observed with a maximum strength of 4γ at the outboard magnetometer.

At this early date, the accuracy of the measurements, combining all sources of error, is estimated to be approximately ±1γ on each axis. The nature of the results and the magnitude of the fields measured are such that this is not a source of significant error in this preliminary report.

Mercury encounter observations. The trajectory of Mariner 10 during Mercury encounter was uniquely well designed for a study of the planetary magnetic field and solar wind interaction. The spacecraft path was approximately perpendicular to the planet-sun line on the dark side of the planet, very close to the antisolar point. See Fig. 2 for a presentation of the trajectory in Mercury-centered solar ecliptic (SE) coordinates. As is readily evident, the spacecraft moved rapidly past the planet, the relative velocity being 11 km/sec. Thus, accurate information relating the time of data acquisition to the time when Mariner 10 was at a particular position relative to the planet is very important.

Magnetic field observations during a 2-hour time interval surrounding closest approach are shown in Fig. 3. The format for presentation incorporates 6-second averaging periods for each orthogonal component of the magnetic field and a reconstituted average vector represented by a field intensity $\bar{F}$ at latitude θ and longitude ϕ in SE coordinates. The RMS parameter, which is invariant with respect to coordinate system, is sensitive to fluctuations on the time scale of tens of seconds or less.

Shortly after closest approach, the acecraft passed into a period of radio cultation during which data were or[illegible]n a spacecraft magnetic tape co[illegible]r for subsequent retransmission. ecial processing at Jet Propulsion boratory, Pasadena, California, has ade available to us quick-look data es for both the real time data and e playback data at encounter.

As Mariner 10 approached the anet, the interplanetary magnetic ld was slightly disturbed relative to servations made several days previsly, as measured by the RMS value d as noted in the variable average ld magnitude and direction. The agnitude was $18 \pm 2\gamma$, only slightly wer than expected from an extrapola-n of the average magnetic field of observed at 1 A.U. to the Mercury counter heliocentric distance of 0.46 U. The well-known formulas for the chimedean spiral magnetic field emdded in the interplanetary medium edict a field magnitude of 22γ at a ar azimuthal angle ϕ of 155° or 335° for a solar wind velocity of 400 km/sec.

As can be seen from the data in Fig. 3, there are significant discontinuous changes in the magnetic field in the vicinity of Mercury. These cannot be interpreted in terms of a variable interplanetary magnetic field being swept past the spacecraft. The figure includes identification of both inbound and outbound bow shock crossings as well as apparent magnetopause traversals. The interpretation of these phenomena is based on our understanding of the bow shock and magnetopause observed in the terrestrial case. The character of the magnetic field observations is immediately reminiscent of observations obtained with a spacecraft traversing the earth's magnetosphere on the dark side at a distance of approximately 8 to 12 earth radii.

The very sharp change in magnetic field strength to values greater than 40γ noted at 2027 to 2028 U.T. (universal time) represents the inbound crossing of the Mercurian bow shock. In fact, three crossings occur during this time interval. The jump characteristics of the magnetic field at the bow shock are discussed below in a presentation of the more detailed data. Subsequently, the spacecraft is immersed in a sheath or boundary layer in which a disturbed magnetic field regime exists. As the spacecraft continues along the trajectory, the field magnitude decreases steadily to 30γ in a manner characteristic of a steady state magnetosheath. Mariner 10 again traverses a sharp boundary at 2037 U.T. at which the magnitude of the field increases to more than 40γ, while the fluctuations decrease significantly. Most importantly, the direction of the magnetic field simultaneously changes abruptly by 135° (see plot of ϕ in Fig. 3). The magnetic field then increases steadily up to the maximum of 98γ near closest approach at 2047 U.T. The direction of the magnetic field is mainly parallel to the Mercury-sun line with a polarity sense away from the planet. There is also a smooth

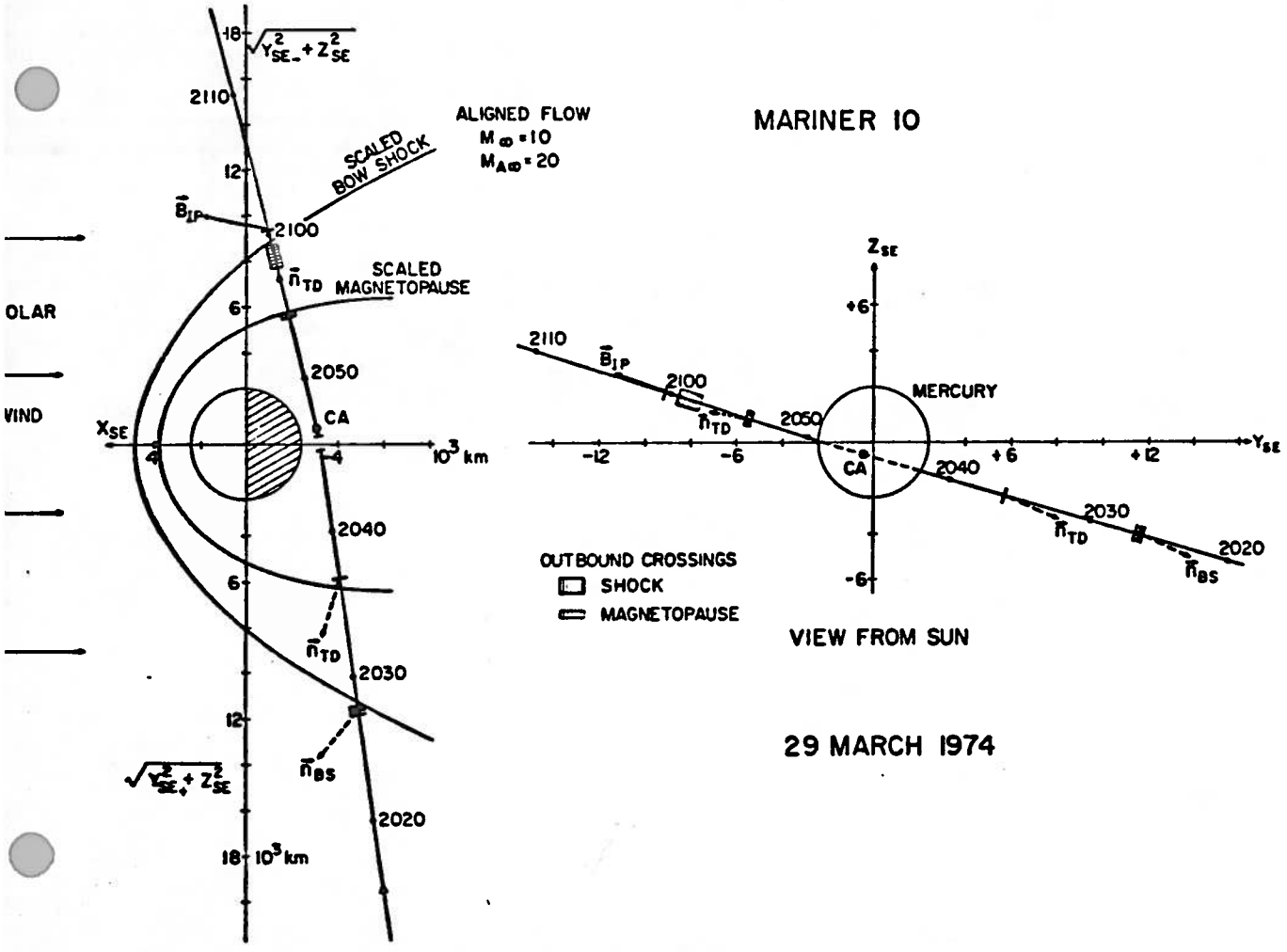

. 2. Encounter trajectory of Mariner 10 in Mercury-centered solar ecliptic (*SE*) coordinates (+ X_{SE} axis toward the sun, Z_{SE} axis pendicular to the ecliptic, and Y_{SE} axis completing a right-handed coordinate system). (Left). Plot of the distance from the X_{SE} as ordinate; (right) true projection of the trajectory as viewed from the sun. For other abbreviations see Fig. 3 and text.

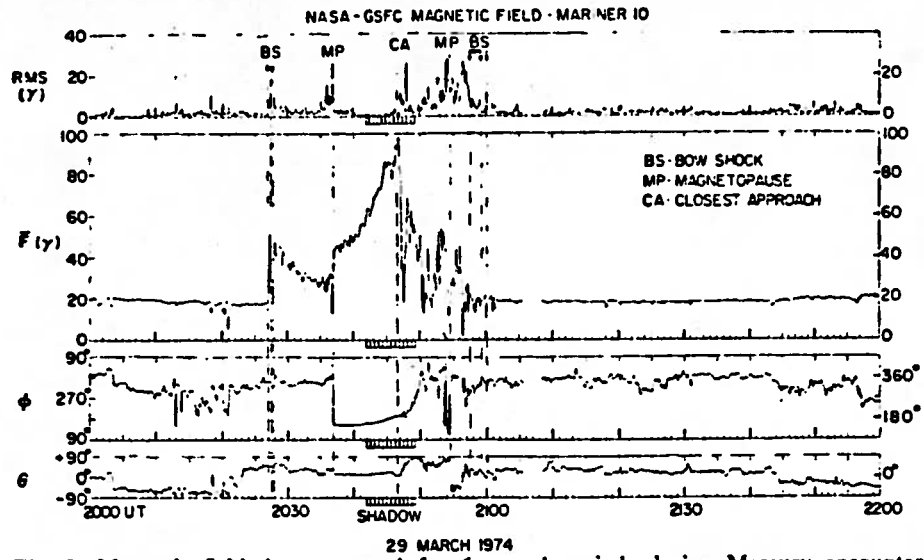

Fig. 3. Magnetic field data averaged for 6-second periods during Mercury encounter in spacecraft-centered solar ecliptic coordinates. The latitude of the magnetic field vector is represented by θ and the longitude by ϕ; the field intensity is $\overline{F}$, and RMS represents the Pythagorean mean of the root-mean-square deviations in the X, Y, and Z components computed during the 6-second periods. Significant discontinuities observed in the magnetic field data are identified.

but small variation in the orientation of the field throughout this time period.

Following closest approach, there occurred a distinct change in the character of the magnetic field. Large-amplitude variations over a wide range of time scales are observed. A large field depression with a minimum of 17γ occurs precipitously just after closest approach, with the field magnitude rising back soon afterward to 70γ. Subsequently, the field magnitude varies considerably, while the direction steadily changes to point northward relative to the ecliptic. The considerable variability in the field magnitude is not accompanied by a comparable variability in field direction.

Between 2054 and 2055 U.T. the magnetopause is crossed outbound, although it is a less distinct crossing and the field directional change is primarily a change from northward to southward. As the spacecraft continues on in the sheath, it encounters magnetic fields highly variable in both direction and magnitude, and the bow shock crossing is not readily apparent in this format.

The detailed 40-msec data, to be presented shortly, indicate that the outbound bow shock crossing (or crossings) occurred somewhere between 2057 and 2059 U.T. within the region indicated in Fig. 3. This bow shock crossing is similar to that observed by Mariner 10 during Venus encounter (*12*) in which there was no abrupt and distinctive jump. This is probably associated with the relative geometry of the upstream interplanetary magnetic field and the shock surface. When the interplanetary field direction is closely aligned with the shock surface normal, the shock is referred to as parallel. Under such circumstances, large-amplitude fluctuations are known to occur from studies of the earth's bow shock (*13*). This type of pulsation bow shock occurs moderately often on the dawn side of the earth's bow shock because of the Archimedean spiral geometry of the interplanetary magnetic field.

More detailed presentations of subsets of the data are given in Figs. 4 and 5. In addition to F, θ, and ϕ describing the instantaneous vector measurements at 40-msec intervals, the X, Y, and Z SE components are also presented. The clear and distinctive appearance of high-frequency fluctuations just outside the inbound bow shock is evident in Fig. 4A. That three crossings occurred is interpreted as representing relative motion of the bow shock across the spacecraft due to moderate changes in the upstream interplanetary medium and the response of the Mercurian bow shock configuration. The nature of the fluctuations in the sheath region is seen to be rather different. High frequencies are observed outside (that is, upstream from the bow shock) while relatively lower frequencies are observed in the sheath (downstream).

Inside the magnetopause, the field is very steady and any fluctuations are very small. This character of the magnetic field is continued through to the maximum field period shown in Fig. 4C. Small sinusoidal perturbations of the magnetic field, analogous to micropulsations observed terrestrially, occur between 2045 and 2046 U.T. However, these detailed data in the magnetosphere-like region show that the field magnitude is extremely steady and give no indication that any of the variability of the interplanetary magnetic field or the sheath region has been transmitted into this region of the Mercurian magnetosphere. This segment of the data reflects what is ideally expected from observations obtained while traversing any planetary obstacle on its dark side if the planet possesses a magnetic field sufficiently strong to deflect the solar wind and lead to the development of a detached bow shock wave.

Details from the outbound magnetopause and bow shock crossings are shown in Fig. 5. The magnetopause is identified at 2054 U.T. by the abrupt change in the latitude angle θ from northward to southward. This is followed by a period of relatively rapidly alternating sign, seen for approximately 40 seconds. This is believed to reflect the relative motion of the magnetopause and the variability of the magnetospheric structure, probably due to variations in the interplanetary medium and the response of the Mercurian environment to these fluctuations. It may also reflect the close proximity of the spacecraft to a neutral sheet–field reversal region such as is found in the earth's magnetic tail. The sheath region is again well defined by relatively larger amplitude fluctuations of all three field components.

With the better time resolution, the bow shock is now somewhat more distinctive. The fluctuations change from relatively lower frequencies and larger amplitudes to higher frequencies and smaller amplitudes. The period of bow shock crossings is extended, however, from 2057 to 2059 U.T., with a more distant bow shock crossing apparently observed just after 2100 U.T.

The identification of the time of occurrence of these various boundaries is important in determining the relative positions of the solar wind obstacle boundary, the magnetopause, and the detached bow shock. The identified positions of the boundaries are superimposed on the trajectory plot of Fig. 2 with uncertainties indicated accordingly. Also included are two curves representing a scaled magnetopause and bow shock, both obtained from

oretical studies of the solar wind eraction with the geomagnetic field. e shape of the magnetopause shown ') is computed for the case of the ir wind incident on a Mercury- te magnetic dipole orthogonal he solar wind flow (assumed along V_{SE}) and the plane of the figure. e bow shock shown (*15*) is scaled ording to a sonic Mach number $_s$) of 10 and Alfvén Mach number $_{As}$) of 20 at the subsolar point. ese values correspond approximately the measured values of the inter- netary magnetic field, plasma den- , and velocity. The theoretical bow ck position presented here is for the y solvable case so far in magneto- rodynamics, that of aligned flow, which the upstream magnetic field solar wind velocity are parallel. ce it is assumed that the apparent ir wind direction is parallel to the rcury-sun line, this implies a true from 3.7°E, when the effect of rration due to planetary heliocentric ital motion is allowed for.

No direct attempt has been made to ust the scaled curves to exactly fit observed boundary traversals. But comparison with the observed ndary positions is remarkably good, s ng the normal variability of the solar wind and its concomitant effects.

For this fit, the value of the stagnation point distance (*14*)

$$r_{s_p} = 1.07\left[\frac{M^2}{4\pi mnV^2}\right]^{1/6}$$

has been assumed equal to 1.6 Mercury radii (R_M) ($R_M = 2434$ km). (Here M is the magnetic moment, m the proton mass, n the plasma density, and V the solar wind velocity.) With the measured value of $n = 17$ particles per cubic centimeter and the estimate of $V = 600 \pm 50$ km/sec, M is determined to be $380 \pm 32\gamma\ R_M^3$.

Analysis of boundary crossings. The relative position of the bow shock and magnetopause boundaries is important in determining the geometry of the obstacle to solar wind flow. In order to obtain accurate estimates of the appropriateness of the fit of the bow shock and magnetopause boundaries, normal vectors to these surfaces have been calculated where possible. They are valuable since they augment the discrete point location by permitting extrapolation of the surface shape beyond the point of observation. This is analogous to a classical boundary value problem in which one has information that fixes the slope as well as the magnitude of a quantity of interest at a specific boundary.

The inbound bow shock was first observed at 2027:20 U.T., immediately followed by another crossing, which appears as a reverse shock, and finally the third and last crossing at 2027:50 U.T. Average magnetic field quantities were used in estimating the shock normal. An analysis interval of 84 seconds immediately preceding the first crossing and another interval of 84 seconds after the last crossing were used. It is implicitly assumed that the interplanetary magnetic field is stationary during 3½ minutes. The preshock and postshock field averages in standard X, Y, Z SE coordinates, normalized to unity, and their respective magnitudes were found to be

$$\hat{B}_{pre} = (0.630, -0.237, 0.740)$$
$$|\bar{B}|_{pre} = 17.3\gamma$$

and

$$\hat{B}_{post} = (0.497, -0.119, 0.860)$$
$$|\bar{B}|_{post} = 40.3\gamma$$

Hence, the field magnitude jump ratio was 2.3 and the angle between the preshock and postshock field vectors was 12°, implying that the field vectors were almost parallel. Under this condition, the shock normal cannot be cal-

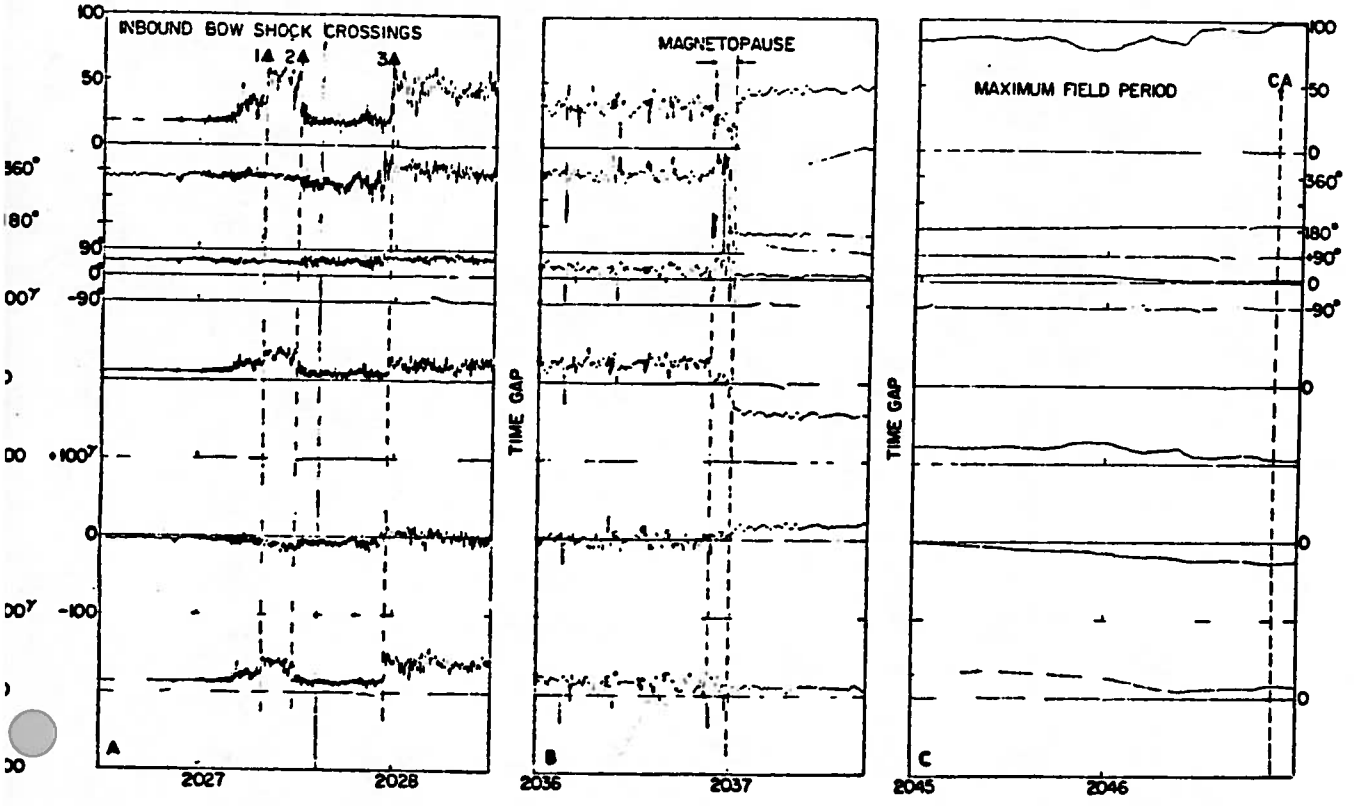

4. Detailed magnetic field data taken with an instrument sampling rate of 25 hertz during the inbound bow shock and netopause crossings and near closest approach (*CA*). The three orthogonal components are presented in the bottom three s.

culated by using the magnetic coplanarity theorem (*16*) because of an unacceptable magnification of errors (*17*). Since data for the ion component of the plasma were not available, a more sophisticated method of least squares fitting to the shock conservation equations was not possible either (*17*).

However, the data show that the shock character was typically that of an approximately perpendicular type (that is, the shock surface normal is perpendicular to the upstream field). Thus, this was assumed as was the cylindrical symmetry of the bow shock surface about an axis parallel to the X axis. With knowledge of the spacecraft position at the crossing, this is sufficient to yield an accurate estimate of the bow shock normal

$$\hat{n}_{BS} = (0.65, 0.70, -0.30)$$

This corresponds to longitude $\phi = 47°$ and latitude $\theta = -18°$, while the angle between the bow shock normal and the X axis is 50°. The angle between the projection of the bow shock normal onto the YZ plane and the Y axis is found to be $-23°$. Figure 2 shows the bow shock normal in terms of the relevant angles.

Using the upstream field magnitude of 17γ and the plasma density of $n =$ 17 particles per cubic centimeter from the Mariner 10 plasma science experiment, we compute the upstream Alfvén speed to be $V_A = 90$ km/sec. Assuming that the protons behave according to the relation between plasma bulk velocity and temperature valid at 1 A.U. (*18*), we calculate the sound speed to be $V_s = 60$ km/sec. The component of the upstream plasma bulk speed along the bow shock normal is 390 ± 42 km/sec, with 600 ± 50 km/sec as the value for the solar wind speed. Hence, the upstream fast mode Mach number is 3.6 ± 0.3 and the sonic Mach number is 6.5 ± 0.5. This yields good agreement with the magnitude of the field jump ratio of 2.3 (*19*).

The inbound crossing of the obstacle to solar wind flow was assumed to be a classical magnetohydrodynamic tangential discontinuity (TD) (*16, 20*), across which no plasma flow takes place and perpendicular to which no magnetic field exists. Hence, using the magnetic field data alone, we computed a normal to this boundary observed at 2036:50 U.T. with 84-second averages for precrossing and postcrossing observations. This yields a normal of

$$\hat{n}_{TD} = (0.30, 0.88, -0.36)$$

The angular coordinates of this normal are longitude $\phi = 72°$ and latitude $\theta = -21°$. Accordingly, the angle with respect to the X axis is 73° and the angle to the Y axis in the YZ plane is $-22°$. The field magnitude jump ratio across this boundary was 1.6. Such a tangential discontinuity is expected at a classical magnetopause boundary crossing. It is often the case for the terrestrial magnetopause.

A similar calculation has been done for the outbound crossing of the obstacle boundary, which occurred at 2054:15 U.T. For the analysis 42-second intervals were used to obtain preboundary and postboundary averages; a 42-second interval including the crossing was omitted because of the high RMS values of the components. From these data, the normal to the tangential discontinuity on the outbound crossing is

$$\hat{n}_{TD} = (0.26, -0.94, 0.21)$$

The longitude $\phi = 285°$ and latitude $\theta = 13°$. Accordingly, the angle with respect to the X axis is 75° and the angle to the Y axis in the YZ plane is 13°. The normal is not as accurately determined for the outbound crossing as for the inbound crossing because of the greater fluctuations of the magnetic field near the outbound obstacle boundary.

The outbound bow shock crossing, occurring between 2057 and 2059 U.T. and briefly at 2100 U.T., appears to be a multiple crossing of a pulsation shock. This occurs, as previously mentioned, when the shock is of the parallel type, that is, when the field direction

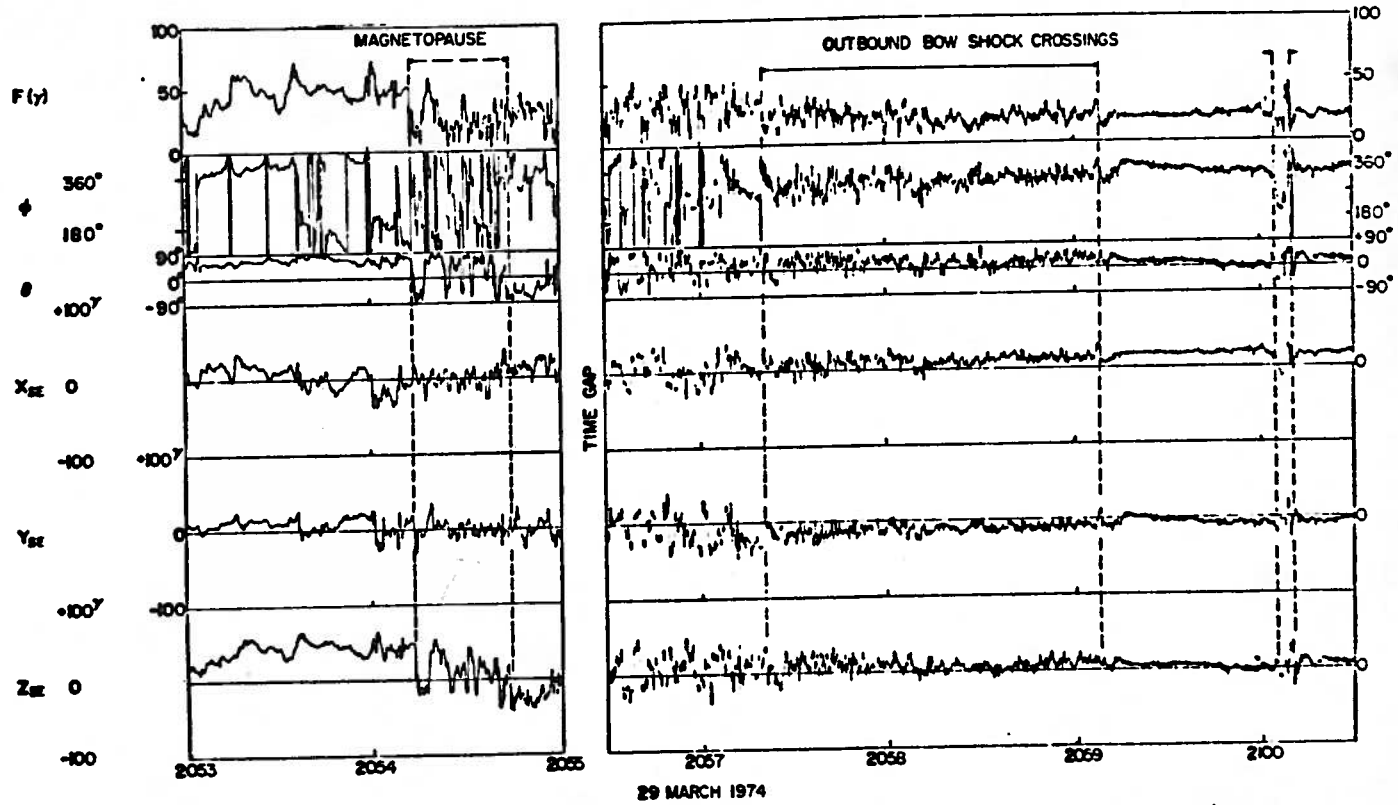

and shock normal are aligned with each other (*13*).

Figure 2 shows the projections of the tangential discontinuity normals on the trajectory. In addition, the solid in Fig. 2 correspond to theoretical boundary positions, as discussed above. There is remarkably good agreement between the computed normals and the calculated boundary positions. This agreement between extrapolated surfaces determined from the normals computed at the boundary crossings and the boundary positions themselves leads us to conclude that the obstacle to solar wind flow is global in size. That is, it is not plausible to expect that a trailing shock such as a limb shock, due to the deflection of the solar wind near the terminators of the flow, would lead to the geometrical configuration and the shock strength measured by the Mach number which are required by these magnetic field data.

It should be noted that both the identification of the time of occurrence of these boundaries (bow shock and magnetopause) and the nature of their signatures (abrupt or diffuse) are in excellent agreement with the results of the plasma science experiment on iner 10.

Interpretation of the origin of the magnetic field. The origin of the interplanetary magnetic field upstream of either the bow shock or the magnetopause is the solar magnetic field. Within the magnetopause boundaries, the field is the vector sum of secondary magnetic fields associated with the solar wind interaction and any intrinsic planetary magnetic field.

There is no unique characteristic of the data that makes it possible to separate the internal and external contributions, since the data are only for a very restricted region of space along the spacecraft trajectory. If magnetic field data were available over a closed surface enclosing the planet, it would be possible to separate the internal and external sources by using classical methods of mathematical analysis (*21*).

Thus, in our preliminary interpretation, we have considered the simple model of an offset, tilted dipole as representing the intrinsic field of the et. Further, we have assumed that this represents the major contribution of the observed magnetic field only during the interval from 2041 to 2050 U.T., surrounding closest approach, when the spacecraft is within 2400 km of the planetary surface. By using selected data from this interval and minimizing the mean-square fit of the assumed dipole, we obtain a result whose fit to the data is illustrated in Fig. 6. The observed and theoretical orthogonal magnetic field components are presented, and a reasonably good fit is obtained. Discrepancies, especially in the X component, may be due to the secondary magnetic fields associated with currents flowing on the magnetopause extending the planetary magnetic field out behind the planet to form a magnetic tail. While there are indications that the discrepancies after closest approach may be due to complex local fields on the planetary surface, they probably represent time variations of the structure of the Mercurian magnetosphere.

The coordinates and values of the dipole so determined are as follows: The position is offset 0.47 R_M at $\phi = 62°$ and $\theta = 17°$; the moment has magnitude 227γ R_M^3 at $\phi = 209°$ and $\theta = -70°$. These preliminary values are uncertain, in a mathematical sense, by approximately 10 percent in offset distance, 20 percent in the magnitude of the dipole moment, and 10° in all direction angles.

This intrinsic magnetic dipole is oriented within 20° of the ecliptic pole, or almost aligned with the axis of rotation of the planet, considering that there is an uncertainty of some 10° in the planetary rotation axis. The large offset might appear at first to be anomalous. However, considering the very large core size (*22*) indicated by the anomalously high average density of the planet, it is quite acceptable.

A further implication of this dipole concerns the magnetic field configuration of the Mercurian magnetosphere. An isointensity map of the intrinsic magnetic field on the surface of the planet is presented in Fig. 7A. Also included are intersections of the magnetic poles and equator and the trace of the Mariner 10 subspacecraft point. The field at an altitude of 0.6 R_M (1460-km elevation) is presented in Fig. 7B. This is the appropriate distance for the stagnation point inferred in the previous section, when the interpretation of the obstacle boundary and bow shock position was made.

Immediately evident in these two isointensity contour maps is the asymmetry due to the dipole offset. The magnetosphere of Mercury is clearly not as symmetrical about the Mercury-sun line as the earth's is about the earth-sun line. However, it is plausible to assume that a magnetic tail and embedded neutral sheet–field reversal region will be developed on the dark side, similar to the earth's. Then the effect of the dipole offset and tilt would be to bring the neutral sheet region closer to the surface of the planet near the dawn terminator than at the dusk terminator at the time of encounter, 29 March 1974. The weaker fields and closer proximity to the magnetic equator, as Mariner 10 approached the outbound magnetopause, combine to yield a consistent image of the origin of the field as due to an intrinsic but modest magnetic field of the planet Mercury.

The offset of the dipole in the YZ plane will have an effect on the positions of the magnetopause and bow shock. However, there is some compensation due to the dipole tilt, so that the net effect may not lead to a significant inconsistency with the results illustrated in Fig. 2 where a centered dipole with no tilt was assumed. Similarly, the offset in the $+X$ direction, 0.21 R_M, compensates the lower moment determined, 227γ R_M^3, relative to the value of 380γ R_M^3 inferred only from the boundary positions. The stagnation point distance from the YZ plane is then found to be approximately 1.7 R_M, which compares favorably with the previously used value of 1.6 R_M, considering the uncertainty associated with the fitting of the theoretical bow shock and magnetopause surfaces to the observed crossings and normals.

Possibilities of induction mode. The steady state or unipolar induction mode is generated by the electrical field $\mathbf{E} = -\mathbf{V} \times \mathbf{B}$ associated with the solar wind convective transport of the interplanetary magnetic field $\mathbf{B}$ past the planet (*23*). The resulting electrical currents close in the solar wind, regardless of whether they are induced in the ionosphere or the planetary interior (*24*). For such a mode there must be direct electrical contact between the ionosphere or planetary surface and the solar wind. Thus, the solar wind cannot be completely deflected away from the ionosphere or the planet itself.

The observations by Mariner 10 of the Mercurian bow shock and magnetopause correspond to positions and characteristics which are not consistent with such a postulated geometry, where only a portion of the flow is deflected and this occurs very close to

the planet. Also, the magnetic field topology as observed at the magnetopause is not consistent with the theoretical field configurations in which the magnetic field is draped around the planet (*24*). A recent quantitative study of the steady state induction mode appropriate to the moon assumes complete absorption of the solar wind on the upstream hemisphere (*25*). The magnetic field configuration obtained confirms the earlier qualitative studies (*24*) and does not show large directional changes at what would correspond to the magnetopause, which are clearly seen in the Mariner 10 data. Finally, no modest-sized magnetosphere-like region was observed at Venus (*12*), the normalized stagnation point distance being only 1.025 whereas at Mercury it is ~ 1.6. These many considerations of boundary positions and inferred obstacle size, as well as the solar wind deflection, existence of a magnetosphere-like region, magnetic field topology, and comparative solar interaction studies, lead us to conclude that the unipolar steady state induction mode was not active at Mercury encounter.

The transient induction mode is generated by an implicit time variation of the interplanetary magnetic field as seen by the planet. This can be due to either an explicit time variation of the interplanetary magnetic field, $\partial \mathbf{B}/\partial t$, or a spatial variation, $\mathbf{V} \cdot \nabla \mathbf{B}$, due to the convection past the planet of a spatially varying interplanetary field. For this mode, electrical currents circulate completely within the planetary ionosphere or interior and no direct electrical contact with the solar wind is required. Again, the absence of a modest-sized magnetosphere at Venus during the extended period when such a feature could have been observed suggests that, even if a significant Mercurian ionosphere existed, the transient induction mode would not be active.

The quasi-static nature of the magnetic field observations during the inbound portion of the Mariner 10 trajectory at Mercury encounter implies that a magnetosphere-like region had existed on a time scale at least of the order of the time interval from inbound bow shock crossing to closest approach. This places a constraint on the minimum conductivity of the planetary interior since the characteristic time constant for decay of electrical currents in such a mode is given by

$$\tau = \frac{\mu_0 \sigma R_M^2}{\pi^2}$$

Assuming a magnetic permeability (μ_0) of free space and a uniformly conducting planet, we obtain a minimum conductivity (σ) of 10^{-4} mho per meter. This is not an unreasonable value for silicates at the elevated temperatures which must be appropriate in the Mercurian interior, and it is easily satisfied by any metal phases, although it depends very much on the detailed grain structure and intergrain electrical connections. However, the value is rather implausible for near-surface material, even at the subsolar point.

A model of a uniformly conducting planet is not a reasonable assumption, and a model of an insulating shell surrounding a conducting core requires a combination of higher magnetic permeability and conductivity. Neither of these two requirements create special problems for Mercury because its high aver-

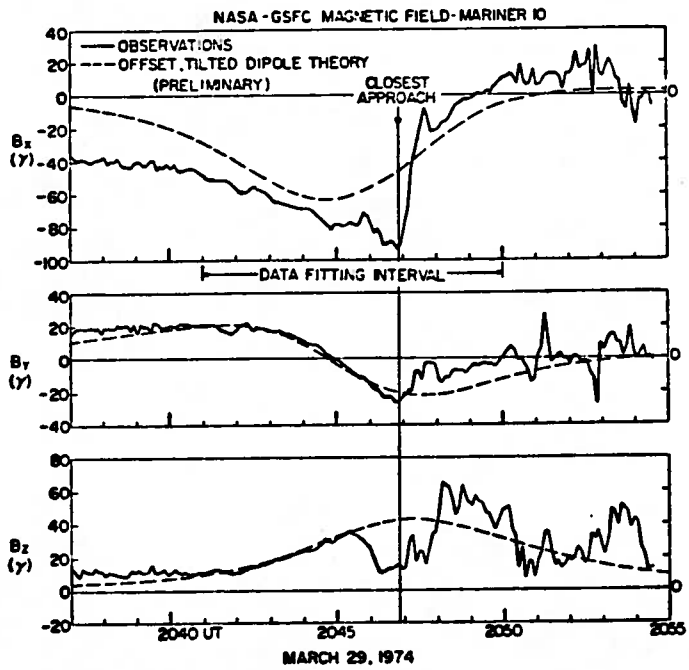

Fig. 6 (left). Comparison of observed and theoretical orthogonal components (B_X, B_Y, B_Z) of the magnetic field near closest approach. The observational data are averaged over 6-second periods. The theoretical planetary magnetic field is represented by an offset, tilted dipole chosen to best fit the data in a least-squares measure during the interval 2041 to 2050 U.T. (see text).

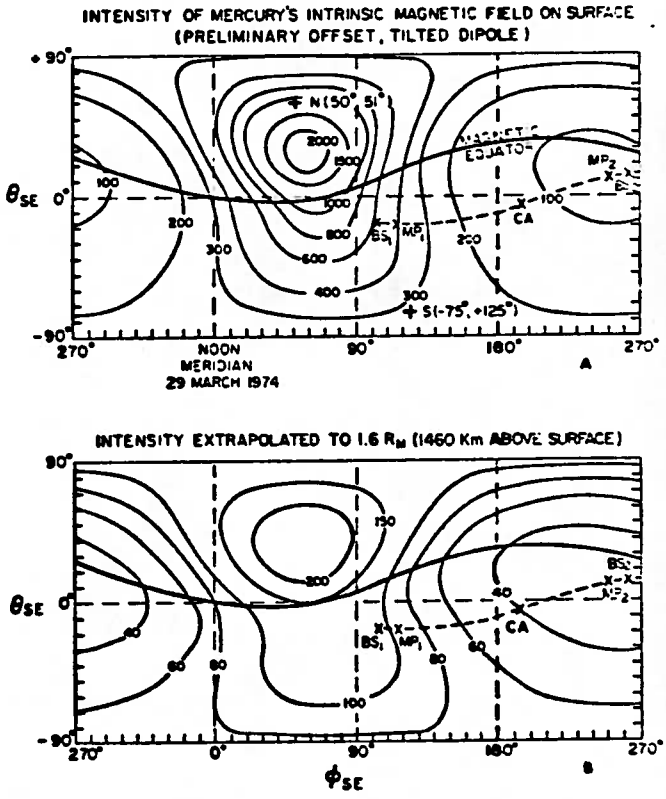

Fig. 7 (right). Predicted isointensity contours and characteristics of an intrinsic magnetic field on the surface of Mercury (A) and at an elevation of 1460 km from the surface (B). The magnetic polarity is in the same sense as the earth's. The appreciable offset distorts the surface field so that it varies by more than an order of magnitude over the surface. The position of Mariner 10 during encounter trajectory and the associated bow shock (*BS*) and magnetopause (*MP*) crossings are indicated relative to the magnetic equator.

age density implies a substantial iron-rich core (22). Moreover, the secondary magnetic field which would develop in such a mode is dominated by a dipole t[illegible] Since there were significant, abrupt changes in the interplanetary magnetic field direction near 2020 U.T., we do not believe it possible at present to reject the possibility of an induction mode. However, it requires a unique combination of circumstances coincident with the time of encounter and also a very strong secondary field, much stronger than in the lunar case, in order that the obstacle be as large as has been inferred. We believe the most plausible explanation is the conclusion offered in the previous section, that Mercury has a modest intrinsic magnetic field.

Discussion. In the previous sections, arguments for the interpretation of the magnetic field observations in terms of a modest intrinsic planetary magnetic field have been presented. In the analysis yielding an offset, tilted dipole it was explicitly assumed that there were no time variations in the structure of the Mercurian magnetosphere during Mariner 10 observations. However, it should be noted that the characteristic c[illegible]ge in magnetic field data from a tail-like configuration to a more dipole-like configuration following closest approach may be due to a temporal change in the Mercurian magnetospheric structure. By intercomparing these data with the plasma and particle measurements, it should be possible to clarify this possibility.

One effect of such a temporal variation on the interpretation would be that it could masquerade as a spatial variation of the magnetic field and lead to an erroneous conclusion regarding the magnitude of the dipole offset and tilt.

These results have significant implications regarding the present state and past history of formation of Mercury. The intrinsic planetary magnetic field may be due to a dynamo currently active within the planetary interior, or it may be a residual remanent magnetic field associated with a now extinct dynamo. Thus, it is possible that Mercury rotated faster earlier in its history than at present. On the other h[illegible] if the transient induction mode is the source of the field, it places a constraint on the interior electrical conductivity.

Assuming that the intrinsic dipole interpretation is correct, we can reach some conclusions regarding the interaction of the solar wind with Mercury in its present state. The large offset and modest size of the dipole moment suggest that, under normal conditions, Mercury should not have a permanent trapped radiation belt. However, a magnetic tail should exist and should contain an embedded neutral sheet–field reversal region where particles are accelerated by field line merging.

Because the dipole is approximately perpendicular to the planet's orbital plane, the size of the Mercurian magnetosphere and tail would not change significantly during the Mercurian year. However, the distance of the stagnation point of solar wind flow relative to the subsolar point on the planetary surface would change considerably because of the large dipole offset. Because of the variation in the heliocentric distance of Mercury, the temporal variations in the solar wind momentum flux, and the changing value of the planetary field in the subsolar region, it should be possible for the solar wind to compress the planetary field to the surface. Thus, since the surface of the planet would not always be protected from the direct impact of solar wind flux, the optical properties of the planet's surface in certain regions should reflect the effects of proton bombardment characteristically observed on the lunar surface.

If Mercury also has a weak atmosphere, then acceleration of particles in the neutral sheet might lead to precipitation of particles into the polar regions and to "auroral" events. Direct access of particles from the interplanetary medium to the polar region is always possible.

These are speculative remarks, but represent logical conclusions based on the existence of an intrinsic Mercurian magnetic field. We once again emphasize the preliminary nature of the interpretation. The offset, tilted dipole result inferred in this first analysis should not be taken as more than a logical and simplified starting point for studying what is certainly a complex interactive process. We interpret these results, however, as strongly suggesting that an intrinsic field does indeed exist. Final confirmation of this conclusion will be possible if another appropriately configured Mercury encounter takes place. Unfortunately, the second encounter by Mariner 10 will not satisfy this requirement and it is not expected therefore to contribute any additional useful data to these investigations.

Conclusions. Direct observations of the magnetic field environment of Mercury by the magnetic experiment on Mariner 10 show the presence of a well-developed bow shock wave and magnetosphere region. A fundamental question not yet uniquely resolved is whether the magnetic field observations are consistent with an intrinsic planetary magnetic field or with a field induced by solar wind interaction. Considering the well-studied solar wind interaction with the moon and the recent Mariner 10 observations at Venus, it appears that the magnetic field data are not consistent with the steady state induction mode of interaction but may be consistent with the transient mode.

The modest size of the apparent magnetosphere of Mercury precludes a determination of an assumed intrinsic magnetic moment with high confidence. Preliminary analysis of a restricted data set obtained near closest approach yields an offset tilted dipole whose parameters are generally consistent with other aspects of the data. The moment's magnitude is $227\gamma\ R_M^3$, which is 4.1×10^{-4} that of the earth's dipole moment. Whereas the dipole's offset, $0.47\ R_M$, is significant, the tilt is within 20° of the ecliptic pole. This is probably close to the planetary rotation axis, itself uncertain to 10°. With the anomalously high average density of this small terrestrial planet, such a large dipole offset is not implausible. It should be noted, however, that temporal variations of the structure of the magnetosphere of Mercury would masquerade as spatial variations of the magnetic field in the interpretation of data from a single flyby encounter.

If the interpretation of an intrinsic planetary magnetic field at Mercury is validated by future studies and additional observations, it will represent a substantial discovery in the exploration of the solar system and will contribute significantly to the study of its origin.

N. F. NESS
K. W. BEHANNON
R. P. LEPPING
NASA–Goddard Space Flight Center, Greenbelt, Maryland 20771
Y. C. WHANG
Catholic University of America, Washington, D.C. 20017
K. H. SCHATTEN
Victoria University, Wellington, New Zealand

12.

Electrons and Protons Accelerated in Mercury's Magnetic Field

Abstract. *Fluxes of protons with energies of ~550 kev and electrons with energies of ~300 kev which exceed approximately 10^1 and 10^5 cm^{-2} sec^{-1}, respectively, have been discovered in the magnetosphere of Mercury. Electron fluxes > 10^1 cm^{-2} sec^{-1} also are observed in the outbound pass of the Mariner 10 spacecraft through the magnetosheath. The intensity versus time profiles of the particle fluxes in the magnetosphere appear with sudden onsets of ~ 10^1 cm^{-2} sec^{-1} beginning at interplanetary background levels and persisting for times equivalent to their being distributed spatially over regions having a scale size comparable to the planetary radius. For a spectral form* $dJ/dE \propto E^{-\gamma}$, *where J is the differential particle intensity and E is the kinetic energy, the typical values of* γ *are* $\gamma_p = 5.5$ *for protons above 500 kev and* $\gamma_e \geq 9$ *for electrons above 170 kev. Large coherent electron intensity oscillations (variations of factors of 10 to 100) have been discovered with characteristic periods of ~6 seconds and with higher frequency components. In some cases proton bursts are found in phase with these oscillations. On the basis of the experimental evidence and a knowledge of the general magnetic field intensities and directions along the trajectory of Mariner 10 provided by the magnetic field observations, it is shown that the radiation events observed in the magnetosphere and magnetosheath are transient and are not interpretable in terms of stable trapped particle populations. Furthermore, experimental evidence strongly supports the view that the particles are impulsively accelerated and that the acceleration source is not more distant from the point of observation along lines of force than ~ 8×10^3 to 16×10^3 kilometers (3 to 6.5 units of Mercury's radius). Candidates for the regions most likely to be sources of particle acceleration are discussed, namely, the magnetotail and the magnetosheath. It is pointed out that the phenomena discovered at Mercury will place more stringent conditions on allowed models for electron and proton acceleration than have heretofore been possible in studies within the earth's magnetosphere.*

One of the outstanding problems of common interest for planetary electrodynamics and high energy astrophysics is the acceleration of electrons and protons arising from the solar wind interaction with the induced or intrinsic magnetic fields of the planets. A wide range of in situ measurements already made at four planets and at the moon serve as a basis for an investigation of the physical conditions necessary for particle acceleration. Only at the earth and Jupiter, which have intrinsic magnetic fields with extensive magnetospheres, has local acceleration been shown to exist for both trapped radiation and impulsive events of electrons and protons. For Venus and Mars, without intrinsic magnetic fields but with ionospheres which provide a conducting surface for the interaction with the solar wind, induced magnetic fields are generated and standoff bow shocks have been observed. No evidence has been found for particle acceleration above an energy of ~ 50 kev in either the bow shock or the plasma wake region of either Venus or Mars. The moon represents the extreme case of a solid body without appreciable intrinsic magnetic field, ionosphere, or any conducting surface to deflect the solar wind. It has neither a bow shock nor significant induced magnetic fields which could lead to charged particle acceleration. Therefore, in attempts to predict the conditions for particle acceleration at Mercury the evidence derived from these earlier studies suggested that unless Mercury had a significant intrinsic magnetic field (*1*, *2*), which was believed doubtful on the basis of its slow rotational period (*3*), the planet would most likely have a moonlike interaction with the solar wind (*1*, *4*, *5*). This prediction was supported by the fact that nonthermal radio emissions from Mercury had not been detected. Hence it appeared most probable that we would find no locally accelerated electron or proton fluxes in the 100-kev energy range associated with Mercury.

This is a preliminary report of our measurements from the Mariner 10 spacecraft, which show the presence at Mercury of large and impulsive fluxes of electrons with energies > 170 kev and protons with energies > 500 kev distributed over regions comparable in size to the planet itself. Our observations reveal physical conditions substantially different from those predicted for Mercury (*1*, *2*) based on the analogies mentioned above with other planets and the moon. The observed

References and Notes

1. G. H. Pettengill and R. B. Dyce, *Nature (Lond.)* 206, 1240 (1965).
2. G. Columbo, *ibid.* 208, 575 (1965); P. Goldreich and S. Peale, *Astron. J.* 71, 425 (1966); G. Columbo and I. I. Shapiro, *Astrophys. J.* 145, 296 (1966).
3. G. P. Kuiper, *Commun. Lunar Planet. Lab.* 143, 165 (1970).
4. S. J. Peale, *Icarus* 17, 168 (1972); *Astron. J.*, in press.
5. G. Field, in *The Origin and Evolution of the Atmospheres and Oceans*, P. J. Brancazio and A. G. W. Cameron, Eds. (Wiley, New York, 1964).
6. S. I. Rasool, S. H. Gross, W. E. McGovern, *Space Sci. Rev.* 5, 565 (1966).
7. D. Morrison and C. Sagan, *Astrophys. J.* 150, 1105 (1967); D. Morrison, *Space Sci. Rev.* 11, 271 (1970).
8. W. Elsasser, *Phys. Rev.* 9, 106 (1946); E. C. Bullard and H. Gellman, *Philos. Trans. R. Soc. Lond. Ser. A Math. Phys. Sci.* 247, 213 (1954); W. V. R. Malkus, *Science* 160, 259 (1968); D. Gubbins, *Rev. Geophys. Space Phys.* 12, 137 (1974).
9. N. F. Ness and Y. C. Whang, *J. Geophys. Res.* 76, 3136 (1971).
10. P. M. Banks, H. E. Johnson, W. I. Axford, *Comments Astrophys. Space Phys.* 2, 214 (1970).
11. C. P. Sonett and D. S. Colburn, *Phys. Earth Planet. Interiors* 1, 326 (1968); J. L. Blank and W. Sill, *J. Geophys. Res.* 74, 736 (1969); G. Schubert and K. Schwartz, *Moon* 1, 106 (1969).
12. N. F. Ness, K. W. Behannon, R. P. Lepping, Y. C. Whang, K. H. Schatten, *Science* 183, 1301 (1974).
13. E. W. Greenstadt, I. M. Green, G. T. Inouye, D. S. Colburn, J. H. Binsack, E. F. Lyon, *Cosmic Electrodyn.* 1, 160, 279, and 316 (1970); E. W. Greenstadt, *J. Geophys. Res.* 77, 1729 and 5467 (1972); T. G. Northrop and T. J. Birmingham, *ibid.* 78, 2308 (1973).
14. J. Y. Choe, D. B. Beard, E. C. Sullivan, *Planet. Space Sci.* 21, 485 (1973).
15. A. W. Rizzi, thesis, Stanford University (1971).
16. D. C. Colburn and C. P. Sonett, *Space Sci. Rev.* 5, 439 (1966).
17. J. K. Chao, *MIT Report CSR TR-70-3* (1970); R. P. Lepping and P. D. Argentiero, *J. Geophys. Res.* 76, 4349 (1971).
18. L. F. Burlaga and K. W. Ogilvie, *Astrophys. J.* 159, 659 (1970).
19. G. R. Smit, *ESRO Report SN-17* (European Space Research Institute, Frascati, Italy, 1967); B. Bavassano, F. Mariani, U. Villante, N. F. Ness, *J. Geophys. Res.* 76, 5970 (1971); *ibid.* 77, 2004 (1972).
20. L. F. Burlaga and N. F. Ness, *Solar Phys.* 9, 467 (1969); D. M. Willis, *Rev. Geophys. Space Phys.* 9, 953 (1971).
21. S. Chapman and J. Bartels, *Geomagnetism* (Clarendon, Oxford, 1940).
22. S. Plagemann, *J. Geophys. Res.* 70, 985 (1965); R. A. Lyttleton, *Astrophys. Space Sci.* 5, 18 (1969).
23. D. S. Colburn, C. P. Sonett, K. Schwartz, *Earth Planet. Sci. Lett.* 14, 325 (1972).
24. A. J. Dessler, in *Atmospheres of Venus and Mars*, J. C. Brandt and M. B. McElroy, Eds. (Gordon & Breach, New York, 1968), p. 241; F. S. Johnson and J. E. Midgeley, *Space Res.* 9, 760 (1969); F. C. Michel, *Rev. Geophys. Space Sci.* 9, 427 (1971); J. L. Blank and W. R. Sill, *Bellcomm. TM 72-2015-1* (1972); P. A. Cloutier and R. E. Daniell, *Planet. Space Sci.* 21, 463 (1973).
25. G. Schubert, and B. Horning, in preparation.

26. We appreciate discussions of these results with our colleagues from the plasma science experiment and charged particle experiment teams. In addition, our colleagues at Goddard, D. Howell, H. Burdick, R. Hoffman, J. Seek, and J. Scheifele, contributed significantly in the phases of the mission concerned with the magnetometer boom, instrumentation, and data analysis. Lastly, we recognize the contributions of the technical teams at Jet Propulsion Laboratory and the Boeing Company to the successful conduct of the overall mission; we especially acknowledge J. Bruns of Boeing in connection with this experiment.

29 May 1974

nena provide important clues r understanding the interaction of e solar wind with Mercury's mag-tosphere which leads to the energizing charged particles. We have benefited eatly in our interpretative work on ie Mercury encounter of 29 March 974 as a result of the exchanges of ata with the magnetometer group (*6*) nd the plasma science group (*7*) in ie weeks preceding the preparation f this report. However, it is clear that quantitative physical picture of the article–magnetic field–plasma inter-ctions will become possible only after n extensive collaboration of the three roups.

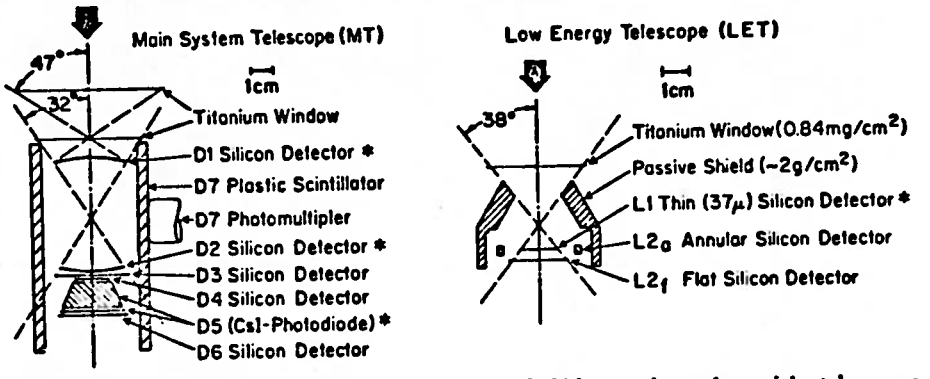

Fig. 1. Cross-sectional view of the University of Chicago charged particle telescopes. The view axes of the MT and the LET are parallel to within 5 degrees. This instrumentation is almost identical to the MT and LET onboard the Pioneer 10 and Pioneer 11 spacecraft (*10*).

Instrumentation. A general description of the University of Chicago nstrument, its location on the Mariner 0 spacecraft, and the spacecraft rajectory has been published (*8*, *9*). n the following discussion we have xtended the description only to in-lude those details essential for under-tanding our observations at Mercury. Cross-sectional views of the two charged article telescopes in the instrument r own in Fig. 1. Charged particles which enter the acceptance cones of hese telescopes are identified as elec-rons, protons, and helium nuclei by oth range of penetration in the letector stack and energy loss or esidual energy deposited in those letectors (identified by an asterisk in Fig. 1) which have pulse height nalyzers. Thus, the analysis of a given article consists of the simultaneous utput once each 0.33 second of the ulse height analysis and range in-ormation. The pulse height analysis perates in a statistical sampling mode or identification of particles during eriods of large fluxes. The absolute luxes are determined from the outputs f the counting rate accumulators, which count all particles satisfying the various range requirements. For nstance, a particle entering detector D1 but not penetrating to detector D2 is called an ID1 event and is counted by the ID1 accumulator, whereas a particle entering detectors D1 and D2 but not detector D3 would be called a 2 event and would be counted by the ID2 accumulator. There is a measurement of the accumulated number of events for each range inter-val every 0.6 second. From the known geometrical factors, the particle iden-tification, and the counting rates we can determine the absolute fluxes and energy spectra of electrons and pro-tons which are reported here. The rapid readout of the data was essential during the encounter in order to resolve the rapidly changing fluxes. For ex-ample, since the spacecraft velocity was ~ 11 km sec^{-1}, the flux was measured in increments of ~ 7 km (1/350 of the p'anetary radius) along the trajectory.

Our measurements at Mercury have shown that the energy ranges for electrons and protons were such as to restrict our measurements to detectors D1 and D2 in the main telescope and to the low energy telescope. The ID1 accumulator responds to protons and helium nuclei in the energy range 0.62 to 10.3 Mev per nucleon. It has an electron sensitivity which begins at an electron kinetic energy of approximately 170 kev. The experimentally determined efficiency, ϵ, for electron detection in ID1 is $\epsilon = 8$ percent at 170 kev, 50 percent at 300 kev, and a maximum of 70 percent at 750 kev. The ID1 geometrical factor for electrons is approximately ϵG_e where $G_e = 14$ cm^2 sr; for protons $G_p = 7.4$ cm^2 sr.

The low energy telescope (LET) was designed to respond to 0.53- to 1.9-Mev protons, which trigger detector L1 but not L2 (designated as L1N2), and 1.9- to 8.9-Mev protons (designated as L12) without responding to elec-trons over a wide range of electron energies and intensities. To achieve this discrimination against electrons the L1 detector thickness was made ~ 37 μm and the energy threshold for accepting pulses from L1 was set at 350 kev. Laboratory experiments have shown that the detection efficiency for low energy electrons for detector L1 is ~ 1×10^{-5} (*10*). The dynamic range of the pulse height analyzer associated with detector L1 provides for the identification of protons and helium nuclei. A passive shield defines a geometrical factor of 0.49 cm^2 sr.

Experimental results. Before present-ing the detailed analysis of our ex-perimental results and their interpreta-tion we have prepared in Fig. 2 a simplified overview of our measure-ments during the encounter, which places in perspective the time-intensity profiles of the locally accelerated energetic particles with respect to the main features of Mercury's magnet-osphere (*6*, *7*) and which relates all of these observations to the physical scale of the planet. To represent the particle measurements in Fig. 2 we choose the ID1 counting rate, which is the counting rate of electrons with a mean kinetic energy of ~ 300 kev. We find four major features in the time-intensity profiles, which we designate as the A, B, C, and D events. The events are separated in time and space by flux levels which were close to the inter-planetary background fluxes measured before and after encounter, as shown by the dashed line in Fig. 2. Since the Mariner 10 mission has occurred near solar minimum activity in the 11-year cycle, extensive periods of interplane-tary quiet time (periods free from fluxes of particles accelerated in solar flares) exist throughout the mission, including the period of several days before, during, and after the Mercury encounter. We have reported the dif-ferential energy spectra for inter-planetary electrons and protons under these conditions (*9*).

It is also important to emphasize the small scale of Mercury and its magnetosphere relative to the earth. The region over which the physical

interactions occurred at Mercury is ~ 60 times smaller than the earth's magnetosphere for a similar trajectory. Hence, major magnetospheric features of global extent at Mercury are to be observed on time scales on the order of minutes along the Mariner 10 trajectory. The A, B, and C events are all within the magnetospheric boundaries of the planet, whereas the D event was observed in the magnetosheath on the outbound or "dawn side" pass. The asterisk at the intensity peak of the B and C events designates a period when the electron flux was so high that the ID1 counting rate became a nonlinear function of the true rate of incidence of electrons on D1; this is due to the electronic circuit response at these high counting rates (*10*).

In the following discussion we examine each of the four events in detail with respect to the kinds of particles present and their energy spectra, in order to decide whether the particles were trapped in the magnetic field of Mercury or whether they were transient phenomena.

The A event. We found no significant time-intensity structure in the A event for periods shorter than the 30-seconds used for the counting rate averages shown in Fig. 2. The electron flux increased by a factor of 10 over a distance of 1600 km from interplanetary background levels at the magnetospheric boundary. This was a region of generally increasing magnetic field intensity, with the field direction approximately radial from the planet (*6*) and within the view cones of both telescopes. The flux was ~ 99 percent electrons with a differential energy spectrum of $dJ_e/dE \propto E^{-3.0 \pm 0.5}$ derived from pulse heights corresponding to electrons of kinetic energy E from 200 to 600 kev. Less than 1 percent of the measured flux could be nucleons: the LET detected no flux of nucleons during this event.

The B event. At the onset of the B event shown in Fig. 3 the flux of ~ 300-kev electrons measured by the ID1 counting rate channel rose four orders of magnitude within 1.2 seconds, during which time the L1N2 counting rate channel, which measures the ~ 550-kev protons, remained at background level. Since the L1N2 and ID1 counting rate channels respond to protons of nearly the same energy, we conclude that the ID1 counting rate results only from electrons. Further, the lack of response of the LET during this time interval shows that the L1N2 counting rate channel has negligible electron sensitivity over the electron intensity range measured by the ID1 counting rate channel during this time interval. This immunity of the LET to electrons is in agreement with laboratory calibrations (*10*). The proton flux showed a similar abrupt increase at 2048:05 U.T. and returned to background at 2048:15 U.T. From the same arguments we also conclude that after the proton flux returned to background level, the remainder of the B event and B′ event (see Fig. 3) was due exclusively to electrons. We also found that at no time could the electron contamination of the L1N2 counting rate channel exceed 3 percent.

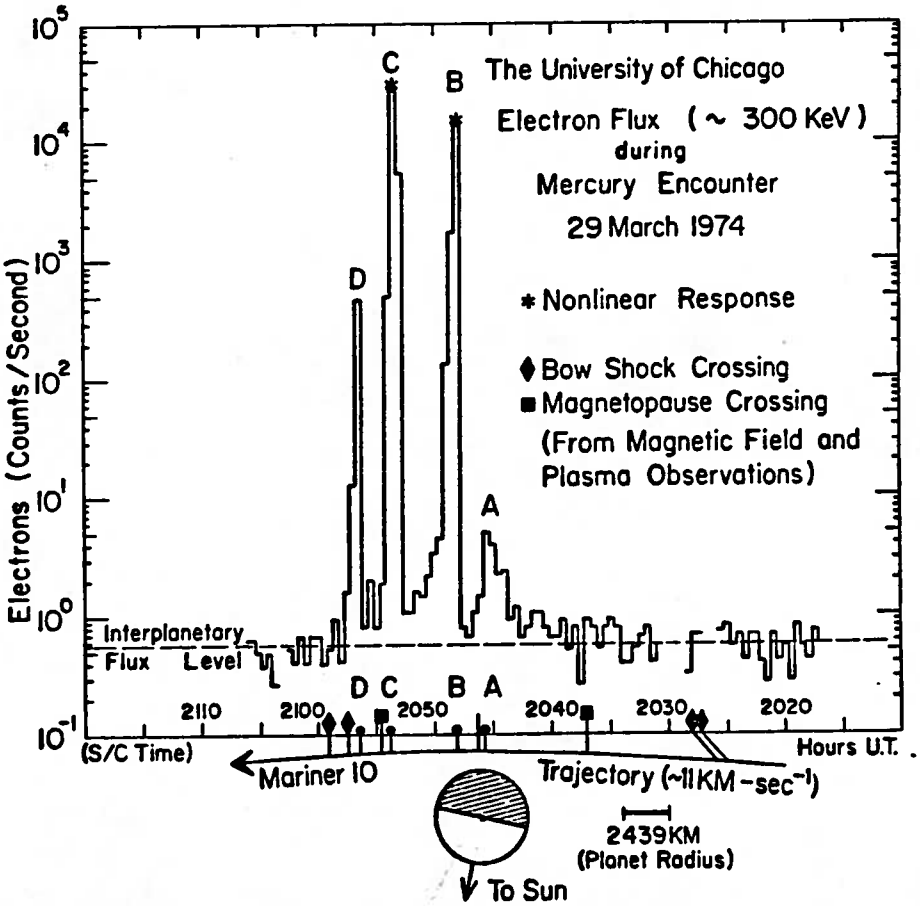

Fig. 2. Superposition of the ~ 300-kev electron counting rate and the main magnetospheric features (*6*, *7*) projected onto the Mercury encounter trajectory of Mariner 10. Four charged particle events, A, B, C, and D, were observed. The position of maximum flux for each event is projected onto the trajectory. The trajectory is plotted in a plane defined by the centers of the sun, Mercury, and the spacecraft, with the sun-Mercury line held fixed.

Whenever the true flux leads to a counting rate in ID1 or L1N2 above ~ 3×10^4 counts per second, the electronics respond nonlinearly to the higher flux levels (*10*). Although the absolute counting rate is not directly determined above ~ 3×10^4 counts per second, approximate values for the true counting rate can be deduced from the observed counting rate by using experimentally determined conversion factors (*10*). The counting rates for the ~ 550-kev protons never reach the nonlinear region. However, the fluxes of ~ 300-kev electrons in both the B and C events (see Fig. 4) were in this region for approximately 10 seconds. These periods are identified in Figs. 3 and 4 by the "flat-tops" on the observed counting rates at ~ 5.5 $\times 10^4$ counts per second. The true counting rates at these times were higher by a factor of 10 to 20 than the indicated values shown in Figs. 3 and 4.

In addition to the evidence presented above that the LET was measuring protons and the ID1 was measuring electrons in the B event, we have examined the question whether these detector systems could be responding to a pulse pile-up effect from electrons with energies below the ID1 electron threshold, under the assumption that

the flux of lower energy electrons would continue to rise steeply below this threshold energy. We found from a study of the rate of change of the ID1 and L1N2 counting rates and the experimentally determined L1 electron efficiency that such an assumption of subthreshold energy electron pileup is inconsistent with the data.

We also note that the simultaneous observations of approximately equal proton and electron fluxes such as observed at 2048:05.2 U.T. proves that there can be no substantial spacecraft charge contributing to local acceleration of the protons or electrons which we measure.

If the differential energy spectrum for protons is represented as $dJ_p/dE \propto E^{-\gamma_p}$ then we find $5 \leq \gamma_p \leq 7$ as the range for γ_p in the B event. Both counting rate data from L1N2 and L12 and pulse height distributions lead to this conclusion. The energy spectrum of the protons measured by the LET implies that the ID1 flux was always dominated by electrons. The electron energy spectrum in the B event is difficult to determine because the flux decreases extremely rapidly with increasing energy. The ID1 pulse height analysis and the fact that no protons are observed to penetrate to detector D2 set a limit of $\gamma_e \geq 9$ for an assumed spectral form of $dJ_e/dE \propto E^{-\gamma_e}$ for $E > 170$ kev.

The magnetic field intensity decreased rapidly in coincidence with the onsets of both the B event and the B′ event and then increased rapidly (*6*). The direction of the magnetic field in the B event was such that for electrons and protons to enter the cone angle of acceptance of the telescopes they must have pitch angles with respect to the magnetic field of ≥ 20 degrees and ≥ 40 degrees, respectively. The electron detector in the plasma instrument observed an enhanced electron flux, beginning with the onsets of the B and C events (*7*).

The B event provided sufficient information for us to decide whether the particle fluxes are stably trapped or are transient. The spacecraft velocity was ~ 11 km sec^{-1}, and for a stable trapping region the spacecraft would require 4 seconds to move one electron gyroradius in the magnetic field of $\sim 10^{-4}$ gauss which was typical of the region. Since the gyroradius of the protons is ~ 2100 km, the time to move one proton gyroradius would be ~ 200 seconds. However, from

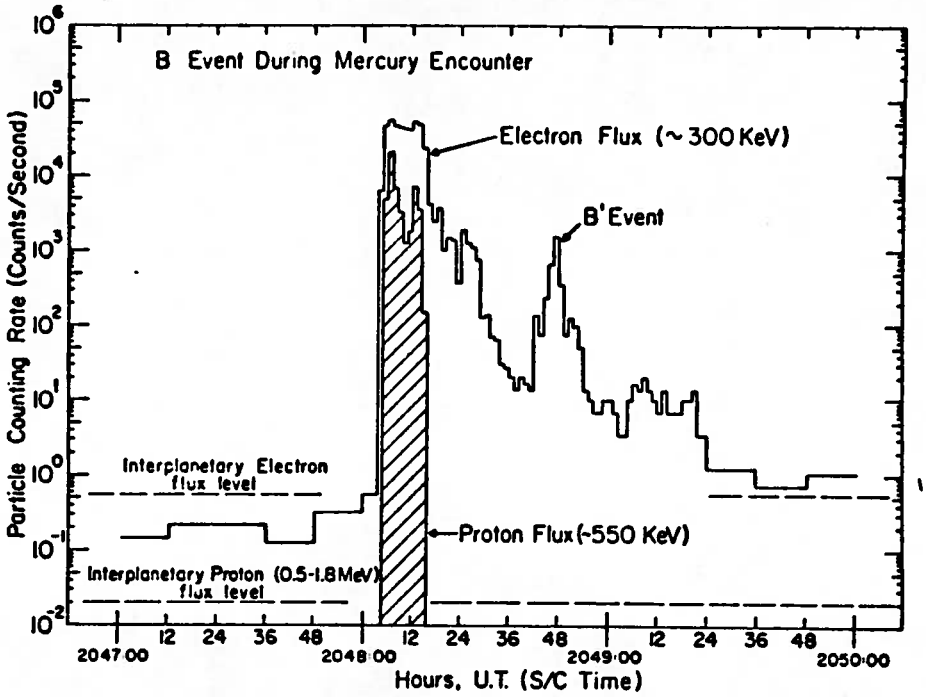

Fig. 3. The B event counting rates of ~300-kev electrons and ~550-kev protons. Tick marks on the abscissa represent 12-second intervals. The counting rates are averaged over 1.2 seconds whenever they are significantly above 1 count per second. Note that ~6 seconds separate the two proton peaks and that the three peaks in the B′ event are also separated by ~6 seconds.

Fig. 3 it is clear that the flux increase of both electrons and protons occurred within ~2.5 seconds. Therefore the fluxes are either transient effects or represent particles transported by the magnetic field past the spacecraft at high velocity to simulate a rapid onset and rapid intensity variations. Although the magnetic field did switch direction near the onset of the B event, it returned to its pre-onset direction within ~1 second (*6*). There was no subsequent correlation of magnetic field directional variations with particle intensity variations. We consider this evidence that the particle fluxes observed in the B event (and later in the C event) were transient phenomena.

Additional evidence that the events are impulsive may be derived from the B event, namely, that the duration of the enhanced proton fluxes in the B event is only 12 seconds, corresponding to a spatial extent of only ~1/16 of the proton gyroradius. Furthermore, since the spacecraft was only about 1200 km or about 0.5 of a proton gyroradius above Mercury's surface during the B event, we see that the protons in this event must have been captured by the planet.

The small upper limit set by dispersion of ~1.2 seconds between the onsets of the electron and proton fluxes is also important to note since the velocity ratio $V_e/V_p \geq 30$. This is strong evidence that the particles, if produced simultaneously in an impulsive event, have not traveled great distances before detection.

The C event. Between the end of the B event and the onset of the C event shown in Fig. 4, the electron and proton fluxes were at interplanetary levels for approximately 3.5 minutes. The initial rate of increase of the electron flux was slower than for the B event by a factor of approximately 3; that is, there was an increase of $\sim 10^4$ in electron flux in 4 seconds. The arguments applied to the B event to show that the ID1 counting rate channel was measuring the electron flux and that the L1N2 channel was measuring the low energy proton flux are found to hold for the C event. In addition, similar arguments can be invoked to show that the L12 channel was measuring protons for event C.

In Fig. 4 it is clear that there is an approximately 6-second periodicity in the electron and proton counting rates. From a power spectrum analysis (*11*) of the electron intensity variations from 2052:57 to 2053:24 U.T. we obtained a characteristic period of 6.6 ± 1.2 seconds and higher frequency components, while in the interval 2053:36 to 2054:12 we obtained a strong peak at

~ 10 seconds in addition to the one at 6.6 ± 1.2 seconds and the higher frequency components. We have made a detailed study of these periods to decide whether they could have been artifacts arising from spacecraft noise, instrument malfunction, or noise introduced in the data system. We conclude that the oscillations or "ringing effects" are variations of particle intensity and may reflect the dynamics of the energizing process, which we shall discuss later. Although the magnetic field shows considerable structure in intensity and direction during the C event, no readily apparent magnetic field signature was noted which could be considered coincident with any particle intensity change except that the flux level in the C event terminated abruptly by dropping three orders of magnitude at the magnetospheric boundary (*6*, *7*). Since the mean magnetic field was approximately 5×10^{-4} gauss during the C event, if we were to interpret the 6-second periodic variation as a spatial feature it would correspond to twice the electron gyroradius and 1/30 of the proton gyroradius. This is independent evidence that the electron and proton fluxes are transient phenomena.

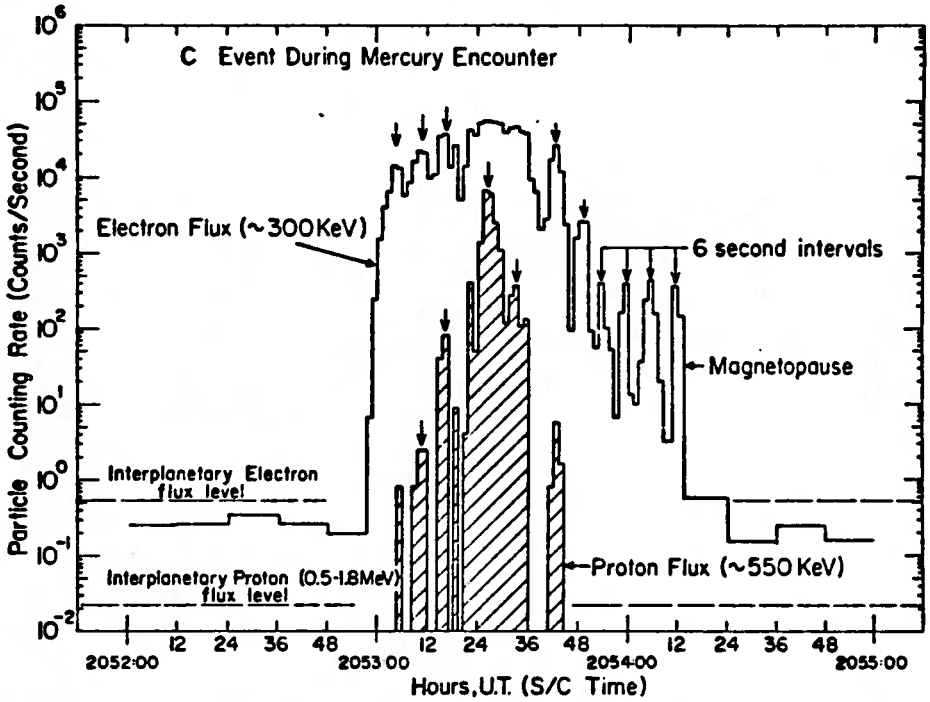

Fig. 4. The C event counting rates of ~ 300-kev electrons and ~ 550-kev protons averaged over 1.2-second intervals. These fluxes exhibit a periodicity of ~ 6 seconds and terminate at the magnetopause (*6*, *7*).

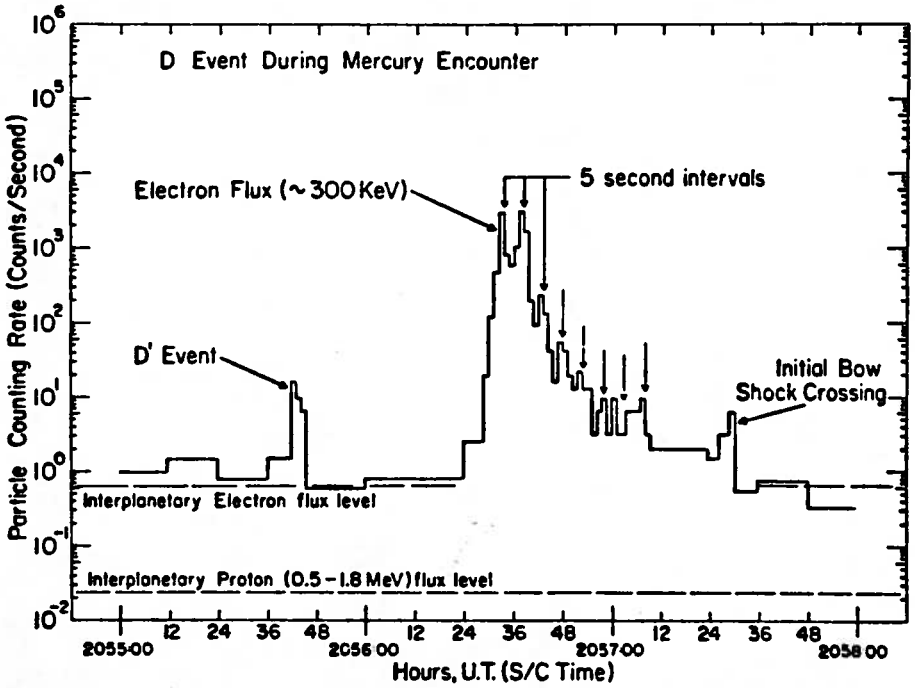

Fig. 5. The D event counting rates of ~ 300-kev electrons. Both the D' event and the D event occurred within the magnetosheath. Note the marked 5.0-second periodicity of the D event. The bow shock crossing was identified by magnetic field (*6*) and plasma (*7*) observations.

The D event. The electron flux as measured by the ID1 counting rate channel was at interplanetary levels during passage through the magnetosheath except for the D' and D events as shown in Fig. 5. Throughout the magnetosheath crossing and bow shock crossings the ~ 550-kev proton flux remained at the interplanetary level which existed before encounter and which persisted beyond the bow shock after encounter. The electron pulse height distribution for the D event was similar to that for the B and C events: namely, for an assumed power law spectrum, $\gamma_e \geq 9$. No additional electron flux increases were observed in the successive bow shock crossings (*6*, *7*) which arose from the motion of the bow shock across the spacecraft. We note that the intensity increase was ~ 10^3 in 2.4 seconds and that the oscillations of electron intensity displayed an approximately 5-second period for at least eight periods.

We analyzed this oscillation by using the method of Blackman and Tukey (*11*) to obtain the power spectrum of the spectral density versus frequency displayed in Fig. 6. The maxima are at 0.20, 0.40, and 0.66 hertz. These frequencies (ν) correspond to periods of 5.0 ± 1.0, 2.5 ± 0.3, and 1.5 ± 0.1 seconds. In Fig. 6 we note that the maxima are modulated by an intensity dependence which is proportional to exp ($-a\nu$), where a is a constant.

In contrast with the B and C events, where no correlation between electron and magnetic field intensity variations were observed, we found that the D event intensity variations were strongly correlated with oscillatory changes in direction of the magnetic field. The electron intensity maxima occurred when the magnetic field was approxi-

on, whereas the intensity minima ccurred when the field was approxi- northward and antisolar in irection (*6*).

Discussion and conclusions. So far this report we have presented only ie experimental facts obtained by irect analysis of the data. We now examine their interpretation in terms of lternate models for acceleration and ropagation of the electrons and pro- ons to demonstrate that the unique haracter of the phenomena discovered Mercury's magnetosphere eliminate ome magnetospheric acceleration ypotheses and place strong constraints n others.

The first question to settle is whether ie radiation is primarily trapped (that , whether there is a spatial distribu- on of fluxes) in the magnetic field, r is transient radiation. If the radia- on is transient, we want to know hether the accelerating region is ontinuously feeding particles to the eld lines on which the observations re made, or is impulsively injecting ie particles. We first consider the vents within Mercury's magnetospheric o ary. No unambiguous answer to ie questions can be obtained from ie A event, which could, for example, orrespond to a trapped electron pop- lation, especially if the dipole model or the magnetic field suggested by Ness *al.* (*6*) is confirmed. Such a popula- on would be rapidly depleted by radient drifts in the magnetic field, ie depletion being dependent on the agnetic field geometry or the source f the electrons. Two possible sources or these electrons are a remnant flux om an impulsive event like the B vent, or radioactivity from the planet's rface. However, our observations of ie B and C events enable us to choose nong the above alternatives. Namely, e conclude that

1) The transitory nature of both ie electron and proton fluxes is not ue to the magnetic field carrying these rticles swiftly past the spacecraft to mulate rapid intensity variations.

2) The B event occurred when the stance of the spacecraft to the planet's rface was less than the proton gyro- dius in the observed magnetic field. h ore the observed protons must e captured by the planet. Thus, if lercury has an atmosphere this radia- on may produce aurora-like effects.

3) The duration of the enhanced roton fluxes in the B and C events only ~2 to 15 seconds. This corresponds to a spatial extent of less than 0.1 of the proton gyroradius in the measured magnetic field. Consequently these protons must be bursts and cannot be part of the stably trapped population.

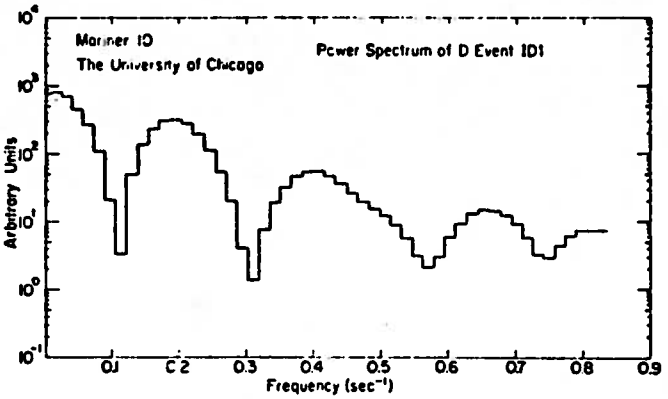

Fig. 6. Power spectrum of the ~300-kev electron counting rate during the D event. The fundamental frequency response is at 0.2 hertz with higher frequency components at 0.4 and 0.66 hertz. If the periodicity in the D event were not coherent, the frequency response would average out to a straight line.

4) The approximate 6-second oscillations observed for both events are not due to periodic changes in the magnetic field geometry or intensity. The periodicity and near simultaneous observations of both electron and proton fluxes require that the particles of opposite electric charge are accelerated in the source at, or near, the same time. It appears that the oscillations are to be associated with the source mechanism.

Since the electrons and protons in the B and C events have such strikingly similar characteristics—including their energy spectra—we are led to the conclusion that they are both manifestations of the same kind of acceleration mechanism. Furthermore the high intensity electron and proton events observed inside the magnetosphere are transient events and are not interpretable as spatially distributed trapped particle populations.

We can estimate the distance that particles travel along the magnetic field lines between the point of impulsive acceleration and the point of observation if we make the assumption that both protons and electrons are accelerated to their observed energies simultaneously. Since the ratio of particle velocities along the magnetic field line is $V_p/V_e \cong 0.03$ and the difference in observed rise times is 1 to 2 seconds for the burst events, we see that the source could not be more than $\sim 8 \times 10^3$ km ($\sim 3\ R_M$, where R_M is the planetary radius) for the B event and less than 16×10^3 km ($\sim 6.5\ R_M$) for the C event. Since the proton cyclotron period in the observed magnetic field is itself ~1 second we see that the above values derived from time dispersion must be upper limits.

Before discussing possible acceleration mechanisms, we compare the D event to the B and C events. The D event occurred within the magnetosheath before the first outbound crossing. The electron intensity shows a marked periodicity of 5 seconds, comparable to the 6-second periodicity observed in the B and C events, but was much more coherent, as demonstrated in Fig. 6. Otherwise, except for intensity, we conclude that the D event is similar in characteristics to the B and C events.

The most likely candidates for the magnetospheric regions in which the impulsive acceleration could occur are either the region between the bow shock and the magnetopause, or the magnetotail extending behind the planet between magnetospheric boundaries.

The features of the D event could possibly be explained by assuming particle acceleration in the magnetosheath associated with the moving bow shock. The absence of protons in this event may be due to the large proton gyroradius relative to the distance between the bow shock and the magnetospheric boundary. A strong correlation of the magnetic field variations with the ~5-second periodic electron intensity variation leaves open the question of whether the electron flux is being modulated by the local magnetic field changes, or whether the oscillation is to be associated with the acceleration region. On the other hand, if the magnetosheath were the only region for particle acceleration at Mercury it would be difficult to account for the appearance of both electrons and protons far inside the magnetospheric boundary where the B and C events were observed, and at the same time preserve their persistent ~6-second

periodicity and very sharp rise times.

Alternatively, impulsive acceleration of electrons and protons in the magnetotail of the planet is an attractive possibility since it can account for the major features of the B and C events. There are several analogies which can be made with the phenomena observed in the earth's magnetotail, such as the so-called substorm effect in which electrons and protons are accelerated as a result of a sudden instability occurring in the magnetic tail region.

The phenomena we discovered at Mercury, however, place more stringent conditions on allowed models for impulsive acceleration than have heretofore been possible in studies of the earth's magnetosphere. For example, the rise times for each proton burst—and therefore the time limit for energizing protons to $\gtrsim 0.5$ Mev—is less than the time required for a proton to undergo one cyclotron period in the magnetic field (which we have assumed to be $\sim 5 \times 10^{-4}$ gauss). Therefore, no theories or models for magnetic field interactions involving many cyclotron periods can be operative. The consequence of this conclusion is that models invoking strong, impulsive electric fields appear to be required for the simultaneous acceleration of protons and electrons. For example, ion–acoustic wave acceleration (*12*) and even slow neutral sheet merging of magnetic fields may not account for the observations. The question of whether phenomena such as fast neutral sheet merging, sheet pinch instabilities (*13*), or runaway processes (*14*) can account for the postulated impulsive acceleration remains to be explored later.

The periodic oscillation of the electron intensity in the B and C events without accompanying periodic variations in the local magnetic field points strongly to the acceleration region as the source of the oscillation or "ringing effect." Indeed, this is fully supported by the series of impulsive proton bursts accompanying electron oscillations in the C event (Fig. 4). This effect will undoubtedly place strong constraints on models to be developed for explaining the impulsive acceleration of the particles.

Mercury's magnetosphere can provide sufficient energy for the observed bursts of electron and proton fluxes. We find that the maximum rate of energy input required to accelerate the protons and electrons we observed in the B event is $< 10^{-2}$ of the rate of energy input of the solar wind into the magnetosphere. Therefore the mechanism of acceleration must also be very efficient. Since the energy spectra of the protons and electrons undoubtedly extend to lower energies and higher flux levels below our observational thresholds, it is quite clear that although there is sufficient energy via the solar wind–magnetic field–charged particle interactions, the energy spectra of protons and electrons must turn over below the detection thresholds in our experiment in order not to exceed the magnetic field energy density.

Clearly, a second encounter of Mariner 10 with Mercury through the magnetotail region of the planet would be of major importance for resolving the remaining questions on impulsive acceleration of Mercury's electron and proton fluxes.

J. A. Simpson, J. H. Eraker
J. E. Lamport, P. H. Walpole
Enrico Fermi Institute, University of Chicago, Chicago, Illinois 60637

References and Notes

1. S. J. Bame, H. S. Bridge, L. A. Frank, J. W. Freeman, K. W. Ogilvie, C. W. Snyder, J. H. Wolfe, C. M. Yeates, "Final report of the plasma instrument team for the 1973 Mercury/Venus mission design study," preprint.
2. J. A. Simpson, S. M. Krimigis, J. E. Lamport, C. O. Bostrom, J. W. Kohl, W. T. Huntress, Jr., *JPL Document 615-5* (Jet Propulsion Laboratory Pasadena, Calif., 1970).
3. P. Goldreich and S. J. Peale, *Astron. J.* **71**, 425 (1966).
4. N. F. Ness and Y. C. Whang, *J. Geophys. Res.* **76**, 1316 (1971).
5. F. C. Michel, *Comments Astrophys. Space Sci.* **3**, 27 (1971).
6. N. F. Ness, K. W. Behannon, R. P. Lepping, Y. C. Whang, K. H. Schatten, *Science* **185**, 151 (1974).
7. K. W. Ogilvie *et al.*, *ibid.*, p. 145.
8. J. A. Dunne, *ibid.* **183**, 1289 (1974); *ibid.* **185**, 141 (1974).
9. J. A. Simpson, J. H. Eraker, J. E. Lamport, P. H. Walpole, *ibid.* **183**, 1318 (1974).
10. J. A. Simpson, D. C. Hamilton, R. B. McKibben, A. Mogro-Campero, K. R. Pyle, A. J. Tuzzolino, *J. Geophys. Res.*, in press.
11. R. B. Blackman and J. W. Tukey, *The Measurement of Power Spectra* (Dover, New York, 1958).
12. F. L. Scarf, W. Bernstein, R. W. Fredricks, *J. Geophys. Res* **70**, 9 (1965); R. W. Fredricks, F. L. Scarf, W. Bernstein, *ibid.*, p. 21.
13. B. Coppi, G. Laval, R. Pellet, *Phys Rev. Lett.* **16**, 1207 (1966).
14. M. J. Houghton, preprint.
15. We wish to acknowledge the support of many individuals and groups which made these experiments possible. At the University of Chicago the instrument was designed and built in the Laboratory for Astrophysics and Space Research of the Enrico Fermi Institute and the preparation of programs and preliminary analysis were undertaken by G. Lentz, J. Coates, S. Christon, S. Daly, and A. J. Tuzzolino. The laboratory electron calibrations were carried out with the assistance of R. Zamow. We thank E. N. Parker for a valuable discussion of our results. At the Jet Propulsion Laboratory we are especially grateful for the support of W. Giberson, J. Dunne, A. Matzke, D. Swenson, and J. Tupman. It is clear that this mission could not have been successful without the strong support of J. E. Naugle, N. W. Cunningham, and S. E. Dwornik at NASA Headquarters. This research was supported in part by JPL contract 953091, NASA grant NGL 14-001-006, and NSF grant GA-38913X.

14 June 1974

1a. Mercury's Atmosphere from Mariner 10: Preliminary Results

Abstract. *Analysis of data obtained by the ultraviolet experiment on Mariner 10 indicates that Mercury is surrounded by a thin atmosphere consisting in part of helium. The partial pressure of helium at the terminator is about 5×10^{-12} millibar. The total surface pressure of the atmosphere is less than about 2×10^{-9} millibar. Upper limits are set for the abundance of various gases, including hydrogen, oxygen, carbon, argon, neon, and xenon. The wavelength dependence of Mercury's surface albedo is similar to that of the moon over a broad range of wavelengths from 500 to 1600 angstroms. Strong signals were recorded by the airglow instrument as Mariner 10 passed through the cavity behind Mercury. They are as yet unexplained but may provide information on the properties of the local plasma.*

Two instruments sensitive in the extreme ultraviolet were carried aboard Mariner 10: an occultation spectrometer to measure the extinction properties of the atmosphere as the sun is occulted by the limbs of the planet, and a spectrometer to search for airglow at wavelengths elected to identify specific atmospheric gases. The airglow instrument has previously observed constituents in the upper atmospheres of the earth and Venus (*1*).

We concentrated attention on noble gases such as He, Ar, and Ne, since there are several obvious supply processes for these gases. Helium and neon can be captured from the solar wind; helium and argon may be released by decay of radioactive elements in Mercury's crustal rocks. A preliminary examination of the mass balance for the various species on Mercury leads us to conclude that the most probable species would be Ar, Ne, and He. The choice of airglow channels reflects this analysis. However, the instrument was also designed to detect emissions associated with H, O, and C.

Occultation experiment. The absorption cross sections of all common atmospheric gases and their photochemical products are large in the extreme ultraviolet (300 to 900 Å). Values for absorption cross sections range from 1×10^{-17} to 7×10^{-17} cm^2. Since the sun is a bright source of extreme ultraviolet radiation, the occultation experiment provides a sensitive test for the presence of an atmosphere almost regardless of its composition.

The occultation spectrometer has a plane grating which operates at grazing incidence (*2*). Channel electron multipliers measure the solar flux at four wavelength positions, 470, 740, 810, and 890 Å, chosen to straddle the first ionization edges of Ne, He, Ar, and Kr. Pinholes isolate spectral bands of ~75 Å full width at half maximum (FWHM) and also define the effective field of view of the instrument, which is 0.15° FWHM. The instrument, which is body-fixed to the spacecraft, observed the sun continuously for several days during Mercury encounter. The solar flux was sampled in each channel every 0.6 second. Raw data received at ingress and egress are plotted in Fig. 1.

There are no obvious effects in these data due to atmospheric extinction. The intensity variations that are evident are due to the motion of the projected field of view of the instrument on the solar disk. This motion is caused by the spacecraft's limit cycle motion (*3*). The characteristic time scale for atmospheric effects is quite short (1 to 50 seconds) and is determined by the velocity of the spacecraft (approximately 11 km/sec) as it passes behind Mercury, the scale height (H) in the planet's atmosphere, and the angular field of view of the instrument. At encounter the height resolution at the occulting limb was about 16 km. In the absence of an atmosphere the signal cutoff should occur in about 2.4 data sample periods. The observed cutoff took place, in all channels, within three data samples,

Table 1. Upper limits to the abundances of atmospheric constituents on Mercury deduced from the ultraviolet observations. The data were obtained on 29 March 1974 at 2028 G.M.T. The 0.13° field of view was 15 km above the bright limb at a range of 12,400 km. A temperature of 550 K was assumed in calculating the vertical column densities. These data are not corrected for background.

Probable emitting species	Channel (Å)	Upper limit to limb brightness (rayleighs)	g-Value at Mercury (photon sec^{-1} atom^{-1})	Vertical column density (cm^{-2})	Partial pressure (mbar)
He*	304	1200			
Background	430				
He	584	84	2.0×10^{-6}	7×10^{12}	2×10^{-12}
Ne	740	23	5.1×10^{-8}	3×10^{13}	4×10^{-10}
Ar	869	85	4.2×10^{-7}	1×10^{13}	3×10^{-10}
Ar	1048	150	1.4×10^{-6}	5×10^{12}	
H	1216	5000	1.5×10^{-2}	1×10^{13}	1×10^{-11}
O	1304	240	1.3×10^{-1}	1×10^{11}	2×10^{-12}
Xe (1470 Å)	1480	490	1.0×10^{-5}	1×10^{12}	1×10^{-10}
C	1657	870	1.4×10^{-3}	5×10^{10}	4×10^{-12}

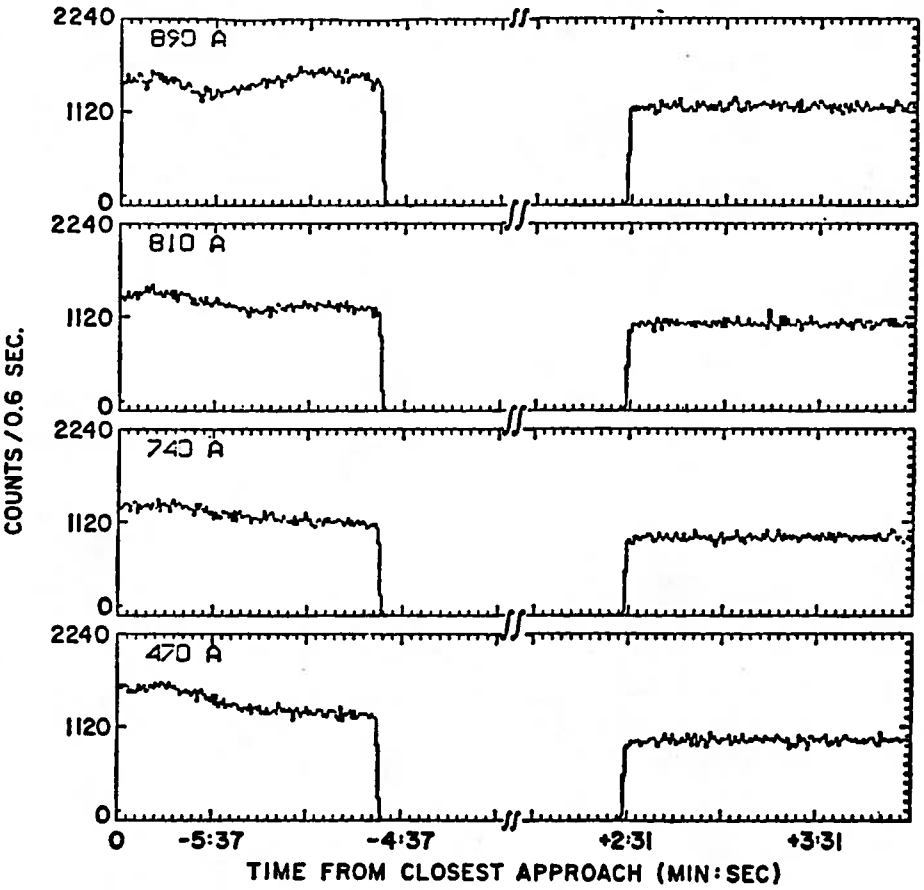

Fig. 1. Sample of data from the occultation spectrometer as the spacecraft moved into and out of occultation at Mercury.

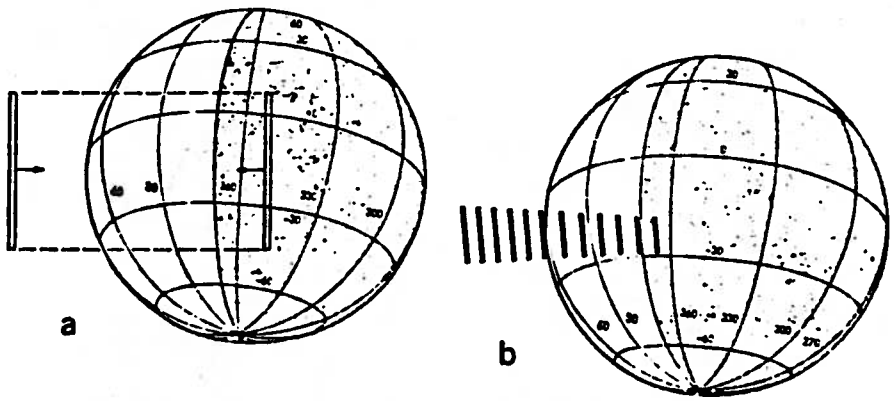

Fig. 2. (a) Geometry of the field of view with respect to the planet at encounter minus 1 hour. The field of view is 0.13° by °. The planet was at a range of 43,000 km. A 5° slew was used at a rate of ⅛ sec^{-1}. The data taken during this scan are shown in Fig. 3. (b) Geometry of the field of view with respect to the planet during the limb drift experiment 21 minutes before closest approach. The planetary phase angle is 114° and the range to the limb is ~ 12,400 km.

Fig. 3. Data obtained from the sequence shown in Fig. 2a. Counts from the four scans were summed and smoothed. The 1216-Å data were scaled by a factor of 0.63 for comparison. Points on the 584-Å curve represent the number of counts accumulated in 2.4 seconds.

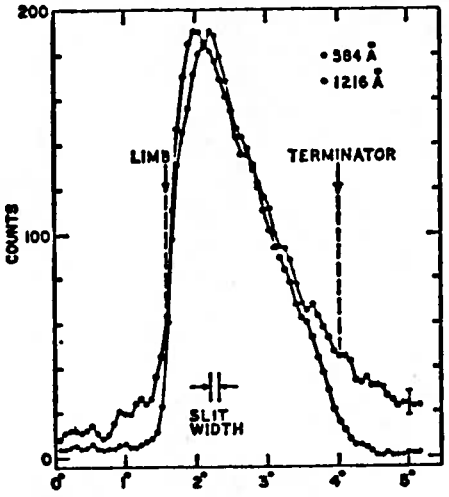

consistent with a sharp edge—that is, planetary limb occultation.

An estimate of the maximum possible attenuation, 16 km above the limb, gives an upper limit to any atmosphere on Mercury. We feel that a drop in intensity in the last few samples of more than 10 percent is excluded by the data. This corresponds to a maximum vertical optical depth of $8 \times 10^{-4} H^{1/2}$ in the extreme ultraviolet. Here H is measured in kilometers. For CO_2 near the terminator, at an assumed temperature of 100°K, this corresponds to an upper limit of 4×10^{13} cm^{-2} for the column density or a surface pressure of 1×10^{-9} mbar. This decreases the best previous limit on the surface pressure for CO_2 [approximately 2×10^{-5} mbar (*4*)] by a factor of 2×10^4. For He and Ar the limits for the column densities are 4×10^{14} and 8×10^{13} cm^{-2}, respectively; the corresponding surface pressures are 1×10^{-9} and 2×10^{-9} mbar.

Considerable improvement in these figures is anticipated with further processing of the data. Signal variations due to the limit cycle motion of the field of view on the sun can be removed in the following way: Data from the many hours of observation preceding and following the encounter can be used to build up an intensity picture of the sun as a function of the spacecraft attitude sensor signals, and a correction can then be applied to the data taken at occultation.

Airglow experiment. The airglow spectrometer (*1*) has ten detectors which accept emission over 20-Å bandwidths about the central wavelengths 304, 430, 584, 740, 869, 1048, 1216, 1304, 1480, and 1657 Å. These wavelengths correspond to the positions of strong lines of He^+, He, Ne, Ar, H, O, and C (see Table 1). In addition, there are two zero-order channels which provide checks on the total incident extreme ultraviolet flux to the spectrometer. One of these channels is open, the other has a MgF_2 filter and CuI photocathode. The instrument is mounted on the scan platform which provides considerable pointing versatility. The effective field of view of the instrument is 0.13° by 3.6°.

The sequence of operation at Mercury consisted of three separately identifiable modes: (i) A mode in which the instrument was moved at a constant rate, ⅛° per second, by the spacecraft scan platform, as illustrated in Fig. 2a. At 1, 2, and 4 hours before encounter, four scans were made across the planet. (ii) A fixed pointing mode in which the objective was to build up the signal to a statistically significant total count in each channel. (iii) A drift mode in which the field of view moves across the limb as a result of spacecraft motion. This is illustrated in Fig. 2b. Limb drifts were performed 21 minutes before encounter and 9 minutes after encounter. The latter gave the highest spatial resolution (~15 km) at the limb.

Figure 3 shows the results of four scans made across the planet at 1 hour before encounter. Only the data from the 1216- and 584-Å channels are shown. Individual scans have been summed and smoothed. A significant signal is seen in the 584-Å channel. The signal extends beyond the bright limb and well into the dark side across the terminator. The signal in the 1216-Å channel rises abruptly at the limb and falls to the background level at the geometrical terminator; it is similar to the signal in the zero-order channels, which is predominantly due to sunlight scattered from the surface of the planet.

We interpret these data for the 584-Å channel as indicating the definite presence of neutral He on the planet. Further processing of the data is required to remove the effects of limit cycle motion before the actual distribution of intensity can be derived. However, a preliminary estimate of the brightness at the terminator is about 45 rayleighs. The derivation of global He abundance requires proper modeling. The effects of scattering of sunlight, of collisional processes, surface albedo, solar wind interaction, and variable surface temperature should be included. However, if the 584-Å emission is entirely due to single scattering in a homogeneous atmosphere, then the vertical column density of neutral He atoms near the terminator would be 2×10^{12} cm^{-2}, well below the exospheric limit of ~10^{15} cm^{-2} (*5*). The observed column density corresponds to a He partial pressure of 5×10^{-12} mbar near the terminator.

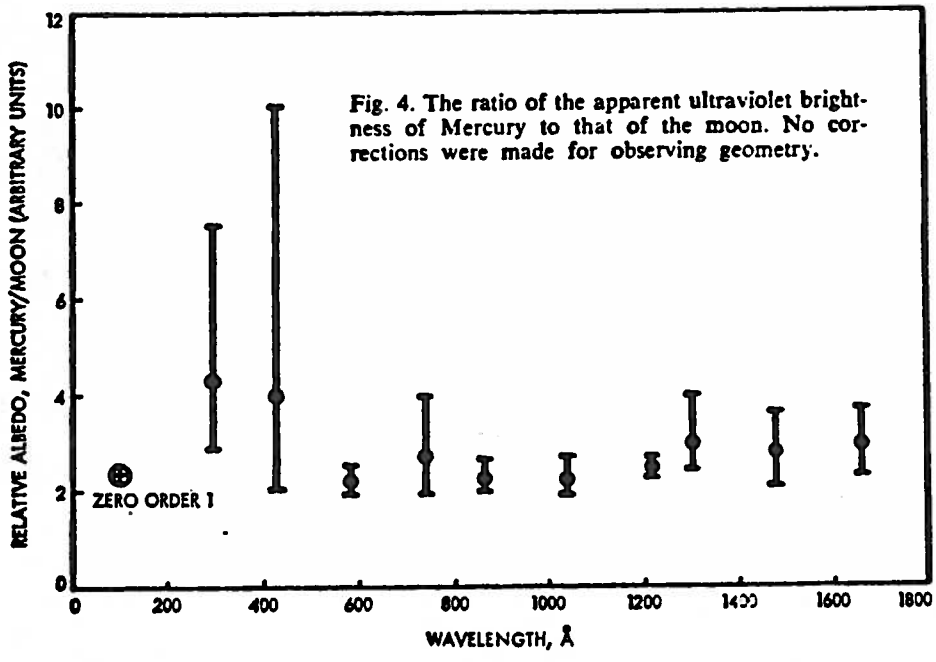

Fig. 4. The ratio of the apparent ultraviolet brightness of Mercury to that of the moon. No corrections were made for observing geometry.

If He is lost primarily by thermal escape, we estimate that the atmospheric residence time should be of the order of 10^5 seconds. The source strength required to supply the observed He atmosphere would then be of the order of 10^7 cm^{-2} sec^{-1}, which is comparable to the He source in the earth's atmosphere (*6*).

The drift sequence across the bright limb (Fig. 2b) provides stringent upper limits to the abundances of probable atmospheric constituents. These are listed in Table 1 and were estimated from data taken 15 km above the limb. For these calculations we have assumed the local surface temperature at the limb to be 550°K (*7*). Scattering efficiencies and *g*-values for the resonance emissions of H, O, C, and Xe were scaled from the compilations of Barth (*8*) and Fastie *et al.* (*9*). For the other species the *g*-values were based on reported solar fluxes (*10*), oscillator strengths (*11*), and assumed solar line widths (*12*).

Inspection of the results in Table 1 shows that the airglow spectrometer is far more sensitive to individual species than the occultation instrument. Of particular interest is Ar, which should be produced radiogenically in the planet. If we assume that Ar is removed primarily by interaction with the solar wind, we can deduce an upper limit to the supply rate. Its residence time should be similar to the ionization time of the gas, that is, $\sim 10^6$ seconds. Combining this number with the column density upper limit in Table 1, we find a maximum source strength of $\sim 10^7$ cm^{-2} sec^{-1}. This is consistent with the terrestrial supply rate of 2×10^5 cm^{-2} sec^{-1} (*6*).

During the Mercury encounter channels at wavelengths short of 1216 A observed sporadic emission. This emission was seen during the limb drifts and while observations were being made of the dark side of the planet. The spacecraft was also within the solar wind cavity during most of these bursts of emission, but we have found little correlation with the fluxes observed by the plasma and energetic particle experiments (*13*).

Extreme ultraviolet albedo. Observations of the bright side of the moon were obtained with the airglow instrument shortly after launch. These were compared with similar measurements on Mercury made several hours before encounter. The ratio of the apparent brightnesses is plotted in Fig. 4 on an arbitrary scale. The marked similarity between the two is obvious in spite of the poor statistics in the two short-wavelength channels at 304 and 430 A. Evidently the similarity of the run of albedo with wavelength between Mercury and the moon that has been reported throughout the visible (*14*) extends far into the ultraviolet and probably at least down to wavelengths of 500 A.

Conclusions. The Mariner 10 ultraviolet spectrometer experiment has achieved its primary objective of detecting a neutral atmosphere on Mercury. Evidently neutral He is a prime constituent. The column density is very low, such that the atmospheric atoms follow ballistic trajectories. The occultation experiment places an exceedingly low limit to the total atmospheric content, far lower than indicated by any previous measurements. Further reductions in these limits are expected when the effects of spacecraft limit cycle motion are included in the analysis. Similarly, further analysis should provide information on the neutral He scale height and also on the origin of the unexpected "emission" seen as the spacecraft flew behind Mercury.

A. L. BROADFOOT
S. KUMAR
M. J. S. BELTON
Kitt Peak National Observatory, Tucson, Arizona 85726
M. B. MCELROY
Harvard University, Cambridge, Massachusetts 02138

References and Notes

1. A. L. Broadfoot, S. Kumar, M. J. S. Belton, M. B. McElroy, *Science* 183, 1315 (1974).
2. J. A. R. Samson, *Techniques of Vacuum Ultraviolet Spectroscopy* (Wiley, New York, 1967), p. 76.
3. The solar disk had an angular diameter of 1.18° at Mercury encounter. The intensity distribution in the extreme ultraviolet is very inhomogeneous over the disk [see E. M. Reeves and W. H. Parkinson, *Astrophys. J. Suppl.* 21, 1 (1970)]. The spacecraft limit cycle was ± 0.3° in all three axes.
4. U. Fink, H. P. Larsen, R. F. Poppen, *Astrophys. J.* 187, 407 (1974).
5. M. J. S. Belton, D. M. Hunten, M. B. McElroy, *ibid.* 150, 1111 (1967).
6. P. M. Banks, H. E. Johnson, W. I. Axford, *Comments Astrophys. Space Phys.* 2, 214 (1970).
7. S. C. Chase, E. D. Miner, D. Morrison, G. Münch, G. Neugebauer, M. Schroder, *Science* 185, 142 (1974).
8. C. A. Barth, *Appl. Opt.* 8, 1295 (1969).
9. W. G. Fastie, P. D. Feldman, R. C. Henry, H. W. Moos, C. A. Barth, G. E. Thomas, T. M. Donahue, *Science* 182, 710 (1973).
10. H. E. Hinteregger, *Ann. Geophys.* 26, 547 (1970).
11. W. L. Wiese, M. W. Smith, B. M. Glennon, *Ref. Data Ser. U.S. Natl. Bur. Stand.* 1, 4 (1966).
12. For the He 584-A line, we have used the solar line width measured by G. Cushman, L. Farwell, G. Goden, and W. A. Rense (in preparation).
13. We wish to thank J. A. Simpson and H. S. Bridge for providing us with their unpublished data.
14. T. B. McCord and J. B. Adams, *Science* 178, 745 (1972); *Icarus* 17, 585 (1972).
15. We would like to express our appreciation for the assistance of Frank E. Stuart and the Electronics Laboratory at Kitt Peak National Observatory in construction of the instrument. We are especially grateful for the exceptional effort put forth by Sam S. Clapp, senior engineer at Kitt Peak. Special thanks are due to Jet Propulsion Laboratory personnel, particularly Clayne M. Yeates and James A. Dunne for providing the science support. We also thank D. G. Rea for a critical review of the manuscript. This research was sponsored by the National Aeronautics and Space Administration. Kitt Peak National Observatory is operated by the Association of Universities for Research in Astronomy, Inc., under contract with the National Science Foundation.

3 June 1974

Mercury's Surface: Preliminary Description and Interpretation from Mariner 10 Pictures

Abstract. *The surface morphology and optical properties of Mercury resemble those of the moon in remarkable detail and record a very similar sequence of events. Chemical and mineralogical similarity of the outer layers of Mercury and the moon is implied; Mercury is probably a differentiated planet with a large iron-rich core. Differentiation is inferred to have occurred very early. No evidence of atmospheric modification of landforms has been found. Large-scale scarps and ridges unlike lunar or martian features may reflect a unique period of planetary compression near the end of heavy bombardment by small planetesimals.*

Mariner 10 acquired 2300 television pictures in the vicinity of Mercury in order to investigate the geologic history of the planet as manifested in the morphology and optical properties of the surface. A unique surface history could have been indicated by the planet's Earth-like density (5.5 g/cm^3) and small size (4870 km) (*1*). Instead, an extraordinary similarity to the surface of the moon has been found; the implications of this lunar-like exterior and probable Earth-like interior provide insight into very early stages of planetary formation.

A brief description of the first images

Table 1. Sequence summary.

Phase	Range (km)	Resolution (km)	Frames
Incoming far encounter, −6 days to −1 day	4,500,000–800,000	127–20	716
Incoming color mosaicking, −1 day to −3 hours	800,000–100,000	20–4	212
Close encounter, −3 hours to +3 hours	100,000–10,000	4–0.15	548
Outgoing color mosaicking, +3 hours to +1 day	100,000–800,000	4–20	220
Outgoing far encounter, +1 day to +3 days	800,000–2,000,000	20–60	112
Satellite search, +1 day to +3 days	1,000,000–3,500,000		555
Total			2363

Table 2. Normal albedos.

Feature (Fig. 5)	Earth-based	Mariner 10
Lunar		
Mare Crisium	0.085	0.10
Mare Serenitatis	0.09	0.10
Highlands between Crisium and Serenitatis	0.16	0.17
Brightest crater	0.23	
Integrated disk*	0.125	
Mercurian		
Bright craters and rays (1, 6, 7, 11, 14, 22, 23, 28, 29, 30, 31)		0.19–0.25
Heavily cratered terrain and textured plains (4, 9, 10, 12, 13)		0.11–0.19
Flat-floored craters (3, 2)		0.10, 0.13
Smooth plains (15, 16, 17, 18, 20, 26, 27, 33)		0.08–0.12
Integrated disk*	0.125	

* From (5).

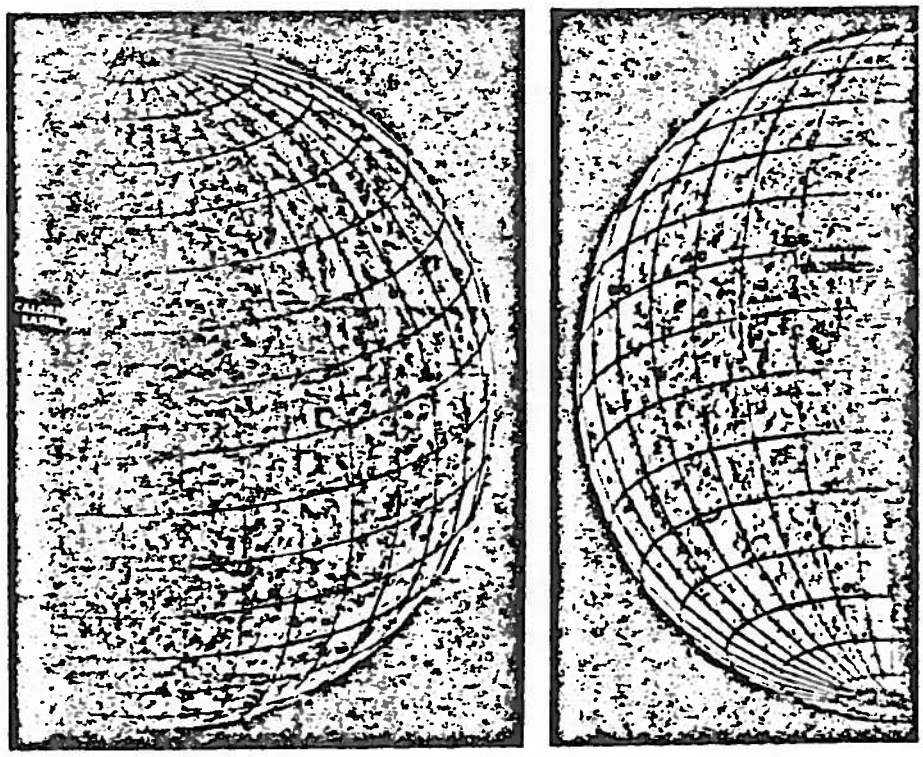

Fig. 1. Photomosaic of the incoming (right) and outgoing (left) view of Mercury with the approximate coordinate system. The provisionally named features discussed in the text are indicated.

has already been published (*2*). We present here further experimental results and consequent interpretations from preliminary study of all the pictures received in the March 1974 encounter as well as a quantitative analysis of about one-tenth of the total. Table 1 summarizes the data set. High-resolution photomosaics covering nearly all the lighted hemisphere of the planet were constructed from specially processed frames of the close encounter phase (Figs. 1 and 2). In regions of favorable lighting and viewing geometry the resolution is 1.5 to 2.0 km, comparable to good Earth-based photography of the moon. There are about 200 additional individual pictures of resolution ranging from 1.5 to 0.15 km.

Pictures from the satellite search phase of the imaging experiment reveal no mercurian satellites, only stars (Fig. 3). We place an upper limit of 5 km on the diameter of any hypothetical mercurian satellite with an albedo similar to that of the planet. Spatial coverage is estimated to be at least 95 percent complete for equatorial satellites within 30 planetary radii. Further processing is expected to improve the detection limit to about 2 km in diameter and to increase the completeness of spatial coverage.

The photographic coverage provided by Mariner 10 is so extensive that a mercurian surface coordinate system and control net is necessary. Coordinates of features (control points) on Mercury are being computed photogrammetrically by methods similar to those developed for use with Mars (*3*). As of May 1974, 635 measurements of 151 points on 45 pictures had been incorporated into the control system. A series of maps, to be produced by the U.S. Geological Survey, is planned as the cartographic base for future systematic geologic mapping.

In the Mariner 10 coordinate system the axis is assumed always to be normal to the orbital plane of Mercury (0° obliquity). The crater Hun Kal, about 1½ km in diameter, has been chosen to define the system of longitudes; the 20° meridian passes through its center at latitude about 0.4°S (Fig. 4). Thus, the 20° meridian defines the longitude on Mercury in the same way that the 0° meridian (Greenwich) does on Earth (*4*).

Surface optical properties. Earth-based observations indicate that the integral optical properties of Mercury are closely similar to the global average

of the moon (*5–7*). The average microrelief and surface composition of the two objects, therefore, have been inferred to be similar. Mariner 10 provided an opportunity to determine whether this similarity extends to regional variations in optical properties such as the highland/maria dichotomy of the moon. In addition to a comprehensive preflight photometric and geometric calibration, extensive photography of Earth and the moon was carried out from Mariner 10 shortly after launch to permit direct comparison between Mercury and the moon.

The relative brightness distribution in a selected image of Mercury, taken on the incoming leg of the trajectory, is virtually identical with similar plots of lunar data made from both Mariner 10 and Earth-based observations at similar phase angle. Moreover, the ultraviolet (UV) plane polarization of Mercury in the phase angle range from 80° to 100° is indistinguishable from that of the moon down to a scale of at least 50 km. Evidently the mercurian surface observed by Mariner 10 is everywhere covered with a fine-grained material analogous to the lunar regolith.

The normal albedos (*8*), corrected to a wavelength of 0.55 μm, were measured for 33 representative areas. Their locations are shown in Fig. 5, and the results of the measurements are summarized in Table 2. Relative accuracy is estimated to be 10 to 15 percent; absolute errors may be somewhat larger. Crater Kuiper (number 1, Fig. 5) is one of the brightest areas on the visible hemisphere of Mercury with a normal albedo of 0.24. Both the interior of Caloris Basin and of the smooth plains outside the basin rim have albedos of 0.12. Heavily cratered terrain has approximately the same average albedo as the lunar highlands, and the smooth plains of Mercury are significantly darker. However, Mercury's appearance is blander than that of the moon. Albedo boundaries between light and dark regions are less distinct on Mercury than on the moon, as illustrated in Fig. 6.

We investigated regional color variations by forming ratios of pictures taken with the orange (OR) filter to those taken with the UV filter (see Fig. 7 for the spectral responses of each filter). No pronounced regional color differences were apparent, the maximum dispersion in the OR/UV ratio being approximately ± 5 percent. In particular, no areas with nearly flat

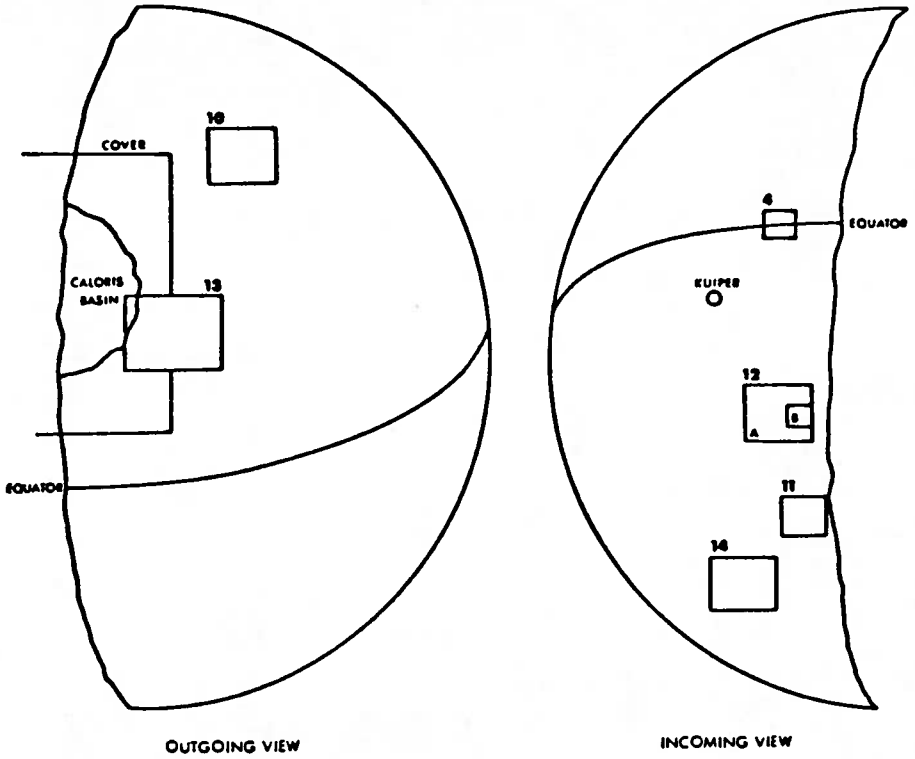

Fig. 2. Index map showing the location and figure numbers (in boldface) of the photographs discussed in the text.

reflection spectra and high plane polarization, which might indicate the presence of significant amounts of metallic iron on the surface, were noted. As for the moon, brighter areas on Mercury are generally redder than average, although many exceptions to this rule occur. For example, Crater Kuiper (latitude, −11°; longitude, 31°) is redder, but the bright crater near latitude 36°, longitude 127° is bluer. The basin 440 km in diameter at latitude −15°, longitude 165° has a light, reddish interior surrounded by a darker, bluish border (Fig. 8). The interior plains of Caloris Basin are also redder than average. Such faint color differences probably correspond to compositional differences in the surface materials on Mercury similar to those

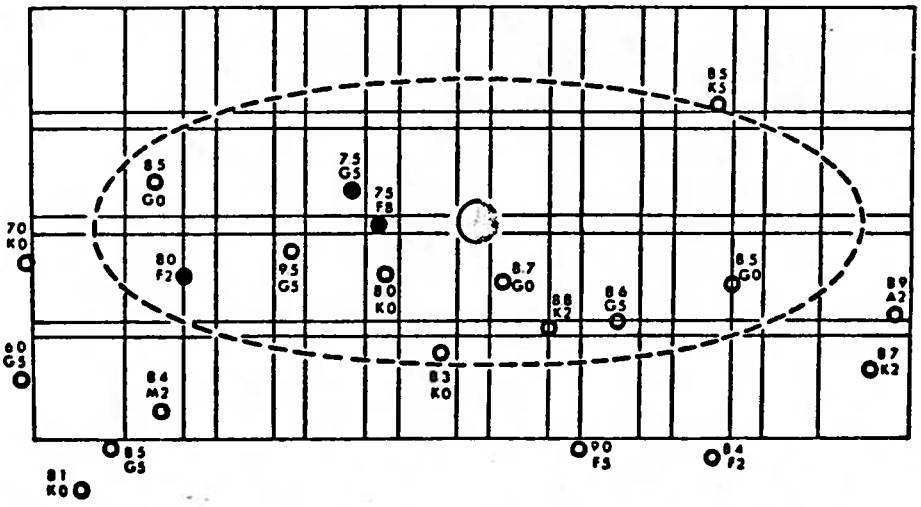

Fig. 3. A 36-picture satellite search sequence, taken 3.5 × 10⁶ km from Mercury, is diagramed with background stars. The actual pointing for individual pictures is still slightly uncertain because of slight spacecraft angular motion. A satellite in a circular orbit at 30 Mercury radii would lie on the ellipse. The closed circles are three stars detected in preliminary processing of the television pictures, and the open circles are undetected stars. The visual magnitude and spectral type of the star are indicated adjacent to each circle. The detectability of the stars sets an upper limit of about 5 km in diameter for a hypothetical satellite.

Table 3. Crater units.

Surface location (Fig. 5)	Number of craters counted	Area (km^2)
Heavily cratered (area A)	1538	4.28×10^4
Plains (area B)	107	2.33×10^4
Plains (area C)	56	1.14×10^4
Caloris Basin	95	4.04×10^5
Area D	261	1.23×10^5
Plains east of Caloris Basin	416	8.50×10^3
Area E	2432	3.11×10^4
Plains (area F)	429	6.33×10^3

found on the moon within individual maria or associated with fresh craters. Thus, Mercury exhibits a surprising similarity to the moon in regional color variations as well as albedo variations. Mercury does indeed resemble the moon on a regional as well as on a global basis. Regional differences in optical properties on the moon generally reflect chemical and mineralogical variations within the overall iron silicate composition of surface material. Grossly similar variations are suggested for the surface of Mercury by the Mariner 10 picture data.

Craters and circular basins. Craters are the predominant landform on Mercury. The areal density differs from one part of the surface to another (Fig. 9), in much the same way as for the highlands and maria on the moon. With increasing size, craters grade into basins—circular structures with an arbitrary lower limit which, for the purposes of this report, is 200 km in diameter. The craters on Mercury are morphologically similar to lunar craters of the same size and evidence the same stages of degradation as their lunar counterparts. This indicates that similar formation and erosive processes have been active, especially meteoroid impact.

Craters smaller than ~10 km in diameter grade from shallow, barely discernible depressions to bowl-shaped cavities exhibiting well-developed raised rims, ejecta deposits, secondary crater fields, and, around some craters, ray systems contrasting in albedo with the surrounding surface. Larger degraded craters, which have lost their ejecta deposits and seondary crater fields and have no prominent raised rims, are typically shallow, flat-floored, and sometimes filled with plains materials. Fresher and presumably younger features commonly exhibit essentially flat floors and terracing on the interior walls; central peaks or ringed complexes are prevalent. The continuous ejecta deposits of the larger craters do not extend as far from the crater rim as for otherwise similar lunar craters. Similarly, the radial distance to the position of maximum areal density of secondary craters is closer to the rim of mercurian craters, and preliminary depth-diameter measurements for 131 craters ranging from 3 to 200 km suggest that mercurian craters are significantly shallower than similar-sized lunar craters. All three differences are consistent with Mercury's greater gravitational acceleration, which can reduce the ballistic range of ejecta and also cause a greater degree of post-cratering collapse through slumping of the rim of the impact cavity.

We obtained crater size-frequency distributions, using the techniques and procedures described by Greeley and Gault (9), as a basis for determining the relative ages of major physiographic provinces and several selected surface units (Table 3 and Fig. 9). Areas in which the crater counts were made are indicated in Fig. 5. The heavily cratered terrain observed prior to encounter is not only grossly similar in general appearance to the lunar highlands but also has a crater frequency distribution (Fig. 9) essentially identical to that of the southern highlands on the nearside of the moon. Both surfaces have attained equilibrium or steady-state conditions (*10*, *11*), with craters as large as at least 100 km in diameter; landforms there have survived since the end of intense bombardment by small planetesimals.

Table 4 lists all basins larger than 200 km in diameter within the areas of favorable viewing areas outlined in Fig. 8. The basins show a variety of morphologies depending on their size, relative age, and degree of flooding by plains materials. The smaller basins tend to have two well-preserved rings, with the diameter of the outer ring close to twice that of the inner ring (Fig. 10). Both rings are of relatively low relief. Radar measurements give a height of 1.5 km relative to the basin floor for the outer ring of basin 5 of Fig. 8 (*12*). In some basins, the inner ring is partially covered with plains materials and the area between the two rings contains irregular hills. Outside the outer ring, radial structures dominate, consisting of hills, valleys, gouges, and strings of craters. Secondary craters and gouges occurs as close as one-fourth crater diameter to the outer ring and extend outward in a continuous field to one crater diameter in the freshest examples (Fig. 10).

Caloris Basin, the largest structural feature apparent in the Mariner 10 pictures, is similar in appearance and size to the lunar Imbrium Basin and undoubtedly originated by impact of a body at least tens of kilometers in diameter. The basin is bounded by a ring of mountains about 1300 km in diameter which forms an irregular scarp averaging around 2 km in height above the basin floor (see cover). Between about 23° and 30°N, the scarp is very subdued and appears to be mantled by plains material. In the northeastern part of the basin, a weak outer scarp occurs at a distance of about 150 km beyond the main scarp. Between these two scarps is a terrain characterized by relatively smooth hills or domes similar in appearance to the terrain adjacent to the Rook Mountains in the lunar Orientale Basin. Surrounding the main scarp and extending outward for at least one basin diameter is

Fig. 4. The 20° meridian passes through the center of the small 1.5-km crater Hun Kal in the Mariner 10 coordinate system. Hun Kal means the numeral 20 in the language of the Maya Indians of Central America; the ancient Maya used a base 20 number system. Hun Kal lies less than 1° south of the equator and defines the Mariner 10 topocentric system of longitudes on Mercury. Numerous elongate craters of probable secondary impact origin are typical of many areas on the planet.

a radial system of linear hills which is best developed northeast of the basin. The radial system is only weakly developed in the terrain between the two scarps; its main development begins beyond the outer scarp in this area. This radial system of hills is embayed by smooth plains material which completely surrounds at least the visible eastern portion of the basin.

Stuart-Alexander and Howard (*13*) counted 24 well-defined basins 300 km in diameter and larger on the moon. In contrast, we have observed eight basins larger than 300 km over approximately one-third of the surface of Mercury, suggesting about the same total of 24 for a body with a surface area twice that of the moon. However, we observe no basins in the size range 500 to 1300 km; the total for the moon in this size range is five (*13*). The relative deficiency of large basins on the surface of Mercury so far viewed probably has affected the regional appearance of the planet as compared to that of the moon. Ejecta blankets and secondary craters are observable around virtually all basins that are not flooded by plains materials outside the outer scarp. Obliteration of these features by subsequent basins larger than 500 km apparently has not occurred on the observed surface of Mercury to the same degree as on the moon (*14*).

Plains. The floors of many basins and craters and the surfaces around several large basins are relatively level, except for scarps and ridges. These surfaces tend to be free of craters larger than 10 km in diameter and are referred to as plains; they are obviously younger than the surrounding heavily cratered terrain. The mercurian plains seen in Mariner 10 pictures strongly resemble the lunar maria. It is important to determine whether a similar volcanic origin also can be inferred for at least some of the mercurian plains. In the following we review morphological evidence which bears on the origin of the plains.

The general distribution of plains visible in the Mariner 10 pictures is plotted in Fig. 8. Many craters in the diameter range 100 to 200 km are filled with plains materials, but others are not, including some that appear to be as old as those that are filled. The plains materials on Mercury fill all of the basins on the planet but to different degrees (see, for example, Fig. 13). Particularly important is the difference between the 350-km north polar basin (number 3, Table 4), which is filled and surrounded by a broad belt of plains, and a basin of identical size at 45°S (number 14, Table 4), which contains only a restricted area of plains on its floor. These relations are more easily explained if the plains are presumed to have formed in episodes of volcanism that followed formation of most of the basins rather than as impact melts at the time of each major cratering event.

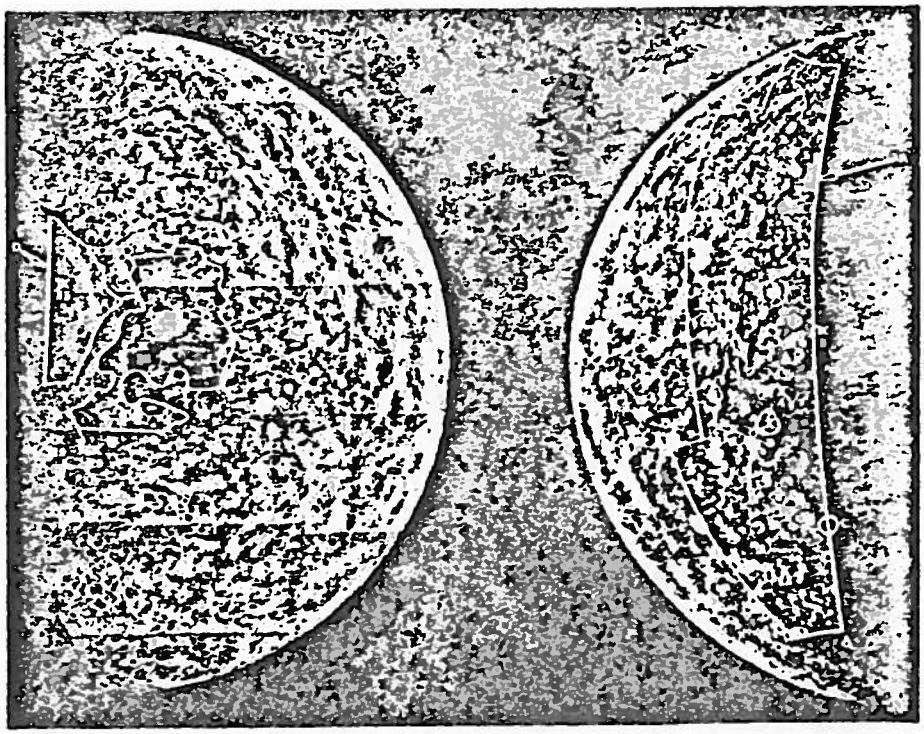

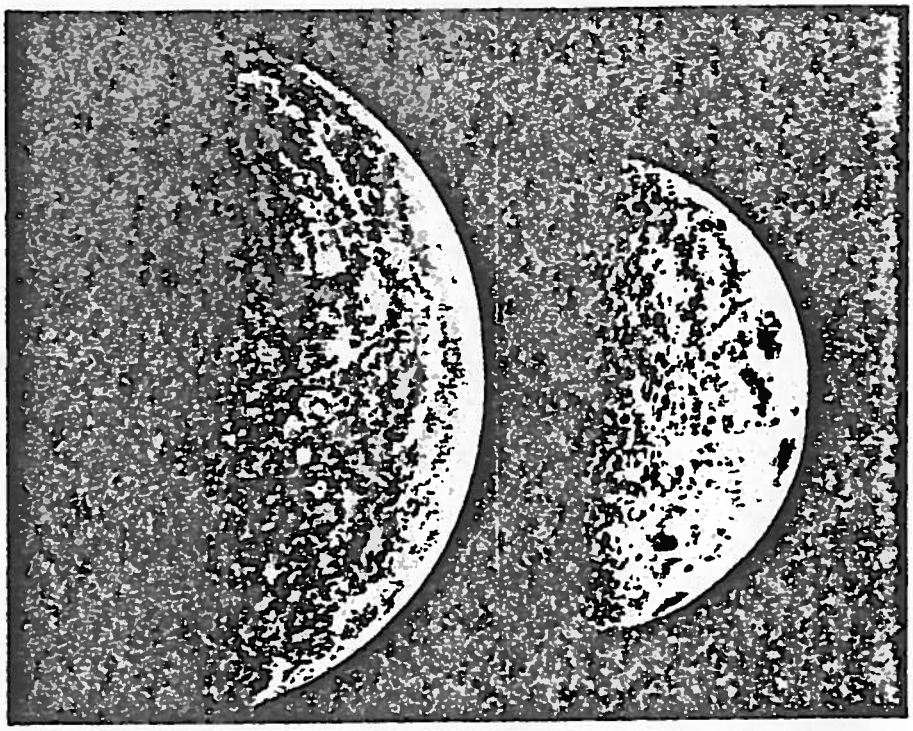

Fig. 5 (top). The incoming (right) and outgoing (left) mosaics of Mercury depicting the points of albedo measurement referred to in Table 2. The enclosed areas indicated by letters are those used in crater counting as listed in Table 3 and shown in Fig. 9. Fig. 6 (bottom). Mariner 10 pictures of Mercury (left) and the moon (right) processed to appear as they would with equal illumination. The relatively lower contrast of Mercury is apparent.

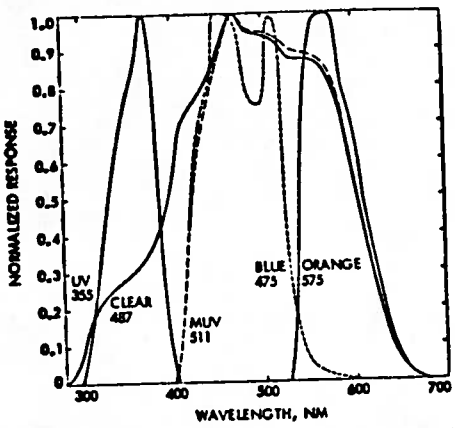

Fig. 7. The integrated optics, filter, and vidicon system response have been independently normalized for each spectral filter on the basis of the absolute Mercury spectrum and plotted as a function of wavelength. The effective wavelength (in nanometers) is shown by each filter name (*UV*, ultraviolet; *MUV*, minus ultraviolet).

Plains containing ridges and scarps surround Caloris Basin in an arcuate band from 1000 to 1500 km wide (Fig. 8 and cover). Radar studies (*12*) suggest that the band continues around at least the southwestern rim of the basin some 1000 to 2000 km on the side not illuminated at the time of the Mariner 10 flyby. In places, hills of more rugged material project through these plains, an indication that the material there is relatively thin. Caloris Basin itself is filled to within about 2 km of the highest peaks in the surrounding mountains.

The plains inside Caloris Basin contain numerous ridges and are intensely fractured (see cover). Ridges range from 1.5 to 13 km in width, have heights of about 300 m and lengths in excess of 300 km, and are grossly similar to lunar mare ridges. The extent and complexity of the ridges and associated fracturing inside Caloris Basin are greater than on lunar maria. Fractures are closely spaced with some forming a polygonal pattern; others are almost sinuous, although unlike lunar sinuous rills in detailed planimetric outline. They range in width from 6 km down to the resolution of the best photography of the basin floor (~700 m). The widest fractures are flat-floored and graben-like. Fractures transect, are parallel to, and even occur along the tops of ridges. The directions of fractures tend to mimic the trend of the ridges, suggesting that the structures are related. The Caloris Basin fracture pattern seems consistent with the gentle subsidence of the central part of the basin floor following emplacement of the plains. Subsidence has also affected lunar mare basins, but not to the same extent or in exactly the same pattern.

Table 4. Circular basins observed in Mariner 10 pictures (March 1974 encounter).

Feature number (Fig. 8)	Latitude	Longitude	Diameter (km)
1 (Caloris)	+30	190	1300
2	−15	165	440
3	+85	30?	350
4	−2	45	385
5	0	37	330
6	+31	159	410
7	+43	158	240
8	−18	52	220
9	−77	100	200
10	+10	190	220
11	+52	133	200
12	−64	20	250
13	−16	13	240
14	−45	178	430
15	+48	150	310
16	+27	163	240
17	+21	19	230

A typical high-resolution view of two areas of plains and their surroundings (Fig. 11) shows that the rims of the enclosing craters have been battered by abundant craters not present on the younger, smooth floors. In another area (Fig. 12a) a series of filled craters shows progressively greater structural disruption of their rims, indicating a lapse of time between crater formation and filling by plains materials. These plains materials are unaffected structurally and appear to be about the same age in each depression. Later plains material fills craters and basins cut into the broad belt of earlier plains around Caloris Basin (Figs. 9 and 10).

Crater populations for plains within Caloris Basin and for surrounding plains east of Caloris (Fig. 9) are indistinguishable, an indication that the emplacement ages of the two surfaces are similar. Plains units exhibit production crater populations (*10*) in contrast to the heavily cratered terrain (Fig. 9) which is in a state of crater saturation. The mercurian plains crater populations resemble those of the more heavily cratered lunar maria. How-

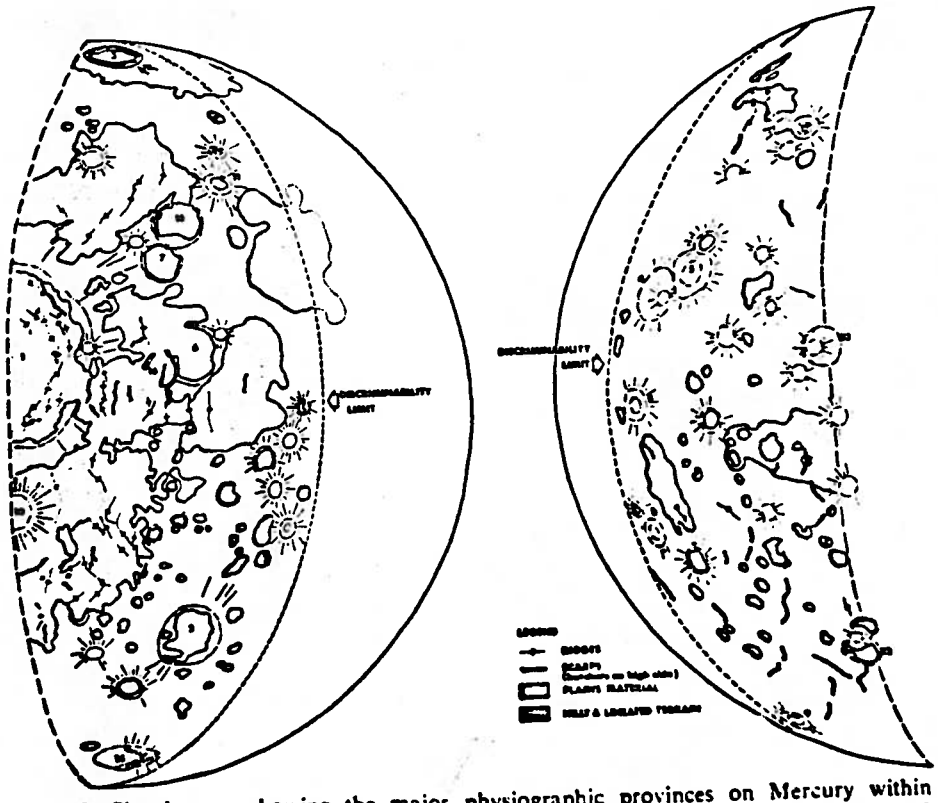

Fig. 8. Sketch map showing the major physiographic provinces on Mercury within approximately 60° of the terminator on the two hemispheres viewed by Mariner 10 approximately 60° of the terminator on the two hemispheres viewed by Mariner 10 and shown in Figs. 1 and 5. The rim crests of basins, arbitrarily chosen as 200 km in diameter or larger, are shown by a dash-dot symbol and keyed by number to Table 4. The more prominent craters larger than 100 km are also shown. Ejecta and secondary craters around craters and basins are indicated by radial lines.

ver, in any attempt to assess the absolute age of the mercurian plains through comparison of their crater number densities with those of the lunar maria, one must take into account the differences in cratering mechanics between the two bodies (*15*) as well as the possibility of differing fluxes of postaccretion impacting bodies.

Patches of plains materials on the floors of craters and basins over the west of Mercury are indistinguishable in age or morphology from the plains concentric to and inside Caloris Basin. Some of these smaller tracts of plains materials could perhaps be impact melt from nearby craters or basins, but for many there is no well-defined source crater (Fig. 11). We have observed no direct evidence of volcanism such as cones, domes, or flow fronts. However, such lunar features are unevenly distributed and best observed under very low sun illumination. The Mariner 10 pictures of Mercury show only a single narrow band on the planet with such lighting.

The origin of the plains material is of key importance because widespread volcanism, in combination with its great bulk density, would strongly imply that Mercury is chemically differentiated. The volumes and areal distribution of the plains materials are the main arguments in favor of a volcanic origin as distinguished from an origin as solidified impact melt or debris flows. Plains materials filling Caloris Basin and the north polar basin certainly cannot be the direct result of the impact which formed these basins because the present volume of the plains fill is very close to the volume originally excavated during the cratering itself. Subsequent filling by fluid material is required, and this has been the case for Mare Imbrium, for example.

Caloris Basin, immediately after it formed, possibly resembled Orientale Basin on the moon which has experienced a minimum of volcanic filling.

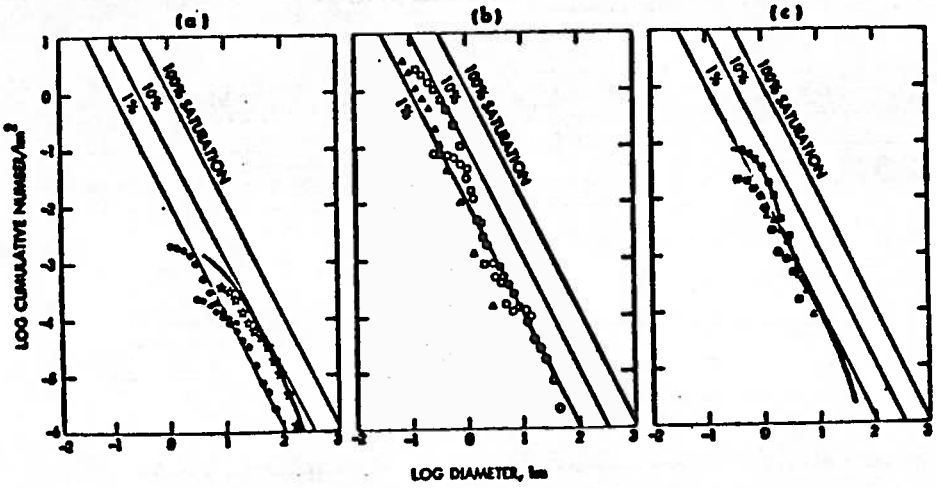

Fig. 9. Crater size-frequency distributions (for major physiographic provinces and selected areas shown in Fig. 5) are expressed as the cumulative number of craters larger than a given diameter and compared with percentages of saturation as defined by Gault (*12*). Equilibrium conditions (that is, when the rate of crater production equals the rate of crater destruction) are attained for crater populations at 5 to 10 percent saturation. Symbol notation: (a) ☆, heavily cratered terrain (area A); ●, Caloris Basin (area D); heavy line, lunar southern highlands (*24*); (b) ○, plains east of Caloris Basin (area E); ▲, Apollo 12 landing site (*23*); □, Apollo 14 landing site (*23*); (c) *, plains filling crater (area B); △, crater floor (area C); ■, plains filling crater (area F); heavy line, plains outside Caloris Basin (area E).

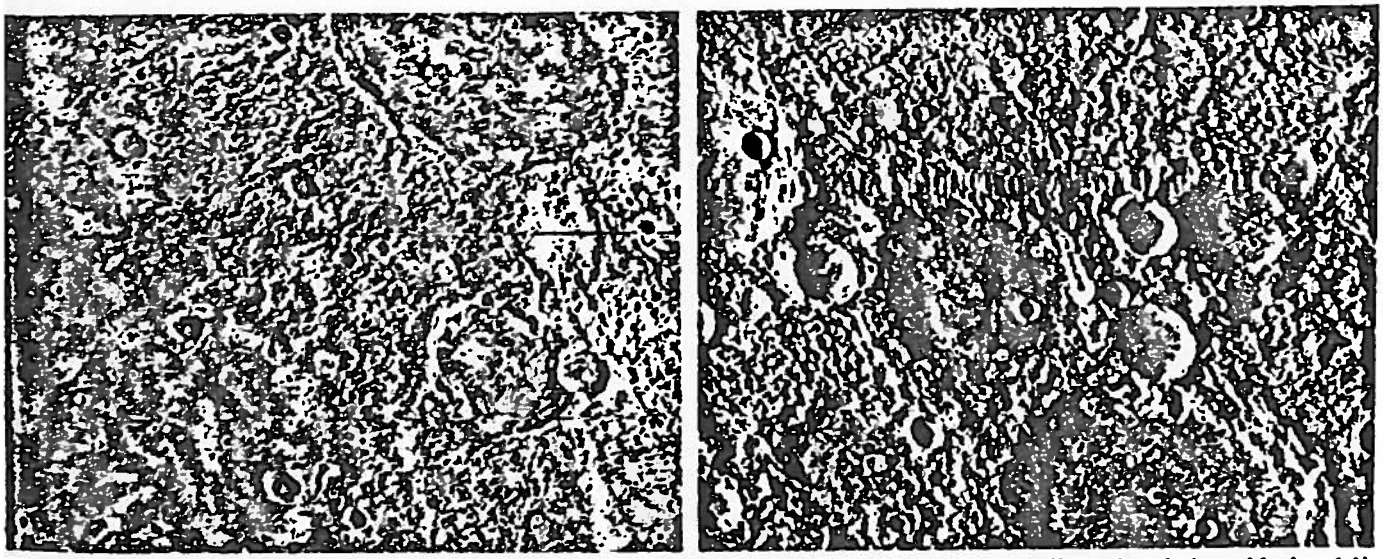

Fig. 10 (left). Typical double-ring basin 200 km in diameter (number 11, Table 4) showing a well-developed ejecta blanket (*A*) and swarm of secondary craters (*B*). The basin is younger than the plains material to the southwest because its secondary craters overlie the plains, which, in turn, are part of a concentric band around the Caloris Basin. This double-ringed basin is also floored by plains material. North is at the top. Fig. 11 (right). Two patches of plains materials covering the floors of older craters (*A* and *C*) whose rims are much more heavily cratered. No external source for the plains material is evident. Hypothetical impact melt from crater C should have filled both craters A and B, but only crater A is filled. A volcanic origin is indicated. The scarp (*d*, *e*) on the floor of crater A is about 400 m high. Similar scarps have been recognized in numerous craters where they appear to be restricted to the crater floor. It is not yet clear whether they are of tectonic or volcanic origin. The blurred stripe about one-third of the distance from the top of the picture is a processing defect. Crater A is 100 km in diameter.

Orientale has numerous hummocky fissured areas on the floor and some smooth plains, probably formed from impact melt. There is also a relatively small area of dark plains (maria) believed to be of genuine volcanic origin. The volume of the Orientale melt material is insignificant compared to the volume of its impact cavity out to its outermost rim. In contradistinction, the plains concentrically surrounding Caloris Basin and the north polar basin involve enormous volumes of melted material—more analogous to the mare flooding of Oceanus Procellarum adjacent to Mare Imbrium than to the light plains materials (sometimes called Cayley Formation) containing impact breccias which concentrically surround Imbrium Basin in disconnected patches (*16*). A volcanic origin for the Caloris Basin plains and surrounding units seems to us quite probable.

Plains-filled basins conceivably may be the sites of gravity anomalies similar to the lunar mascons. O'Leary (*17*) has speculated that a nonuniform distribution of regional gravity anomalies might provide the gravitational inhomogeneity required to keep Mercury in its 3/2 spin resonant period. The location of the large Caloris Basin near the mercurian equatorial region, which is preferentially pointed toward the sun at perihelion, is suggestive in this regard. However, detailed measurements of the nonspherical portion of Mercury's gravity field (probably with an orbiting spacecraft) will be required to verify if Caloris or other circular basins on Mercury actually exhibit mascon-like gravity anomalies.

Unique surface features. Topographic forms are the signature of surface processes of construction and destruction. Features which appear unique to Mercury are therefore of special interest as they may record processes or events, or both, that have not operated on other bodies. The large scarps of great linear extent that transect both craters and intercrater areas on Mercury appear to be just such features. Several of the largest of these are indicated in Fig. 8. These scarps are best seen on the heavily cratered incoming view of Mercury. Preliminary shadow measurements indicate that several of the scarps may attain heights of 3 km or more. They generally have sinuous outlines with slightly lobate fronts and commonly attain lengths well over 500 km (Fig. 14). The scarps face in various directions, although east-facing scarps appear to be more frequent in the incoming view. Often large craters interrupt their paths, suggesting that at least some of the scarps were formed during the final stages of intense bombardment of the surface. The lobate form of the scarps, and their crater transection relation, suggests that they may be thrust or reverse faults caused by compressive stresses. If this interpretation is correct, then Mercury i the first planet other than Earth t show evidence for global compressiv stresses on this scale. Such compressiv deformation evidently was significar during the later phases of heavy bon bardment, if not earlier.

A peculiar terrain of hills and line tions (Fig. 12, a and b), confined a semielliptical area of at least 500,0(km², is centered at latitude 20°S ar longitude 20°, approximately antipod to Caloris Basin. Because the terra extends into the terminator, the are extent may be considerably greate This terrain is somewhat similar to t hilly and furrowed terrain northwe of the lunar Mare Humorum (*16* The hills are generally wider than the lunar example; whether there a other significant differences is not cle without additional picture analysis. T hilly and lineated terrain on Mercu includes craters whose rims have be broken up into hills and depressio Some craters are more strongly mo fied than others of comparable si suggesting that this terrain develop over an appreciable period of ti rather than during a single catastrop event. The extended duration yet l ited geographic distribution point ward an internal origin.

The floors of many craters in hilly and lineated terrain are alm completely filled with plains mate which embays dissected crater r

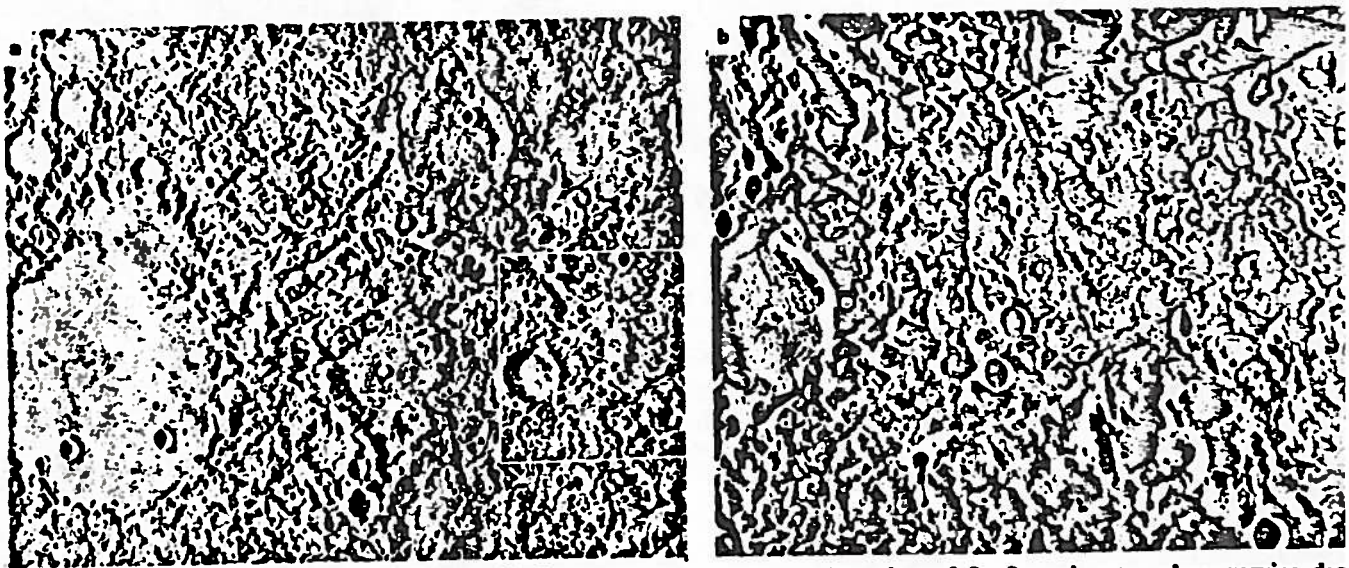

Fig. 12. (a) Hilly and lineated terrain whose distribution is shown in Fig. 8. The rims of flat-floored craters show varying deg of structural disruption, suggesting that the terrain developed over a period of time. Plains materials on the crater floors younger than the surrounding terrain; the plains in the largest crater (170 km in diameter) have a crater number density sim to that of the plains surrounding Caloris Basin. (b) A high-resolution (400-m) picture of area A shown in (a). This terrain sists of numerous dissected hills (~0.1 to 1.8 km high) interspersed with smooth material. The southern rim (*d*) of the 31 crater (*A*) has been severely dissected, but the eastern rim (*e*) is largely intact. The crater rim of the smaller crater (*B* barely recognizable.

and is clearly younger than the hilly and lineated terrain. Hence, the formation of this terrain appears to fall between the end of heavy bombardment and the emplacement of the plains units filling the Caloris Basin and elsewhere.

Planetary history. The Mariner 10 picture data suggest to us that Mercury underwent a period of early heavy bombardment, resulting in the formation of huge basins, and that this was followed by the widespread volcanism represented by the plains materials. The inferred sequence of events is remarkably similar to that deduced for the moon; a strong chemical similarity to the moon on the scale of these plains units is also indicated. But Mercury is much denser on a planetary scale than the moon. Therefore, Mercury must be a chemically differentiated planet; silicate outer layers probably enclose an iron-rich core.

That the materials of the uppermost centimeters to meters on Mercury probably are iron silicates at least grossly similar to those on the moon (density range, 3.0 to 3.3 g/cm^3) has been known for many years on the basis of ground-based radio, radar, spectral, and infrared measurements (*18*). Now, a silicate composition for at least the outer few kilometers is indicated directly by the Mariner 10 pictures because of the strong similarity in albedo and morphology of the mercurian cratered terrains and plains to those of the lunar highlands and maria. Furthermore, the resemblance of Mercury to the moon probably persists to a greater depth. Silicate material must extend to a considerable depth in order to have supplied the large amount of volcanic material that composes much of the extensive plains deposits. Indeed, Reynolds and Summers (*19*) have estimated that an iron core of terrestrial composition for a differentiated Mercury would extend outward 75 to 80 percent of the radius of the planet; the silicate outer layers would be approximately 500 to 600 km in thickness. Alternative interpretations of Mercury's internal structure fail to plausibly account for the close similarity to the lunar surface (*20*).

What additional planetary history is evidenced by Mercury's surface? A striking feature of Mercury (and of the moon as well) is that an ancient heavily cratered terrain has been preserved in extensive regions without major modification by either internal processes such as volcanism or surface processes such as atmospheric erosion. Some of the topographic features comprising such terrain are very probably of considerable antiquity, 4 to 4.5 billion years old if lunar history is relevant. Analysis of samples returned from the moon has raised the possibility that the lunar heavy bombardment may have continued until 4 billion years ago (*21*). Yet, some volcanic rocks returned from the lunar highlands may be as old as 4.5 billion years (*22*). Further resolution of the history of the moon, as well as detailed consideration of intrinsic differences in both accretion and the flux of other solar system objects at Mercury as compared to the moon, seem required before the terminal phases of heavy bombardment of Mercury can be assigned to a time period more precise than 4 to 4.5 billion years ago.

The survival of ancient cratered terrain places limits on the time when material now composing the planet became chemically differentiated. In particular, differentiation must have been complete by the time the oldest surviving landforms were created. The complete planetary heating required for in situ differentiation of an originally homogeneous planet very likely would have significantly modified all surface topography through destructive volcanism, atmospheric effects, or even melting. Consequently, the differentiation of Mercury must have occurred before the end of heavy bombardment. Furthermore, there is no evidence of any atmospheric modification of the ancient land surfaces, making it unlikely that Mercury has possessed any tangible atmosphere since the end of heavy bombardment. The most recent impact craters on Mars, for comparison, have lost their ray systems and

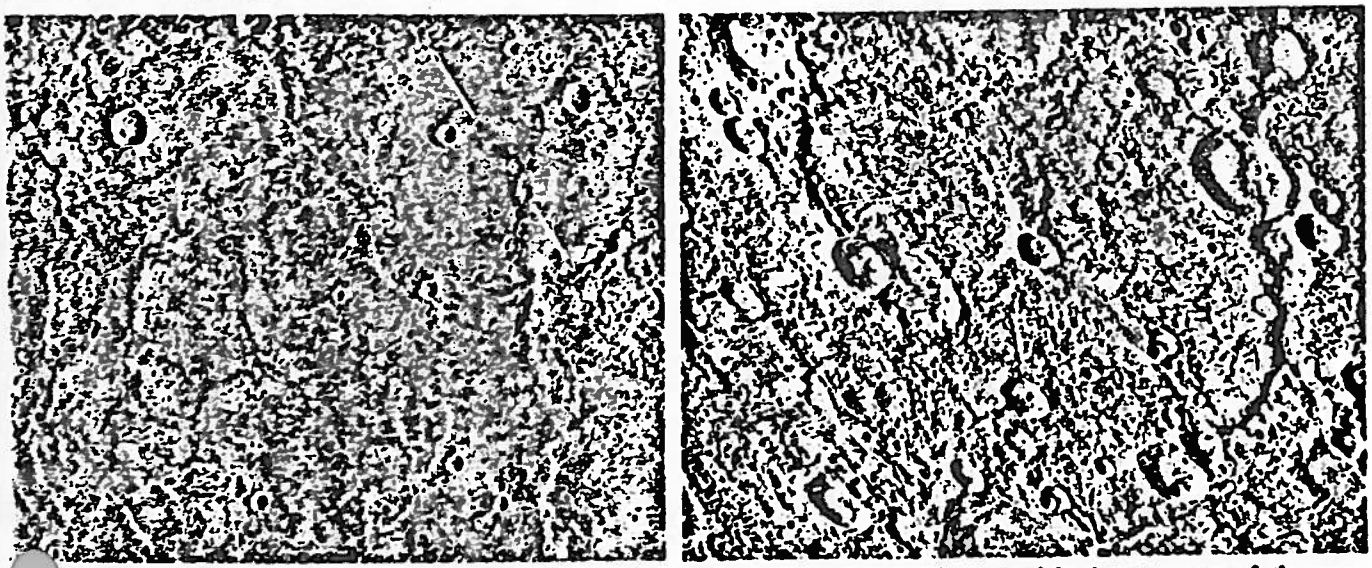

3 (left). A 240-km basin (number 16, Table 4) almost completely floored by plains materials that are part of the concentric band around Caloris Basin. The number 16 is centered in the basin, and arrows point to a ring of low unflooded hills which define the basin. Caloris Basin lies 1300 km to the southwest. North is at the top. Fig. 14 (right). A sinuous, slightly arcuate scarp (*A* through *B*) over 300 km long which transects two craters. Preliminary shadow measurements indicate a maximum height on the order of 3 km. The form, dimensions, and crater transection relations suggest that this structure (and many others of a similar nature) is a thrust or reverse fault due to compressive stresses. Craters cut by scarp are 55 and 35 km in diameter.

Table 1. Mariner 10 Mercury radius.

Occultation	Latitude	Longitude	Solar zenith angle (deg)	Radius (km)	Probable error (km)
Entry	2.3°N	67.4°E	166.7	2439.6	2
Exit	68.4°N	258.8°E	68.4	2438.3	2

dicates that none is larger than the corresponding coefficient for the moon's potential. Further analysis, which will include the calibration of the plasma contribution to the observable deduced from the dual-frequency data, will yield more quantitative results for these harmonic coefficients for Mercury.

The density of Mercury deduced from the mass and radius (see below) determined by Mariner 10, 5.44 g/cm³, is virtually identical with the value determined from radar observations (*7*). Thus any lingering doubts about its validity should now be removed.

Radio science. The data obtained during the spacecraft's entry into, and exit from, occultation by Mercury have been analyzed to obtain preliminary bounds on the density of Mercury's ionosphere and atmosphere, and to deduce the radius of Mercury at the entry and exit points of occultation. The method used to analyze these open-loop and closed-loop data have been described elsewhere (*8*).

The entry, or immersion, of the spacecraft into occultation occurred on the nightside of Mercury near a latitude of 2.3°N and a longitude of about 67.3°E. The solar zenith angle at the point of occulation was about 166.7°. An analysis of the closed-loop differential, dispersive (S- and X-band) Doppler data from the block 4 receivers at Deep Space Station (DSS) 14 (*1*) showed no indication of any ionospheric layers. The data yielded an upper limit for the electron density of about 4000 electron/cm³. Emersion, or exit, occurred on the dayside of Mercury near a latitude of 68.4°N and a longitude of 258.8°E. The solar zenith angle was about 68.4°. No clear signature of a dayside ionosphere was observed. The open-loop data from DSS 14 yielded an upper limit for the electron density of about 1500 electron/cm³ (*9*).

Neither the X-band nor the S-band data provided any indication of propagation effects through a neutral atmosphere, but an upper limit can be inferred from the upper limits of the electron density quoted above. Under the assumptions that any charged particles present on the dayside are the result of photoionization and that the ionosphere would be similar to those of Venus and Mars, it is possible to establish an upper limit for neutral particles near the surface of Mercury of about 10^9 particle/cm³. If a constituent of the largest reasonable molecular weight, such as argon, is assumed, then the surface atmospheric pressure would be less than 10^{-9} mbar.

Mercury's radius can be deduced for two points on its surface from the observations of the time of extinction and reappearance of the spacecraft radio signal and from the relation at these times of the position of the center of mass of the planet relative to the line of sight from Earth to the spacecraft. The accuracy of the radius determination depends on that of the timing of the occultation events and on the accuracy of the ephemeris of the spacecraft relative to Mercury. From the analysis of the open-loop data obtained during entry and exit, the times for the occultation were determined with an error of less than 0.05 second, corresponding to a projected error in the radius determination of about 250 m. However, the uncertainty still existing in the ephemeris of the spacecraft relative to Mercury is the major source of error in the radius determination. The results are summarized in Table 1, which also shows the latitudes, longitudes, and solar zenith angles at the two occultation points as well as the probable errors of the radius estimates. These uncertainties are based on the variations in the values of the radius when computed with different sets of available spacecraft ephemerides. These uncertainties should eventually be reduced by about an order of magnitude. The value of the equatorial radius based on the entry measurement is very close to the mean radius of 2439 ± 1 km obtained from the analysis of planetary radar data (*5*). The difference in radius between the two determinations from the Mariner 10 data is less than the current uncertainty in each. However, even when these uncertainties are reduced, it will not be possible to use these radius measurements to distinguish any overall flattening of the planet from local variations in topography.

H. T. Howard, G. L. Ty
Center for Radar Astronomy, Stanford University, Stanford, California 94305
P. B. Esposito, J. D. Ander
Jet Propulsion Laboratory, California Institute of Technology, Pasadena 91103
R. D. Reasenberg, I. I. Shap
Department of Earth and Planetary Sciences, Massachusetts Institute of Technology, Cambridge 02139
G. Fjeldbo, A. J. Kli
G. S. Levy, D. L. Bru
R. Dickinson, R. E. Edel
W. L. Martin, R. B. Pos
B. Seidel, T. T. Sesplau
D. L. Shirley, C. T. Stelz
D. N. Sweetnam, G. E. W
A. I. Zygielba
Jet Propulsion Laboratory

References and Notes

1. H. T. Howard *et al.*, *Science* **183**, 1297 (19
2. J. A. Dunne, *ibid.* **185**, 141 (1974).
3. Appreciable sensitivity to these terms e only for about 40 minutes, centered on counter; however, no tracking data exist the 12-minute duration of the occulta which started several minutes past encou
4. The corresponding value for the product Mercury's mass and the universal constan gravitation is 22,032 ± 2 km³/sec².
5. Some of the early determinations of the r of the mass of the sun to the mass of M cury from radar data, in chronological or are: 6,021,000 ± 53,000 [M. E. Ash, I. Shapiro, W. B. Smith, *Astron. J.* **72**, (1967)]; 5,983,000 ± 25,000 [W. G. Melbo and D. A. O'Handley, *Jet Propulsion L Space Programs Sum.* **37-53** (1968), vol p. 1]; and 6,025,000 ± 15,000 (*7*). More cent estimates have been made at both Massachussets Institute of Technology and Jet Propulsion Laboratory, a typical v being 6,022,700 ± 3,000 [I. I. Shapiro R. D. Reasenberg, in "Mariner Mars Project Final Report," *Jet Propulsion L Tech. Rep. No. 32-1550* (15 July 1973) vol pp. 460 and 464].
6. Most of the Doppler data are averages o either 600 or 60 seconds. However, withi hour of encounter, the data were avera over only 10 seconds and the root-me square residual for this portion of the d is about 10 mhz.
7. M. E. Ash, I. I. Shapiro, W. B. Sm *Science* **174**, 551 (1971).
8. G. Fjeldbo and V. R. Eshleman, *Planet. Sp Sci.* **16**, 1035 (1968); A. J. Kliore, D. L. C G. Fjeldbo, B. L. Seidel, M. J. Sykes, S. Rasool, *Icarus* **17**, 484 (1972).
9. The difference of nearly a factor of 3 betw the two limits is due to the difference in high-frequency fluctuations in the signals, pr ably attributable to variations in the int planetary medium or in Earth's ionosphere.
10. We thank the personnel of the Mariner Pr ect, the Deep Space Net, and the Project Na gation Team. We are particularly indebted D. W. Brown for his leadership of the grou station tiger team. This report presents r results of one phase of research carried c at the Jet Propulsion Laboratory (JP California Institute of Technology, un NASA contract No. NAS 7-100.

22 June 1974